Review

Catalytic Steam Reforming of Biomass-Derived Oxygenates for H2 Production: A Review on Ni-Based Catalysts

Joel Silva [1,2]**, Cláudio Rocha** [2,3]**, M. A. Soria** [1,2,]***** **and Luís M. Madeira** [1,2]

[1] LEPABE—Laboratory for Process Engineering, Environment, Biotechnology and Energy, Department of Chemical Engineering, Faculty of Engineering, University of Porto, Rua Dr. Roberto Frias, 4200-465 Porto, Portugal; joel.alexandre.moreira.silva@gmail.com (J.S.); mmadeira@fe.up.pt (L.M.M.)

[2] ALiCE—Associate Laboratory in Chemical Engineering, Faculty of Engineering, University of Porto, Rua Dr. Roberto Frias, 4200-465 Porto, Portugal; csrocha@fe.up.pt

[3] LSRE-LCM—Laboratory of Separation and Reaction Engineering—Laboratory of Catalysis and Materials, Faculty of Engineering, University of Porto, Rua Dr. Roberto Frias, 4200-465 Porto, Portugal

***** Correspondence: masoria@fe.up.pt

Abstract: The steam reforming of ethanol, methanol, and other oxygenates (e.g., bio-oil and olive mill wastewater) using Ni-based catalysts have been studied by the scientific community in the last few years. This process is already well studied over the last years, being the critical point, at this moment, the choice of a suitable catalyst. The utilization of these oxygenates for the production of "green" H2 is an interesting alternative to fuel fossils. For this application, Ni-based catalysts have been extensively studied since they are highly active and cheaper than noble metal-based materials. In this review, a comparison of several Ni-based catalysts reported in the literature for the different above-mentioned reactions is carried out. This study aims to understand if such catalysts demonstrate enough catalytic activity/stability for application in steam reforming of the oxygenated compounds and which preparation methods are most adequate to obtain these materials. In summary, it aims to provide insights into the performances reached and point out the best way to get better and improved catalysts for such applications (which depends on the feedstock used).

Keywords: ethanol; methanol; oxygenates; steam reforming; Ni-based catalysts

1. Introduction

The extensive use of fossil fuels over the last few decades has been contributing significantly to the build-up of greenhouse gases in the atmosphere, which on its hand contributed considerably to global warming. Alternative renewable fuels have been studied, among which hydrogen is seen as a potential candidate to replace fossil fuels as an energy carrier [1–4]. Among other advantages, the following are worth mentioning: hydrogen possesses a gravimetric energy density of 143 MJ·kg^{-1}, more than three times higher than that of gasoline and diesel [4]; it can be produced through several processes, many of which include renewable feedstock [5]; hydrogen can be used either in internal combustion engines or in fuel cells [6–8]; the risk associated to hydrogen handling is equal or lower than that of other fuels [4].

Over the last years, hydrogen has been industrially produced mostly through steam reforming of natural gas, naphtha, heavy oils, and to a lesser extent through coal gasification. Only a very small fraction of all of the hydrogen that has been produced worldwide comes from water and other renewable sources [9–12]. Furthermore, if the electricity used in water electrolysis is generated from fossil fuels, the hydrogen produced through this method cannot be considered renewable either.

The steam reforming of oxygenated compounds derived from biomass, namely methanol [13–16], ethanol [17–20], and bio-oil [2,21–23], among others, has been largely studied over the last 20 years as an alternative for the well-established fossil-based processes, such as natural gas steam reforming. Furthermore, their contribution to the build-up of greenhouse gases in the atmosphere is significantly lower than that of fossil fuels (e.g., most of the emitted CO_2 belongs to the natural CO_2 cycle) [24]. If these advantages are combined with sustainable biomass exploitation policies that aim to avoid competition between the use of land for the production of bio-fuels, food, animal feed, fiber and ecosystem services [25], big-scale hydrogen production through steam reforming of biomass-derived oxygenates might be a likely scenario in the near future.

The successful development of the steam reforming process applied to these biomasses derived oxygenates is highly dependent on the choice of a suitable catalyst, since the steam reforming process is already well studied. In terms of catalytic performance, a suitable catalyst for hydrogen production through steam reforming should ideally meet the following criteria: be highly active to produce high amounts of hydrogen; be highly selective towards hydrogen so that the production of secondary products is minimized; be capable of maintaining long term activity without suffering from deactivation [26,27]. Furthermore, an easy protocol to activate the catalyst is desired (e.g., activation with the hydrogen-containing feedstock at the reaction temperature, thus avoiding more complex protocols) [27]. A catalyst must be cheap as its cost can contribute significantly to the overall process expenditure [28]. Finally, and in agreement with the current sensitive environmental situation, catalysts must be as environment-friendly as possible.

Different metallic active phases such as based on Ni, Cu, Co, Pt, Pd, Ru, Rh, and/or Ir, among others, have been investigated for the steam reforming of biomass-derived oxygenates for hydrogen production. However, Ni-based catalysts have been extensively studied over the last decades not only due to the fact that they have the potential to be highly active and stable, but also because they are cheaper than, for instance, noble metal-based catalysts. Ni-based catalysts, although widely used in steam reforming processes, are less active than noble metal-based materials and more prone to deactivation; effectively, noble metal-based catalysts perform well—they are stable and exhibit high catalytic activity [29]. However, they are very expensive and need high temperatures to be reduced. In this way, Ni-based materials are more suitable for industrial-scale applications. Moreover, nickel-based catalysts are inexpensive, but under some reaction conditions they suffer from sintering and deactivation by carbon production [30,31]. Nevertheless, the reaction mechanism over Ni-based catalysts follows the same steps as over noble metal-based catalysts for most steam reforming processes [30].

Still, a careful choice of the Ni loading, support, promoter(s) and synthesis method is of uttermost importance, as these factors have a crucial impact on both catalytic performance and price [32].

Since the steam reforming of biomass-derived oxygenates, such as methanol, ethanol and other oxygenates (e.g., bio-oil and glycerol), is still under intensive study, and considering the above reasons that highlight the potential of Ni-based catalysts, a literature review encompassing a wide range of these materials for the different reactions is hereby carried out. Ultimately, this work aims to understand if Ni-based catalysts currently show enough potential for application in steam reforming of oxygenated compounds and which formulations might be more promising for each application. For the first time, and up to the best knowledge of the authors, this review discusses the results obtained with the best Ni-based catalysts developed so far for the steam reforming of different oxygenated compounds, portraying in detail the effect of the preparation method and the deactivation suffered by these materials in long-term tests. Besides that, this work directs future research works about the most critical properties in preparing catalysts with high catalytic performances for the steam reforming of methanol, ethanol and other oxygenates.
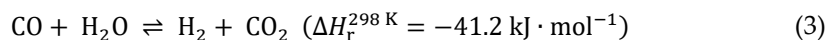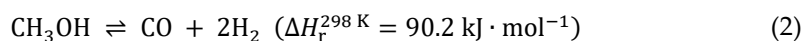
2. Methanol Steam Reforming

2.1. Introduction

Methanol is the simplest of all alcohols and can be produced from several types of biomass such as agricultural waste, forestry waste, livestock and poultry waste, fishery waste, sewage sludge [13,21], among others, through pyrolysis, gasification, biosynthesis, electrolysis and photo electrochemical processes [13]—the main route of methanol formation is the through syngas. Even though some of these processes, such as pyrolysis and gasification, allow a significant hydrogen production directly from biomass [33], the production of methanol, later to be converted into hydrogen, is preferred for the following reasons: it is liquid under room conditions and, for that reason, more suitable for use in fuel cells; it is easier to transport; the required infrastructures are already available; and the production and use of methanol (and other biofuels) are considerably more technologically ready [15].

The methanol steam reforming (MSR) is described by the overall reaction shown in Equation (1):

$$CH_3OH + H_2O \rightleftharpoons CO_2 + 3H_2 \quad (\Delta H_r^{298\,K} = 49.7\,kJ \cdot mol^{-1}) \tag{1}$$
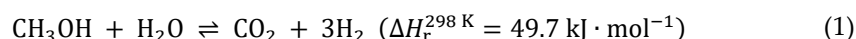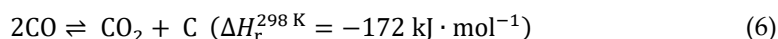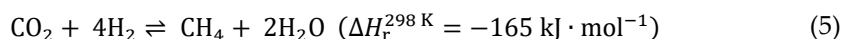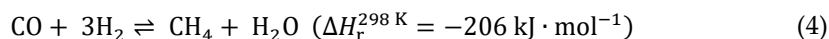
The MSR can be divided into two major reactions: methanol decomposition (Equation (2)) followed by the water-gas shift reaction (WGS) (Equation (3)).

$$CH_3OH \rightleftharpoons CO + 2H_2 \quad (\Delta H_r^{298\,K} = 90.2\,kJ \cdot mol^{-1}) \tag{2}$$

$$CO + H_2O \rightleftharpoons H_2 + CO_2 \quad (\Delta H_r^{298\,K} = -41.2\,kJ \cdot mol^{-1}) \tag{3}$$

This process is globally slightly endothermic and, for that reason, it can be carried out at relatively low temperatures (ca. 200–300 °C) [26] when compared to the steam reforming of methane, for example, which is normally carried out at 700–900 °C [29]. Some of the by-products of this process are CO_2 and CO. The production of CO, in particular, should be avoided, especially if the produced hydrogen is to be used in polymer electrolyte fuel cell applications, where the concentration of CO must be lower than 20 ppm to avoid poisoning of the anode catalyst (low temperature fuel cells) [14]. In fact, for low temperature fuel cells in road vehicles applications, the International Organization for Standardization (ISO 14687) recommends a maximum CO concentration of 0.2 ppm in the hydrogen feed stream [34].

Another frequent by-product in MSR is CH_4, whose formation can happen through hydrogenation of either CO and/or CO_2 (Equations (4) and (5), respectively). Besides that, the highly undesired formation of coke deposits on the catalyst surface may also occur (for instance, the Boudouard reaction—Equation (6)).

$$CO + 3H_2 \rightleftharpoons CH_4 + H_2O \quad (\Delta H_r^{298\,K} = -206\,kJ \cdot mol^{-1}) \tag{4}$$

$$CO_2 + 4H_2 \rightleftharpoons CH_4 + 2H_2O \quad (\Delta H_r^{298\,K} = -165\,kJ \cdot mol^{-1}) \tag{5}$$

$$2CO \rightleftharpoons CO_2 + C \quad (\Delta H_r^{298\,K} = -172\,kJ \cdot mol^{-1}) \tag{6}$$

Even though for fuel cell applications the minimization of CO formation is of extreme importance, its conversion into CH_4 is not desired either as it consumes H_2 (3 mol per mol of CO), the target product. Therefore, choosing an appropriate catalyst that maximizes H_2 production (not only due to higher methanol conversions but also due to lower CO and CH_4 production) could solve, at least partially, this problem.

2.2. Nickel-Based Catalysts

Over the years, several materials were studied as catalysts in the MSR reaction. Among them, Cu-based materials are the ones that have been more targeted for this reaction due to the copper's high surface area, high dispersion and small particle size, among other factors [26]. Furthermore, copper is relatively cheap. On the other hand, copper catalysts can be easily deactivated [35]. Group 8–10 metal-based catalysts have also been of

significant interest and, even though they were, in general, less active towards MSR than Cu-based—group 11, they have shown better long-term and thermal stability [26]. Among those, Ni-based catalysts, which is one of the cheapest metals of such groups, have been a target of huge interest over the last decades for the steam reforming of oxygenates.

2.2.1. Catalytic Activity and H_2 Selectivity

Monometallic nickel catalysts supported on different materials have been extensively explored. Deshmane et al. [36] tested TiO_2 supported Ni, Co, Cu, Zn, Pd and Sn catalysts for the MSR process. The Ni-based catalyst was the second most active after the Pd-based catalyst in terms of methanol conversion and H_2 selectivity, having converted approximately 86% of methanol with an H_2 selectivity of around 97% (at 350 °C). However, it presented the highest CO selectivity, which would be a problem if the product H_2 stream was to be used in polymer electrolyte fuel cell applications. The authors concluded that the specific metal-support interactions, which controlled both reducibility and metal particles dispersion on the TiO_2 support, had a very significant impact on these results. The low activity of the Ni catalyst in the WGS reaction was the main responsible for the high CO selectivities. In a similar work [37], nickel supported on high surface area mesoporous MCM-41 has also been tested for MSR and an H_2 selectivity of 99.9% was achieved at 350 °C (45.1% of methanol conversion) [37]. However, compared to other metals (Cu, Pd, Sn, Zn and Co), Ni was observed to be one of the less active in terms of methanol conversion, contrary to what was observed for TiO_2 support. The authors suggest that the significantly lower reducibility of 10 wt.% Ni/MCM-41 due to silicates and silicides formation could be the reason for its lower activity. It could also be associated with the lower dispersion observed.

In another work [38], it was observed for a Ni/CeO$_2$ catalyst that the strong metal-support interactions play a crucial role in the high selectivity towards CO_2 production in the detriment of CO or surface carbon. Specifically, the enhanced water dissociation over reduced CeO_2 and subsequent oxygen transfer from ceria to nickel enhances the surface oxidation ability of the last. Moreover, the methanol conversion was benefitted over this catalyst and full conversion attained at 400 °C. Other monometallic Ni catalysts supported on other simple oxides have also been studied. For example, 12 wt.% Ni/SiO$_2$ converted 53% of methanol and showed H_2 selectivity as high as 74% at 200 °C only [39], while in another work 10 wt.% Ni/Al$_2$O$_3$ exhibited a conversion of only 24% at 400 °C and a H_2 yield of only about 15% [40]. In this last work, a comparison between the Al$_2$O$_3$ supported catalyst and Ni catalysts supported on MgO prepared through different methods showed that not only did the Al$_2$O$_3$ supported catalyst show higher methanol conversion and H_2 yield (400 °C), but it also showed lower CO selectivity (600 °C). The reason why the MgO-based catalysts showed higher CO selectivity could be due to their higher CO_2 capture ability, which would afterward result in the acceleration of the reverse Boudouard reaction (Equation (6)) and consequent reduction of deposited carbon [40]. This mitigated carbon deposition would certainly be advantageous from a long-term stability standpoint, but the higher CO production would be a problem for polymer electrolyte fuel cell applications. Bobadilla et al. [41] tested Ni nanoparticles supported on a CeO_2 and MgO modified Al$_2$O$_3$ support, having reached a methanol conversion of approximately 66% and H_2 yield of around 70% at 350 °C. The reason why the authors chose this modified support was due to the fact that MgO addition favors the gasification of carbon deposits and CeO_2 modification improves the metal dispersion, which results in a more active and stable catalyst [42].

From this preliminary assessment, one might guess that Ni-Cu-based catalysts are probably a good option for MSR that could assure both high activity and stability. Several catalysts combining both nickel and copper active phases have been reported over the years [43–49]. By studying Cu-Ni bimetallic catalysts with different Cu/Ni ratios (and also the corresponding monometallic catalysts), Khzouz et al. [43] observed that while Ni was related to the enhancement of the methanol decomposition reaction, Cu promoted the

WGS reaction, especially above 250 °C. Furthermore, the bimetallic Ni-Cu catalysts did not yield any CH_4, thus suggesting that Cu alloying in Ni had an inhibiting effect on methanation reactions (Equations (4) and (5)). However, the formation of CH_4 during MSR is not always inhibited over Cu-Ni-based catalysts, as has been reported in several works [46,50–52]. Besides the operating conditions (e.g., reaction temperature or water/methanol feed molar ratio), factors related to the catalysts are also responsible for such different behaviors, namely the support, metal loading and the preparation method adopted.

Lytkina et al. [53] studied bimetallic Ni-Cu-based catalysts supported on ZrO_2 annealed at different temperatures (350 °C or 400 °C), having observed that the higher annealing temperature led to higher crystallization of the support and, consequently, to the deterioration of its adsorption properties. While methanol molecules adsorb on the metal active sites, water molecules adsorb preferentially on the active sites located in the support [54,55]. This was probably one of the causes of the lower H_2 production for the catalysts whose support was annealed at 400 °C. Simultaneous agglomeration of catalyst particles with resulting decreased active surface area was also probably another cause of such decrease in catalytic activity towards H_2 production.

As already mentioned, the loading of the different species is also of crucial importance for catalytic activity. For bimetallic Cu-Ni catalysts, it has been observed that varying the Cu/Ni ratio (0.25–4), while maintaining the total active metal loading, affected the catalytic activity considerably [43,53]. For both studies, while increasing the amount of Ni enhanced methanol conversion, lower Ni contents yielded higher H_2 yields and lower CO production, due to the WGS reaction. It has been suggested that this happens due to a change in the mechanism of adsorption of methanol molecules on the catalyst surface (see Figure 1) [53]. More specifically, for catalysts with higher copper content, there is a higher tendency for single-site (η^1 in Figure 1) methanol adsorption, while two-sites (η^2 according to Figure 1) adsorption through oxygen and carbon atoms is more likely to occur over group 8–10 metals. While in the first case alcohol and water adsorption on adjacent sites with consequently higher yields of H_2 and CO_2 are more likely, in the second case CO production should be more benefited than carbon dioxide [53,56]. The authors suggest that, alternatively, higher Cu content (lower Ni content) might contribute to deeper oxidation of the carbon atoms of the alcohols (i.e., to CO_2) due to a lower Fermi level [53].
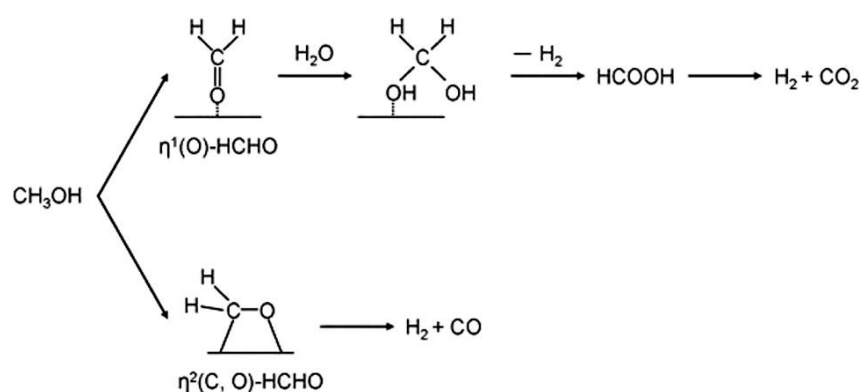
Figure 1. Mechanism of adsorption of methanol molecule over different catalyst surfaces. Reprinted with permission from Ref. [53]. Copyright 2022 Elsevier.

The effect of the total Ni/Cu loading (Ni/Cu of 0.25) on ZrO_2 support has also been analyzed [48]. The increase of the bimetallic loading up to 30 wt.% enhanced the conversion of methanol, having this behavior been correlated to the higher frequency of Ni/Cu core-shell structures observed through transmission electron microscopy (TEM) in the sample with the highest metal content. On the other hand, the sample with a 15 wt.% bimetal loading showed the highest H_2 yield. While only Cu_{core}-Ni_{shell} nanoparticles were identified in the 15 wt.% sample, Cu_{core}-$(NiCu-alloy)_{shell}$ nanoparticles were also observed
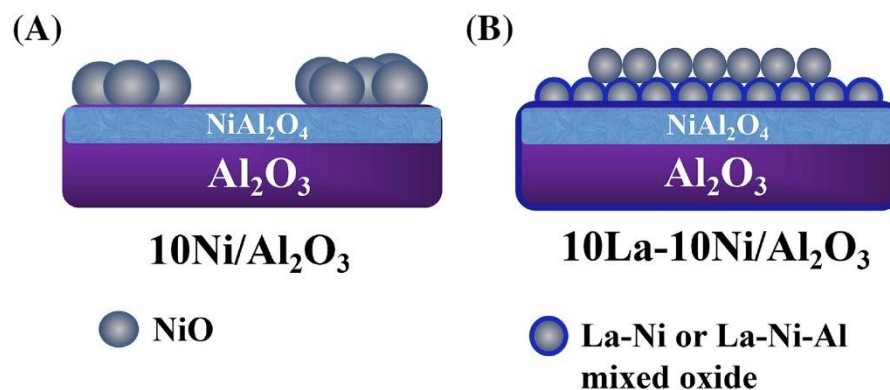
in the 30 wt.% sample. The authors suggested that the nanoparticles with only Ni in the shell presented better H_2 production performance than the nanoparticles whose shell consisted of a Ni-Cu alloy.

Ni-Cu bimetallic catalysts supported on metal oxide-stabilized zirconia (ZrO_2) supports doped with Y, La or Ce were analyzed in another work [57]. The results showed that not only the nature but also the composition of the support influence MSR considerably, which supports the above-mentioned bifunctional mechanism. In fact, while doping the ZrO_2 support with La resulted in higher catalytic activity, doping with Y allowed a higher selectivity towards H_2. This suggests that the doped support influences the process selectivity as well. The modification of the ZrO_2 support with Ce led ultimately to a twofold increment in the activity of Cu-Ni-based catalysts comparatively to the ones modified with Y. It was found that 10 wt.% of Ce was the optimum content that allowed to reach the best catalytic performance, increasing the Ce content beyond that point having been shown as detrimental. The authors suggest that this behavior could be either due to the need of the simultaneous presence of Ce anions (Ce^{3+} and Ce^{4+}), being that the presence of Ce^{3+} on the surface of the particles decreases with increasing Ce content, and Zr, or due to the interaction of defects.

In the work of Huang et al. [58], it has been shown that Ni-Cu/Al_2O_4 materials presented high conversion (>99%), high H_2 yield, and high stability in long-term tests, when used as catalysts in the MSR reaction at low temperatures, in the range of 200–300 °C. In addition, this catalyst exhibits high methanol conversion (very close to 100%), high H_2 yield (always close to 90%) and low CO_2 concentration (around 10%) during the long-term experiment performed in this study. Moreover, it was possible to detect the presence of CO in the reactor outlet (around 5%) during 30 h. These results show that the Ni-Cu bimetallic catalysts present suitable properties to be applied in the MSR process and the promotion of these samples with Ce increases the catalytic performance.

Moreover, it was observed [59] that the simultaneous existence of Pt and Ni elements on the surface of CeO_2 support improved the methanol conversion and H_2 production in comparison with the monometallic samples.

Besides Cu and Pt, other metals such as Sn and La [60,61] have been combined with Ni (using Al_2O_3 as support) in other studies, also aiming to optimize the catalytic performance of the MSR process. While La was observed to enhance the catalytic activity towards H_2 production [61], the presence of Sn was reported to favor mainly the stability of the catalyst [60]. This stabilizing effect of tin is further discussed in the next section (Section 2.2.2). Besides assessing the effect of Sn addition, the authors also evaluated the addition of MgO to the Al_2O_3 support, having concluded that the sample whose support incorporated the highest MgO loading (30 wt.%) presented the highest H_2 production. This enhancement was attributed to the decrease of the support acidity and improvement of Ni dispersion. As for the promoting effect of La, it was observed the interaction between La species and NiO and/or Al_2O_3 (support) to form La-Ni oxide and/or La-Ni-Al mixed oxide, which led to the separation of external NiO particles from the Ni-Al interface. The authors hypothesized that this facilitated the formation of smaller separated NiO particles more highly dispersed (Figure 2), which were ultimately responsible for the improved MSR activity [61]. Furthermore, increasing the Ni loading up to 10 wt.% facilitated the reduction of the catalyst at lower temperatures and improved methanol conversion and H_2 selectivity (lower CO selectivity) for similar reasons as for La.

(A)

NiAl$_2$O$_4$

Al$_2$O$_3$

10Ni/Al$_2$O$_3$

⬤ NiO

(B)

NiAl$_2$O$_4$

Al$_2$O$_3$

10La-10Ni/Al$_2$O$_3$

⬤ La-Ni or La-Ni-Al mixed oxide

Figure 2. Effect of La addition (**B**) on the surface composition of a NiO supported on Al$_2$O$_3$ catalyst (**A**). Reprinted with permission from Ref. [61]. Copyright 2022 Elsevier.

Layered double hydroxides (LDHs) derived catalysts containing nickel have also been a target of interest for MSR over the years. Kim et al. [62] reported a $Cu_{0.55}Ni_{0.10}Zn_{0.10}$ $Al_{0.25}$ LDH which converted about 50% of methanol at 300 °C, being the presence of Ni responsible for a slight improvement of the low temperature activity comparatively to the $Cu_{0.55}Zn_{0.20}$ $Al_{0.25}$ LDH. Qi et al. [63] tested a Ni/Al LDH with a Ni/Al molar ratio of approximately 5.7 which converted 100% of methanol with an H$_2$ selectivity slightly above 50% and CO selectivity below 10% (at 380 °C). In another work [64], another Ni/Al LDH with a Ni/Al molar ratio of around 4.9 converted 87.9% of methanol, provided an H$_2$ yield of approximately 77% and produced low levels of CO at 390 °C. Besides the difference in the Ni/Al molar ratio and reaction conditions between both works, the preparation procedures were also different. The effect of this aspect was, in fact, the target of analysis in both works and was certainly decisive in the results obtained. This will be discussed later (cf. Section 2.2.3). The addition of K to LDHs has been found to further enhance its activity in MSR [65]. The use of K$_2$CO$_3$, during LDH preparation, as precipitating agent combined with no washing, to keep more K in the final solid, increased the conversion of methanol. Furthermore, post-addition of K$_2$CO$_3$ through the incipient wetness method decreased significantly the production of methane. On the other hand, the production of CO suffered a significant increment, which might indicate that the inhibition of methane production could be related to the inhibition of the methanation of CO (Equation (4)). The addition of K also benefited slightly the yield of H$_2$ and the selectivity towards CO$_2$ in detriment of CO, especially at temperatures around 400 °C. The catalytic activity of the K-promoted LDH was superior to that of a commercial Cu catalyst (42 wt.% CuO, 47 wt.% ZnO and 10 wt.% Al$_2$O$_3$), as shown in Figure 3.
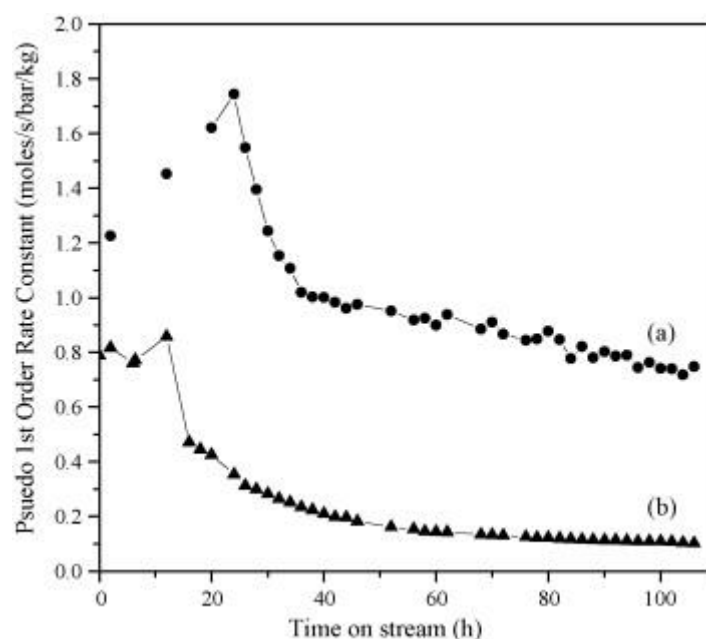
Figure 3. Comparison of the activity in methanol conversion of (**a**) NiAl-LDH with potassium and (**b**) commercial catalyst at 390 °C and steam/carbon molar feed ratio of 1.2. Both catalysts were pre-activated in situ at 240 °C for 6 h on a reactive stream before reaction. Reprinted with permission from Ref. [65]. Copyright 2022 Elsevier.

Different studies using Ni-based catalysts suggested the formation of several intermediates on the catalyst surface during the reaction: according to these works, methyl formate and H_2 were produced via dehydrogenation of methanol, followed by the formation of formic acid [66–68]. Then, CO_2 and H_2 were produced by the decomposition of formic acid. The formation of formaldehyde and dioxomethylene during the MSR process was also suggested by other reactions [66].

2.2.2. Deactivation

High catalytic activity and H_2 selectivity alone do not guarantee that a specific material is a good catalyst for a specific reaction. Long-term stability is another crucial criterion that has to be taken into account when choosing a catalyst. To design a catalyst with long-term catalytic stability, it is crucial to understand what phenomena can disturb such stability. Such phenomena are: (i) coke formation due to hydrocarbons decomposition; (ii) sintering and crystallization or segregation of the metal particles caused by thermal effects; (iii) poisoning originated by chemisorption or reaction of certain substrates on the catalyst surface (e.g., H_2S and CO on Pt-based catalyst in hydrogenation reactions and H_2 dissociation in the anode of polymer electrolyte fuel cells, respectively); and (iv) fouling due to solids deposition caused by dusty materials in the feed [69].

Going back to the bimetallic Cu-Ni catalysts, Qing et al. [44] reported a Cu-Ni-Al spinel with Cu/Ni/Al molar ratio of 1/0.05/3 and calcined at 1000 °C that showed stable conversion of methanol during 300 h (Figure 4). Comparatively to the other materials prepared and tested by the authors, the lower particle size, higher specific surface area and pore volume, more hardly-reducible spinel and better sustained release catalytic performance (catalyst used without being previously reduced and active Cu sites gradually generated during the reaction) probably contributed to the enhanced stability of such catalyst.
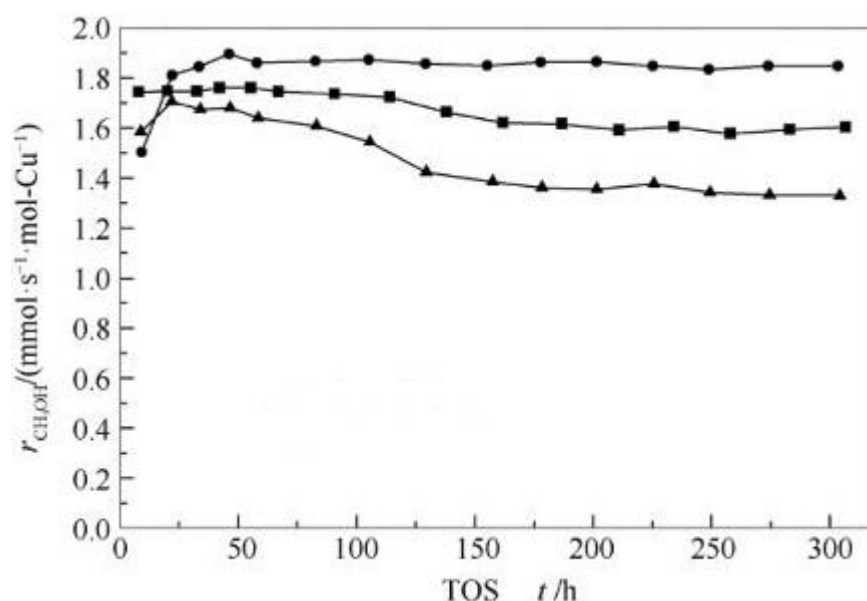
Figure 4. Methanol conversion rate as a function of time-on-stream (TOS) for the catalysts with Cu/Ni/Al molar ratio of 1/0.05/3 calcined at 900 °C (squares), 1000 °C (circles) and 1100 °C (triangles) at 255 °C, 1 bar and WHSV = 2.18 h^{-1}. Reprinted with permission from Ref. [44]. Copyright 2022 Elsevier.

In another work [48], a 30 wt.% Ni-Cu/ZrO$_2$ catalyst showed stable methanol conversion (above 90%) and H$_2$ production (selectivity remained around 60%) for 46 h on-stream at 400 °C, after which the H$_2$-TPR profile of the catalyst was unaffected. In fact, Lytkina et al. [57] tested several Cu-Ni catalysts supported on metal oxide-stabilized ZrO$_2$ supports doped with Y, La and Ce and all of them were reported to work for at least 90 h without visible deactivation (constant H$_2$ selectivity at 300 °C). As already mentioned, even though Cu can be easily deactivated, the presence of a group 8–10 metal, such as Ni, could be partially responsible for this long-term stabilization. In fact, it has been reported that the addition of a second metal improves, in general, the stability of steam reforming catalysts by promoting their hydrogenation activity [69,70] and decreasing the coke deposition [38,40,42,60].

Penkova et al. [60] observed that the simultaneous presence of Ni and Sn results in the formation of an alloy that enhances catalytic stability; this beneficial effect of tin was also corroborated elsewhere [41]. In terms of carbonaceous deposits formation, the addition of Sn resulted in a decrease compared to the monometallic Ni catalysts, indicating that the formation of the NiSn alloy inhibits the formation of NiC and, consequently, coke. It was also observed that the addition of Sn plays an important role in delaying the temperature range of particles agglomeration and, therefore, avoiding low temperature sintering. The authors also concluded that the addition of MgO to Al$_2$O$_3$ in the support results in lower coke formation [60]. In fact, after 20 h on-stream, the decrease of the catalytic activity was negligible. This behavior has been attributed to both a decrease in surface acidity of the Al$_2$O$_3$ support (confirmed from FTIR of adsorbed pyridine) and an improvement of Ni dispersion caused by the formation of MgAl$_2$O$_4$ spinel, which inhibits the incorporation of Ni in the Al$_2$O$_3$ phase. Consequently, the oxidation of carbonaceous deposits was facilitated. The only carbon deposits detected through temperature-programmed oxidation (TPO) were not very stable. A similar result was observed elsewhere [40] for a Ni catalyst supported on MgO. The authors attributed the stable behavior (20 h) of the catalyst to its capacity to mitigate the agglomeration of Ni particles and to the high basicity of the MgO support. The last enhanced the adsorption of CO$_2$ and, consequently, promoted the gasification reaction between CO$_2$ and carbon, as previously discussed.

Concerning bimetallic samples of Ni-Cu, in a recent work by Liu et al. [71] it was observed that the Ni-Cu/Al$_2$O$_3$ materials with higher Al content present higher initial catalytic activity, however, show a quick catalyst deactivation, while the catalysts with less Al content show better catalytic stability. The deactivation of the samples was related to the non-spinel CuO particles that are easier to agglomerate and sinter as compared to that from spinel Cu^{2+} species. In this way, the catalysts with more non-spinel CuO show a high initial catalytic activity but a higher deactivation rate.

A comparison between several metals supported on MCM-41 showed that the Ni-based catalyst was less stable than, for instance, the Cu-based catalyst [37]. Such deactivation of the Ni-based catalyst was attributed to the formation of carbonaceous deposits, thermal sintering and changes in the support structure. It is suggested that the metal particles in MCM-41 behave as bulk materials, thus having little metal-support interactions. This could be one of the reasons why, contrarily to what would be expected, the Ni-based catalyst was less stable than the Cu-based one.

LDHs present good catalytic stability during MSR [64,65]. In both works, the Ni/Al LDHs demonstrated stable MSR activity for approximately 100 h. When the LDH was pre-treated with a diluted H$_2$ stream [64], stable H$_2$ production with low levels of CO and no CH$_4$ occurred. On the other hand, when the catalyst was pre-treated on the reactive stream, it deactivated over time-on-stream with increasing CO formation. The reason for such difference will be further explored in the next section. Besides enhancing the catalytic activity, as already discussed, the addition of K to LDHs also promotes catalytic stability [65]. A K-promoted Ni/Al LDH showed similar stability at 390 °C to that of a commercial Cu catalyst (42 wt.% CuO, 47 wt.% ZnO, and 10 wt.% Al$_2$O$_3$).

2.2.3. Effect of the Preparation Method

The preparation method used is also a very important parameter to be considered. The same catalyst formulation prepared through different methods might result in very different performances and costs. The impregnation method is among the most reported for the preparation of heterogeneous catalysts mainly due to its simple execution and low waste streams [72]. From the works already discussed above, a considerable part of them reported the use of such method [38,40,41,43,45,47–49,53,57,60,61], being that both wet impregnation and incipient wetness impregnation were reported. Furthermore, in the case of the bimetallic catalysts, both co-impregnation and sequential impregnation were used.

A comparison between co-impregnation and sequential impregnation, used for the preparation of bimetallic Ni and Cu over CeO$_2$ catalysts, has been established [73]. The authors observed that the bimetallic catalyst prepared through co-impregnation (Cu-Ni) presented higher methanol conversion and H$_2$ selectivity during oxidative MSR than the homologous catalyst formulation prepared via sequential impregnation (Ni/Cu and Cu/Ni). However, in a different work [74], the Ni and Cu over ZrO$_2$ catalysts prepared by sequential impregnation showed higher oxidative MSR activity than the corresponding co-impregnated material. Fukui's theory [75] indicates that higher reactivity occurs when the system's gap-energy is low and its total energy is high. In other words, higher reactivity corresponds to an easier adsorption or desorption of a molecule for a specific reaction. The molecular simulations carried out by López et al. [74] show that the sequentially impregnated materials on ZrO$_2$ showed lower gap-energy and higher total energy (lower adsorption energy) than the co-impregnated catalyst (Figure 5), thus suggesting that an electron transfer mechanism is benefited at the interface between the support and the bimetallic structures in the first material. This ultimately enhances the redox properties of the catalyst and, consequently, its activity. Furthermore, the observed presence of bimetallic Cu-Ni and core-shell Ni/Cu nanoparticles and crystalline anisotropy of the active phase could have influenced the results greatly. These results show once again that MSR activity is sensitive to the catalyst structure, which on its hand depends on how the bimetallic active phase is impregnated. The opposite behaviors observed in both works could

be due to the different supports, having once again in mind the importance of the active phase-support interface in MSR activity.
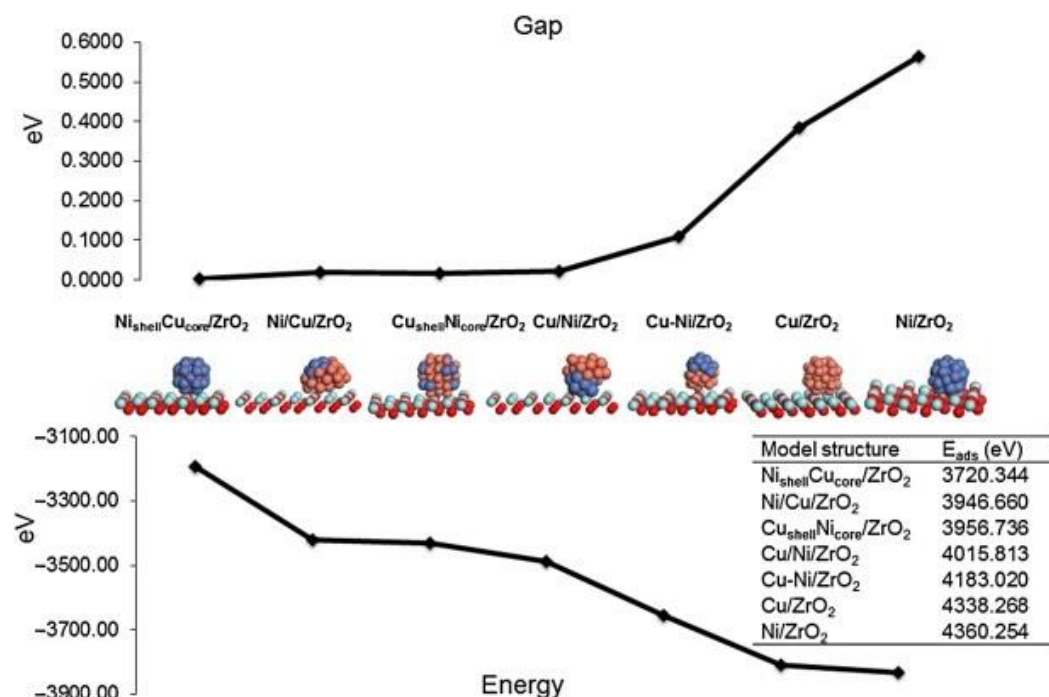

Figure 5. Molecular models of bimetallic and monometallic clusters: the top graph shows the gap-energy, the bottom graph shows the system total energy and the inset shows the adsorption energy of methanol on the surface. Reprinted with permission from Ref. [74]. Copyright 2022 Elsevier.

The precipitation or co-precipitation methods have also been applied to prepare some of the catalysts discussed in this section [40,53,57]. Luo et al. [40] prepared three nano Ni_xMg_yO solid solutions through different methods: (1) incipient wetness impregnation of Ni onto the MgO support prepared via precipitation method; (2) the same method with an added hydrothermal treatment of the support at 100 °C for 24 h after precipitation; (3) co-precipitation of both Mg and Ni salts with the same hydrothermal treatment used in the previous method. Among the three catalysts, the one prepared through the second method showed a superior capacity to convert methanol and produce H_2. By comparing methods (2) and (3), the differences are that while in method (2) Ni was incorporated in the treated support via incipient wetness impregnation, in method (3) Ni was introduced in the catalyst simultaneously with Mg through co-precipitation and went through the same treatment as the support (not Ni) in method (2). Therefore, the lower performance of the catalyst prepared through method (3) is probably associated with these two methodological modifications. TPR analysis showed that the catalyst prepared via method (3) was less reducible than the one prepared through method (2). H_2-TPD results indicated that most Ni species dissolved deeply inside the MgO matrix, being only a minority amount at the subsurface to catalyze the MSR reaction. Furthermore, co-precipitation methods normally involve several washing steps after precipitation, aiming to remove residual nitrates, potassium, sodium and other compounds. This allows avoiding sintering and agglomeration of particles during thermal treatment (higher resistance to sintering was observed for the catalyst prepared through method (3)). Consequently, significant undesired streams contaminated with nitrates are produced. Alternatively, chloride or sulfate-based precursors could be used if they did not poison methanol catalysts. Formate precursors have been researched as possible alternatives that could overcome these limitations [72].

Other methods such as the sol-gel [39,48,50] and polyol method [41,50] have also been used to prepare Ni-based MSR catalysts. The sol-gel method allows the attainment of

good chemical homogeneity, stoichiometry, phase purity, narrow particle size distribution, ultrafine powder and high specific surface area due to molecular and atomic scale mixing and networking of chemical components [76,77]. Regarding the works that used the sol-gel method, none of them established a comparison with other methods. A comparison has, however, been established between Ni/SiO_2 catalysts prepared via wet impregnation and the simple sol-gel method in ethanol steam reforming (ESR) [78]. The catalyst prepared via sol-gel presented good dispersion and considerably higher BET surface area than the catalysts prepared through impregnation. Furthermore, the first produced about twice the amount of H_2 produced by the last. This last result depends not only on the catalyst, but also on the reaction that it catalyzes. In other words, the fact that the sol-gel-prepared catalysts performed better than the catalysts prepared through impregnation in ESR does not guarantee that the same behavior would be observed in MSR. Furthermore, the sol-gel process presents disadvantages such as the high costs of some necessary chemicals and the often large volume shrinkage and cracking due to washing and drying steps mainly [79].

Bobadilla et al. [41] correlated the influence of the synthesis method used to prepare Ni and Ni-Sn supported on CeO_2-MgO-Al_2O_3 with their respective catalytic behavior in MSR. More specifically, the authors established a comparison between the catalysts prepared via deposition of nanoparticles obtained by the polyol method and catalysts prepared through impregnation. The nanoparticles produced via the polyol method presented better activity than the impregnated catalysts, especially the monometallic Ni catalysts. The authors proposed a model of the catalyst surface and phase distribution before and after reduction for the monometallic catalysts prepared through both methods (Figure 6).
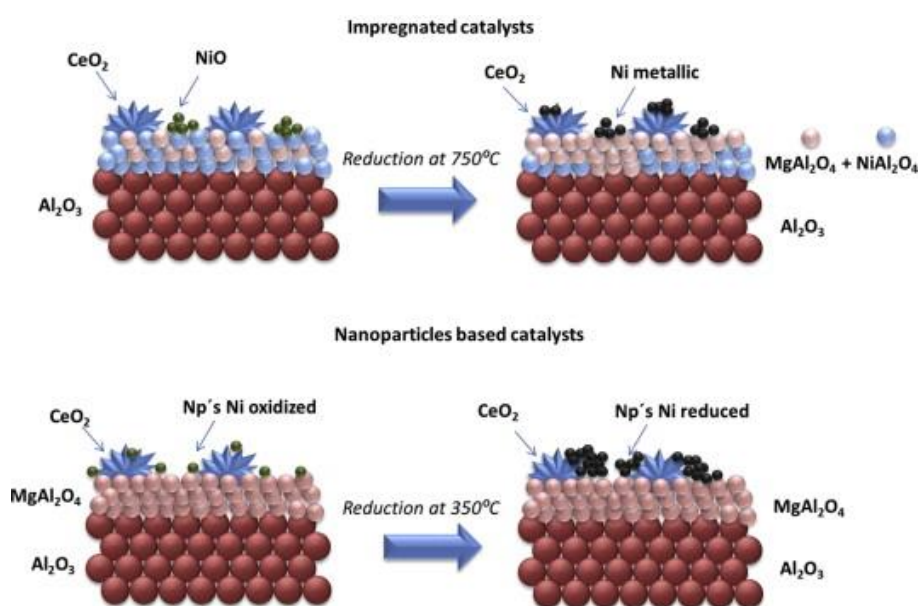
Figure 6. Model of the catalyst surface and phase distribution before and after reduction for the monometallic catalysts prepared through the impregnation method (**above**) and polyol method (**below**). (Np's: Nanoparticles). Reprinted with permission from Ref. [41]. Copyright 2022 Elsevier.

The impregnation method seems to be as good as the polyol method to produce Ni nanoparticles. Even though the catalyst prepared via impregnation required a higher reduction temperature, it also presented higher metal-support interaction and a lower degree of nanoparticles sintering. The monometallic catalyst prepared via impregnation showed CeO_2 fluorite phase and both $MgAl_2O_4$ spinel and $NiAl_2O_4$ spinel, while for the nanoparticles-based catalyst (polyol method) only the CeO_2 fluorite and $MgAl_2O_4$ spinel

structures were observed. The NiAl$_2$O$_4$ spinel in the impregnated sample was transformed into metallic Ni during reduction.

The polyol method was, on the other hand, considered by the authors as the preferable method for the preparation of the bimetallic Ni-Sn catalyst due to its control of composition and the enhanced resistance to sintering and reducibility that it confers to the catalyst. Therefore, polyol method being a better alternative than, for example, impregnation depends significantly on the catalyst being prepared. It has been concluded elsewhere [80] that due to the variety of shapes, compositions and nanostructures that can be produced, significant research has still to be carried out for a better comprehension of the polyol method.

Besides the preparation method, some parameters that are transversal to several methods can also have a significant impact on the catalyst activity and stability. Both drying and calcination conditions are known to be crucial parameters that have to be carefully selected. Going back to the work of Luo et al. [40], the authors observed that the addition of a hydrothermal treatment of the support at 100 °C for 24 h after precipitation increased the methanol conversion from 55.3% to 97.4% and the H$_2$ yield from 30% up to 58.5% at 600 °C, after 20 h on-stream. This enhancement was attributed to the higher reducibility of the catalysts subjected to the hydrothermal treatment. The catalysts hydrothermally treated also showed superior stability, which was ascribed to their higher surface basicity.

In another work [44] the authors observed that increasing the calcination temperature of Cu-Ni-Al spinel catalysts in the temperature range of 900–1100 °C increased the content of spinel. On the other hand, it also increased the spinel's particle size (sintering) and, consequently, led to a decrease in the specific surface area. Ultimately, the catalysts calcined at 1000 °C presented better catalytic activity and stability (Figure 4). Analysis of the used catalysts showed that the catalysts calcined at 1000 °C presented the smallest size of copper species, which took part in the catalysis of the reaction, in line with the catalytic activity results.

Reduction conditions are also of crucial significance in terms of catalytic performance [46,50]. It has been observed that reduction under H$_2$ atmosphere at 400 °C or 500 °C yielded different results [46]. More H$_2$ and CO$_2$ and less CO were produced over the catalyst reduced at 400 °C compared to the one reduced at 500 °C. Reducing the catalyst at 500 °C resulted in the reduction of Fe from Fe$_3$O$_4$, which subsequently reacted with the Ni particles, thus resulting in the formation of a Fe-Ni alloy. It is possible that this alloy covered the pores on the surfaces and lowered the surface area. This benefited the selectivity towards CO at the expense of H$_2$. In another work [50], besides analyzing the effect of reduction temperature (140, 160 and 180 °C), the authors also analyzed the effect of pretreatment atmosphere (4 h under Ar or 4 h under Ar and then 2 h under H$_2$ atmosphere) on the MSR activity of Ni-Cu/CaO-SiO$_2$ prepared via polyol method. Reduction at 160 °C under Ar atmosphere resulted in the highest H$_2$ yield due to, mainly, the higher dispersion of metal on the support. While increasing the reduction temperature from 160 to 180 °C produced larger Ni and Cu particles on the support and, consequently, poorer dispersion, reduction under H$_2$ atmosphere, after treatment under Ar atmosphere, led to metal particles agglomeration [81].

The preparation of LDHs is normally carried out via co-precipitation [62–65], and the addition of promoters such as Na or K normally occurs through impregnation [65]. It has been extensively reported that both calcination temperature and pretreatment conditions are decisive regarding LDHs' activity. The results obtained by Qi et al. [63] show that while calcination at 250 °C allowed attaining full methanol conversion only at 380 °C over a NiAl-LDH, calcination at 330 °C and 500 °C resulted in a progressive dislocation of the full conversion temperature towards lower values, with the LDH calcined at 500 °C achieving total conversion at 360 °C. The catalytic performance of the LDH was not only influenced by the pretreatment temperature [63], but also by the pre-treatment atmos-

phere [64]. While pretreating the LDH under diluted H_2 resulted in high activity and stability, pre-treating it under a reactive stream resulted in higher deactivation, lower H_2 generation and more CO [64].

2.3. Summary

A summary of the MSR catalysts reviewed in this section that showed the most promising results is presented in Table 1. It can be observed that from the list of the 10 most promising catalysts, half of them are bimetallic Ni-and Cu-based materials. All such 5 catalysts showed methanol conversions of at least around 90%, as well as relatively high H_2 yields and selectivities. As already discussed, the catalysts with higher Cu content and lower amounts of Ni tend to be more selective toward H_2 and CO_2 in detriment of CO; almost no CO was produced over $Ni_{0.2}$-$Cu_{0.8}$/ZrO_2 [53]. On the other hand, Ni normally catalyzes mostly the methanol decomposition reaction, thus enhancing methanol conversion. Furthermore, $Ni_{0.2}$-$Cu_{0.8}$/$Ce_{0.1}Zr_{0.9}O_2$-catalyst showed quite promising stable operation [57]. This shows how attractive bimetallic Ni-Cu-based catalysts are for MSR. Moreover, the impregnation method appears to be a critical issue. Finally, the annealing and reduction procedures adopted in both works were carried out at temperatures very similar to those employed during the MSR reaction.

The bimetallic 10 wt.% Ni-10 wt.% La/Al_2O_3 catalyst also showed promising results, not only in terms of methanol conversion and H_2 production but also regarding its low CO generation [61]. The same cannot be said about the monometallic Ni catalyst reported by Deshmane et al. [36], which showed high CO selectivity despite the high conversion of methanol and selectivity towards H_2. Even though the catalyst consisting of nickel nanoparticles supported on CeO_2-MgO-Al_2O_3 mixed oxide [41] showed performance parameters above the average of the catalysts reviewed, it is below all of the others shown in Table 1. More research must be conducted regarding the polyol method. As for the LDH-based materials [64,65], they allowed reaching high conversions of methanol and yields of H_2, while showing promisingly stable operation. However, some CO production was observed in both cases. Nevertheless, it has been highlighted in this review that slight changes in the formulation of the LDHs could reduce this problem. However, the drawbacks of the precipitation method (mentioned in more detail in the previous section), namely the undesired streams resulting from washing, must be considered. If such drawbacks are solved, LDH-based materials might be interesting for the MSR. Finally, considering the emergence of CO_2 sorption-enhanced reactor concepts and the so extensively reported ability of LDHs to capture CO_2 at high temperatures (300–500 °C) [82–84], these materials have great potential to be used as hybrid sorbent-catalyst (so called DFM, or dual function materials).

Finally, along this section, it was observed that the most crucial catalyst properties to achieve high catalytic performance for the MSR process are the metal dispersion and the surface area of the material. In this way, to reach high methanol conversion, high H_2 yield and low sub-products production, it is necessary to prepare a catalyst with a high surface area (for instance, using a porous support with a high pore volume) and with a strong interaction between the active phase and the support.

Taking into account the results presented in Section 2.2 (and the main outputs summarized in Table 1), to achieve high methanol conversion and high H_2 production in long-term MSR experiments, it is suggested the utilization of a bimetallic Ni-Cu catalyst (for instance, prepared by impregnation) promoted with (or supported on) ZrO_2/CeO_2.

Table 1. Comparison of some of the most promising MSR catalysts reviewed in this section.

Catalyst	Temperature	Feed Flow Rate	Mass of Catalyst	S/C [a]	Conversion of Methanol	H$_2$ Yield/Selectivity	Stability	Preparation Method	Refs.
5 wt% Ni-5 wt% Cu/Al$_2$O$_3$	325 °C	0.06 mL·min^{-1}	3 g	1.7	98.5%	2.2 [b]/n.d.	Result after 3 h	Impregnation	[43]
10.8 wt% Ni-Cu/TiO$_2$/Monolith	300 °C	1.8 h^{-1} [c]	n.d.	2	92.6%	n.d./92.7% [g]	n.d.	Impregnation	[49]
Ni/Cu/ZnO/Al$_2$O$_3$ (22.5/22.5/45/10) [d]	350 °C	150,000 mL·g^{-1}·h^{-1}	0.031 g	1	100%	≈83.3% [f]/n.d.	n.d.	Coating and impregnation	[52]
Ni$_{0.2}$-Cu$_{0.8}$/ZrO$_2$ (Metals/Carrier = 0.2/1)	325 °C	n.d.	0.3 g	1	≈100%	≈66.7% [f]/n.d.	n.d.	Sequential impregnation over support prepared via precipitation	[53]
Ni$_{0.2}$-Cu$_{0.8}$/Ce$_{0.1}$Zr$_{0.9}$O$_2$ (Metals/Carrier = 0.2/1)	350 °C	172 h^{-1} [e]	0.3 g	1	≈86%	n.d./ ≈ 99.9% [g]	90 h without deactivation	Sequential impregnation over support prepared via co-precipitation	[57]
10 wt% Ni-10 wt% La/Al$_2$O$_3$	350 °C	0.02 mL·min^{-1} 10,920 h^{-1} [e]	0.2 g	3	100%	n.d./ ≈ 69% [g]	n.d.	Co-incipient wetness impregnation	[61]

10 wt% Ni/TiO$_2$	350 °C	2838 h^{-1} [e]	n.d.	3	≈86%	n.d./ ≈ 97% [g]	n.d.	Facile one-step synthesis	[36]
10 wt% Ni nanoparticles/15 wt% CeO$_2$-10 wt% MgO-Al$_2$O$_3$	350 °C	8000 mL·g^{-1}·h^{-1}	n.d.	2	≈ 66%	66.7%/n.d.	Result after 24 h (no significant deactivation)	Polyol and support via co-impregnation	[41]
NiAl-LDH (Ni/Al = 4.9)	390 °C	0.05 mL·min^{-1}	0.15 g	1	94.6%	70% [f]/n.d.	Result after 100 h (no significant deactivation)	Co-precipitation	[64]
3wt% K/Ni$_{0.78}$Al$_{0.16}$(OH)$_2$(CO$_3$)$_{0.15}$·0.66H$_2$O	390 °C	0.05 mL·min^{-1}	0.15 g	1.2	91%	80% [f]/n.d.	Result after 60 h (no significant deactivation)	Co-precipitation	[65]
(30 wt% Ni)-Cu/Al$_2$O$_4$	300 °C	1 mL·min^{-1}	30 g	1.5	≈100%	98% [f]/n.d.	Result after 30 h (no significant deactivation)	Impregnation	[58]

[a] Steam to carbon molar feed ratio. [b] $mol_{H_2} \cdot mol_{methanol,in}^{-1}$. [c] Weight hourly space velocity (mass flow rate of feed/total catalysts weight). [d] Molar ratio. [e] Entering volume flow rate/volume of catalytic layer. [f] Relative to the maximum of 3 $mol_{H_2} \cdot mol_{methanol,converted}^{-1}$. [g] Selectivity (%) = $\frac{H_2}{\sum F_i} \times 100$. n.d.—Not determined.
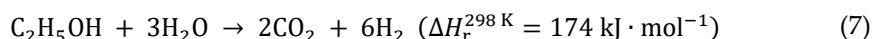
3. Ethanol Steam Reforming

3.1. Introduction

Renewable ethanol can be produced from several feedstocks, as indicated in Table 2. The production of bio-ethanol from algae, even though possible, is still in an early stage of development [85]. The conversion of the different types of biomass into ethanol varies significantly, mainly in terms of the attainment of sugar solutions. While sugar sources only need an extraction process to attain fermentable sugars, starch sources demand previous hydrolysis to convert starch into glucose. Finally, for lignocellulosic biomass, a pre-treatment is required before hydrolysis so that the cellulose structures are modified for enzyme accessibility [85].

**Table 2.** Sources of bio-ethanol [85].

Category	Biomass
Sugar sources	Sugarcane
	Sugar beet
	Sweet sorghum
	Cane
	Molasses
	Beet molasses
	Grape
	Dates
	Watermelon
	Apple
Starch sources	Corn
	Wheat
	Cassava
	Barley
	Canna
	Sorghum grain
	Potato
	Sweet potato
	Yam
	Jerusalem artichoke
	Iles-iles
	Oat
	Banana
Lignocellulosic biomass	Perennial grasses
	Aquatic plants
	Softwood
	Hard wood
	Sawdust
	Pruning
	Bark thinning residues
	Cereal straws
	Stovers
	Bagasse
	Organic municipal solid wastes

Ethanol is highly available, easy to handle, transport and store and is less toxic than methanol [15,20]. Furthermore, it has higher hydrogen content than methanol (six hydrogen atoms instead of four). These are some of the reasons why it has been extensively investigated for hydrogen production through ethanol steam reforming (ESR). The ESR can be described by the overall reaction shown in Equation (7).

$$C_2H_5OH + 3H_2O \rightarrow 2CO_2 + 6H_2 \; (\Delta H_r^{298\,K} = 174 \; kJ \cdot mol^{-1}) \tag{7}$$

This reaction is considerably more endothermic than MSR and for that reason temperatures around 400–600 °C are often adopted, which are still below those typically used in steam reforming of methane.

Contrarily to MSR, the ESR overall reaction is irreversible since at least one of the reaction steps that ultimately and ideally leads to its conversion into 6 moles of H_2 is irreversible. Regarding the reaction pathways involved in ESR, a consensus has not been reached due to the influence of reaction conditions and a considerable variety of catalysts. Still, there has been some agreement towards the reaction network depicted in Figure 7 [17,19,86].
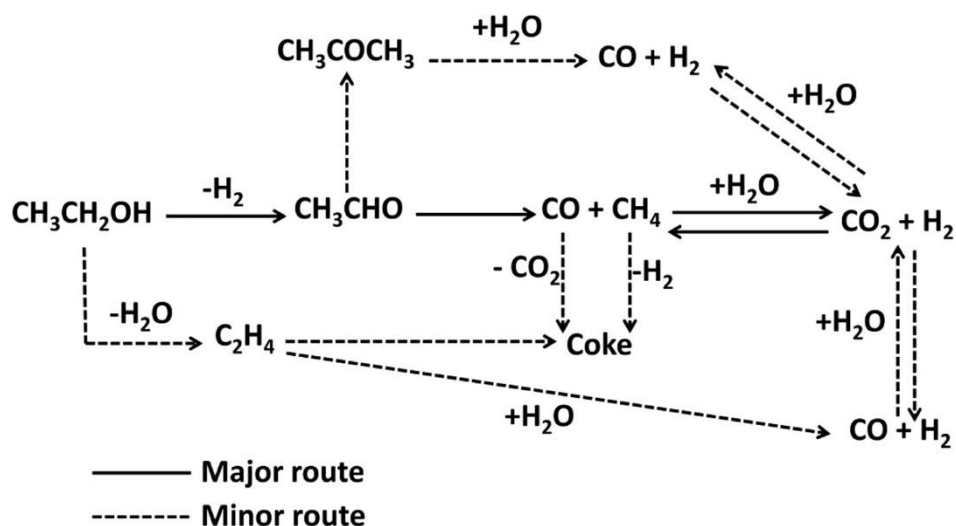
Figure 7. Reaction network proposed for ESR. Reprinted with permission from Ref. [17]. Copyright 2022 Elsevier.

The reactions that have been considered as major and minor routes are presented by order in Table 3. The final major step is the WGS reaction (Equation (3)). Depending on the catalyst that is used, major routes might become minor and vice-versa. Therefore, H_2 production and coke formation in ESR are highly dependent on the catalysts used. Moreover, minimizing CO production is once again crucial if the H_2 that is produced is directed to a polymer electrolyte fuel cell. This will also depend significantly on the choice of an appropriate catalyst. In fact, due to the higher number of possible alternative routes, this choice might be even more crucial here than it was for MSR.

Table 3. Reaction routes considered for the ESR in Figure 7.

Type	Reaction	$\Delta H_r^{298\,K}$ $(kJ \cdot mol^{-1})$	Eq. Number
Major	$C_2H_5OH \rightarrow CH_3CHO + H_2$ (ethanol dehydrogenation to acetaldehyde)	68	(8)
	$CH_3CHO \rightarrow CH_4 + CO$ (acetaldehyde decomposition)	-	(9)
	$CH_4 + H_2O \rightleftharpoons CO + 3H_2$ (methane steam reforming; the reverse of Equation (4))	206	(10)

|			
	$C_2H_5OH \rightarrow C_2H_4 + H_2O$ (ethanol dehydration to ethylene)	45	(11)
	$C_2H_4 \rightarrow C$ (ethylene polymerization to coke)	-	(12)
Minor	$2CH_3CHO \rightarrow C_3H_6O + CO + H_2$ (acetaldehyde condensation into acetone and subsequent decarboxylation)	-	(13)
	$2CO \rightleftharpoons CO_2 + C$ (Boudouard reaction)	−172	(14)
	$CO + H_2 \rightleftharpoons H_2O + C$ (reduction of carbon monoxide)	−131	(15)
	$CH_4 \rightleftharpoons 2H_2 + C$ (methane cracking)	75	(16)

3.2. Catalysts

On contrary to the MSR, ESR requires catalysts that are active in C-C bond cleavage. Hou et al. [17] observed that Rh-based catalysts are the most active in breaking such bonds. On the other hand, and as already mentioned, nickel-based catalysts are normally cheaper and, therefore, might constitute a potential alternative. Furthermore, these Ni-based materials normally also show good C-C bond breaking activity and are very active in CH_4 reforming (they are used industrially for this reaction). However, challenges related to coke formation and sintering have been identified [17]. In this section, a review of the latest Ni-based catalysts reported in the literature is carried out and a thorough analysis of the best strategies to improve their catalytic activity, selectivity and stability are conducted.

3.2.1. Catalytic Activity and H_2 Selectivity

Once again, the nature of the support that is used is vital for the catalytic activity in ESR and selectivity towards H_2 production in detriment of secondary products such as intermediate liquids, CO, CH_4, and coke. Aiming to better understand this, Dan et al. [87] compared the catalytic performance of monometallic Ni catalysts supported on Al_2O_3 and ZrO_2 and analyzed the effect of modifying both supports with CeO_2 and La_2O_3. The Al_2O_3-supported catalyst presented better catalytic activity than the ZrO_2-supported one. The authors reported that this difference could be mainly due to the higher number of active sites, resulting from the higher surface area, higher Ni dispersion and smaller nanoparticle size. In terms of ethanol conversion, while the addition of both CeO_2 and La_2O_3 to ZrO_2 led to significant improvements, for Al_2O_3 only the modification with La_2O_3 improved the conversion. The authors claim that since these modifications do not improve the intrinsic catalytic activity of the Ni sites (based on turnover frequency calculations), the improved results could be due to the participation of the support in the catalysis of ESR and/or due to the higher amount of Ni active sites available. In terms of H_2 production, while the modifications of the Al_2O_3 support did not result in significant improvements, the addition of Ce and especially La to the ZrO_2 support improved the H_2 yield considerably. Besides the mentioned enhancement of Ni dispersion, La_2O_3 is also known to increase the basicity of the modified catalysts [88]. As for CeO_2, it enhances (besides the Ni dispersion) the reducibility of Ni [89] and the capacity of the support to adsorb water [90]. It has been reported for a bimetallic Ni-Cu catalyst that the reduction ability of CeO_2 promoted the intermediate formation of acetone [91]. Overall, the catalyst supported on La_2O_3-modified ZrO_2 provided the best results with total ethanol conversion and H_2 yield of approximately 60% at 350 °C [87].

As already observed for MSR, the number of modifying agents is also very important. Even though modifying the Al_2O_3 support with La resulted in a slight increment in terms of both ethanol conversion and H_2 production [87], it has been observed in other work [92]

that the addition of La_2O_3 to the support could be either beneficial or detrimental depending on the La/Al molar ratio. In this last work, while La/Al ratios in the range of 0.05–0.15 improved the production of H_2 compared to the non-modified catalyst, a La/Al molar ratio of 0.2 was detrimental. Such behavior could be explained by the two opposite trends observed in Figure 8: the Ni surface area and ethanol adsorption capacity. Even though the catalyst with a La/Al ratio of 0.20 presented the highest Ni surface area, it also showed the lowest ethanol adsorption capacity. Although the basicity of La is known to be beneficial to counterbalance the acidity of Al_2O_3, as it reduces the formation of ethylene, too much basicity will negatively affect the dehydrogenation of ethanol [93], thus decreasing H_2 production. For this reason, this catalyst showed not only the lowest H_2 yield, but was also the only catalyst to be unable to fully convert ethanol. The catalyst with a La/Al molar ratio of 0.1 showed the best catalytic performance.
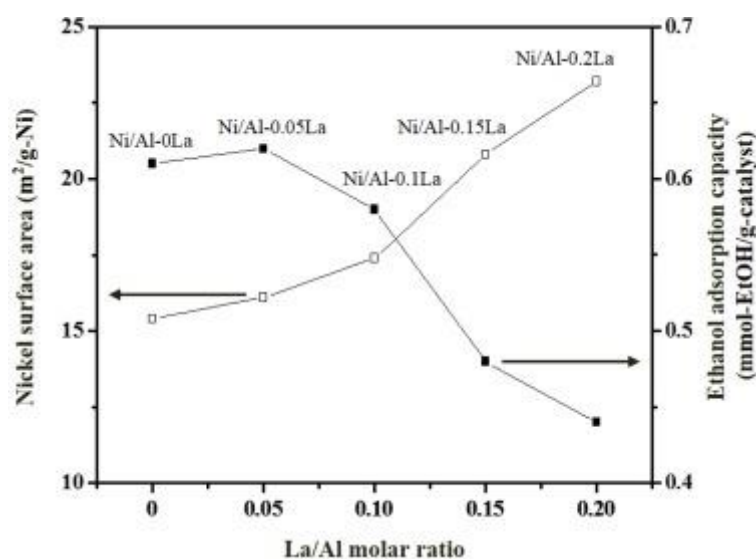
Figure 8. Nickel surface area and ethanol adsorption capacity as a function of the La/Al molar ratio in Ni/xLa$_2$O$_3$-Al$_2$O$_3$ (x = 0, 0.5, 0.1, 0.15 and 0.2) catalysts. Reprinted with permission from Ref. [92]. Copyright 2022 Elsevier.

Trane-Restrup et al. [90] compared the performance of monometallic Ni supported on CeO_2, $MgAl_2O_4$, $Ce_{0.6}Zr_{0.4}O_2$, and $CeZrO_4/MgAl_2O_4$. The catalysts based on the last two supports presented higher catalytic activity, most probably due to their higher water dissociation capacity [94,95]. This would allow higher surface concentrations of OH-species, which would react with carbon species to form H_2 and carbon oxides [90]. It has been proposed that reactions with lattice oxygen on these kinds of supports could also contribute to the enhanced activity of the Ni catalysts over these supports [96]. The particle size of Ni obtained over the different supports could not be responsible for the results obtained as the $Ce_{0.6}Zr_{0.4}O_2$, with the largest Ni particles, presented the highest conversion [90].

Prasongthum et al. [97] prepared a Ni-based catalyst supported on graphene (Ni/CNT-SF) with total ethanol conversion at 300–550 °C. The authors reported that the utilization of this support enhanced the performance of the catalyst due to the tubular structure of the graphene.

In a different work, the effect of modifying Al_2O_3 support with ZnO was analyzed [98]. While for both Ni/Al_2O_3 and Ni/$ZnAl_2O_4$ small amounts of acetaldehyde and ethylene were formed, indicating the occurrence of both ethanol dehydrogenation and dehydration, over the Ni/ZnO-Al_2O_3 only H_2, CO and CO_2 and a small amount of CH_4 were observed. This latter case could be a result of the formation of a NiZn alloy with different compositions (NiZn and Ni_4Zn) on this catalyst, while on the other two catalysts only metallic Ni was present.

The modification of TiO_2 support with montmorillonite (MMT) was also evaluated [99] and an enhancement in the performance during ESR was observed. This modification improved the crystal growth control and produced anatase phase of delaminated MMT/TiO_2 nanocomposite. Also, the formation of a Ni-MMT phase at the surface enhanced both Ni reducibility and dispersion, the last having amplified the ability of Ni to break C-C bonds. Elsewhere [100], it was concluded that organically modifying MMT with cetyltrimethylammonium bromide resulted in higher surface area and pore volume and higher Ni dispersion combined with smaller metal particles.

Musso et al. [101] prepared several Ni-based catalysts supported on La and Y via the sol-gel technique. Samples containing the Y element showed higher catalytic performance and lower production of sub-products. One of these materials (containing Y) also showed no catalyst deactivation even in a 50-h long-term experiment at 650 °C. The higher catalytic performance of this material could be related to its structural properties (namely the higher number of oxygen vacancies and better metal-support interaction). Besides that, several Ni-based catalysts supported on ceria with different Ni loadings (10, 13, and 15 wt.%) were prepared by Niazi et al. [102] for the ESR process. The results showed that the Ni content has a positive impact on the catalytic activity of the catalysts (due to the higher number of active sites available). It was verified that, in a general way, the H_2 and CO yields increased with the temperature using all of the prepared materials. In opposition, the production of CH_4 and CO_2 decreased as the temperature increased.

Two works [103,104] have reported monometallic Ni supported on zeolites with considerable ESR activity. In the first case [103], a comparison between hierarchical and non-hierarchical beta zeolite supported catalysts showed that the first presented superior ethanol conversions and H_2 yields over time. Such superiority of the hierarchical beta zeolite is probably associated with the presence of intra-crystalline mesoporous channels, which confine the well dispersed Ni particles, thus improving mass transfer efficiency. Moreover, catalysts having different loadings of Ni (5–15 wt.%) over the hierarchical beta zeolite were tested under the ESR process, being that a loading of 15 wt.% allowed the attainment of approximately complete ethanol conversion and almost 80% of H_2 yield. This was attributed to the strong metal-support interaction and high active Ni surface area. In the second work [104], Ni was impregnated on non-modified and dealuminated BEA zeolite. Even though Ni supported on dealuminated BEA zeolite showed initially lower H_2 selectivity than Ni supported on non-modified zeolite (full conversion in both cases), the second deactivated rapidly while the first maintained the initial H_2 production. Nevertheless, the first catalyst led to higher CO production, which could be a problem in the case of a fuel cell application. On the other hand, it produced less acetaldehyde for the most of the reaction time and significantly less ethylene, being the last species normally an indicator of coke formation.

The effect of different promoting agents on Ni-based catalysts in terms of ESR activity and H_2 selectivity has been widely researched and, in the last years, several interesting findings have been reported. Using Mg to promote Ni-based catalyst was analyzed by Chen et al. [105] and Song et al. [106], being that both report that Mg addition promotes ESR activity towards H_2 production. In the first work [105], the Mg promoter, added to a Ni supported over attapulgite clay catalyst, anchored the Ni species on the support surface, leading to highly dispersed metallic Ni, high metal surface area and the lowest crystal size, ultimately resulting in improved ethanol consumption comparatively to the unpromoted material. In fact, it was observed elsewhere that the increase in the active Ni surface area was accompanied by enhanced ethanol adsorption capacity [106]. Furthermore, modification with Mg also increased H_2 production, as it benefited dehydrogenation of ethanol to form acetaldehyde, and subsequently H_2, in detriment of ethanol dehydration to form ethylene. This is associated with the lowered acidity of the Mg promoted catalysts. The influence of the Mg loading was also analyzed [105], having been concluded that loading of 10 wt.% provided the highest catalytic activity with around 94% of ethanol conversion and H_2 yield of 85% at 500 °C. A Mg loading of 20 wt.%, however, presented

similar catalytic activity to the unpromoted catalyst at the same temperature This could be once again associated with the excess of basicity mentioned earlier [93].

A comparison of the Mg promoter with other metal promoters (Ba, Ca and Sr) [106] was also carried out. As can be inferred from Figure 9, all promoted catalysts presented higher H_2 production than the unpromoted material and in the following order: Sr > Mg > Ba > Ca. Furthermore, by establishing a relationship between the catalysts' H_2 yields and active Ni surface areas and ethanol adsorption capacities, the authors concluded that higher H_2 productions occurred over the catalysts with higher Ni surface areas and ethanol adsorption capacities, contrary to the study carried out by Song et al. [92]. In other words, the promotion of the Ni/Al_2O_3-ZrO_2 catalyst with Sr resulted in the highest increase in the surface area of the Ni active phase and ethanol adsorption capacity. The same authors analyzed elsewhere the impact of Sr loading over the same catalyst [107]. Different Sr loadings (0, 2, 4, 6, 8, and 10 wt.%) were used, having been observed that even though complete ethanol conversion was attained, regardless of the Sr loading, the highest H_2 yield was obtained over the catalyst with 6 wt.% of Sr, which presented the highest Ni surface area, lowest particle size, highest dispersion and highest ethanol adsorption capacity. It is also argued that an excess amount of Sr covered the catalyst surface, thus harming H_2 production.
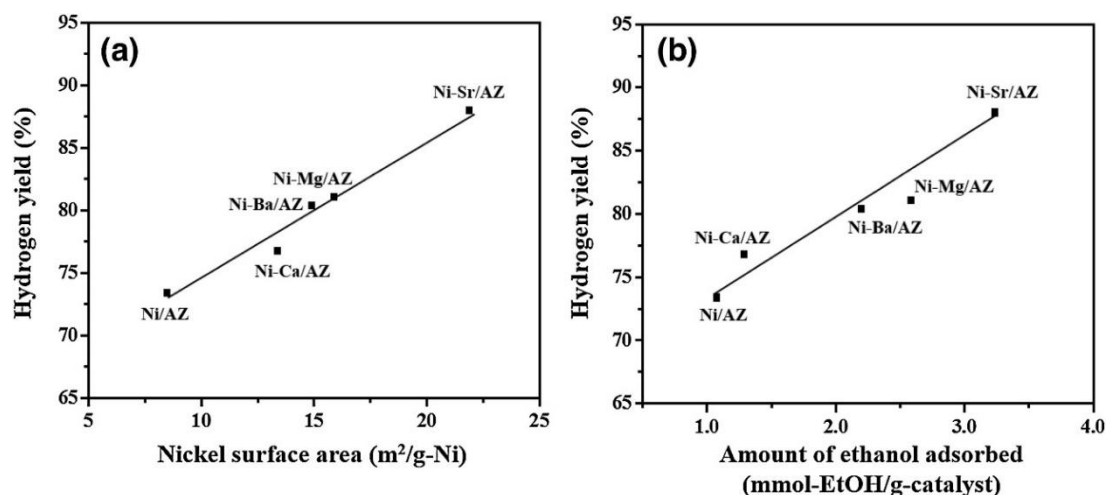
Figure 9. Relationship between the H_2 yield obtained over Ni-X/Al_2O_3-ZrO_2 (X = Ba, Ca, Mg and Sr) and their (**a**) nickel surface area and (**b**) ethanol adsorption capacity. Reprinted with permission from Ref. [106]. Copyright 2022 Elsevier.

A comparison between the promoting effect of K, CeO_2 and ZrO_2 has been established [90]. Enhancement of ethanol conversion was observed for all cases compared to the unpromoted $Ni/MgAl_2O_4$ catalyst, especially when simultaneous modification with K and CeO_2 was carried out. This enhancement in ethanol conversion could be attributed mainly to K modification, as the modification with only CeO_2 did not result in significant enhancement, contrary to what happened when modification with only K was carried out. On the other hand, CeO_2 had a significant role in inhibiting coke formation. Elsewhere [108] it was observed that Ce addition to a Ni/MMT catalyst increased both ethanol conversion and H_2 selectivity by 15% and 24%, respectively. While Ni is responsible for breaking the C-H and C-C bonds of ethanol, CeO_2, with its oxygen vacancies, activates H_2O to produce OH groups, which on their side can react with intermediate products to yield CO_2 and H_2. In fact, the authors observed that increasing the Ce content improved the CO_2/CO ratio, which confirms that CeO_2 benefited the WGS reaction. On the other hand, in a previous work [90], it was observed that when the promotion of the catalyst with $CeZrO_4$ was carried out, higher ethanol conversion was observed. In a different work [109], the addition of Zr to a bimetallic Ni-Co catalyst supported on ordered mesoporous carbon enhanced the ESR catalytic activity in terms of both ethanol conversion and H_2

yield. This was due to the lower crystal size, higher dispersion of the Ni-Co active phase and higher specific surface area of the promoted material.

As for the effect of Co addition, Nejat et al. [110] observed that Co addition benefited both ethanol conversion and H_2 production, regardless of the Co content in the range 1–9 wt.% (constant total metal loading of 10 wt.%). The Co-promoted catalysts showed lower CO and CH_4 production as well. Very similar results were attained elsewhere [111]. Even though neither of these works included a clear explanation of why promotion with Co resulted in enhanced ESR catalytic activity and H_2 selectivity, it has been reported that besides having the ability to break C-C bonds [112], Co also promotes the WGS reaction [113,114]. However, too much Co is detrimental to the desired ESR activity [110] and so a balance between Ni and Co contents is required. The 9 wt.% Ni-1 wt.% Co/MCM-41 catalyst converted 90% of ethanol and produced a H_2 yield of 80%, the best performance among the tested materials in this study [110].

Noble metals have also been combined with Ni aiming to optimize the catalytic activity in ESR towards H_2 production. Combining both Ni and Rh in the active phase has often been observed to be beneficial for ESR activity towards H_2 production [115–117]. The authors in [115] claim that the presence of Rh promotes dehydrogenation of ethanol to acetaldehyde in detriment of ethanol dehydration, as the presence of small quantities of aldehyde was observed for the bimetallic catalysts, but not for the Ni monometallic catalyst. On the other hand, the Rh-promoted catalysts showed higher CH_4 production than the monometallic Ni catalyst, probably due to the higher capacity of hydrogenation of CH_3 species (that were produced during C-C cleavage). However, at higher temperatures (above 500 °C) this trend changed, and the bimetallic catalyst started showing lower CH_4 generation than the monometallic Ni catalyst. This is in agreement with the common report that the promotion of Ni in the active phase with Rh enhances the steam reforming of CH_4 [115–117]. Elsewhere [116] the enhancing effect of Rh promotion was attributed to the easier reduction and smaller crystallite size of Ni on a bimetallic catalyst supported on CeO_2-ZrO_2. Le Valant et al. [117] compared the promoting effect of different metals on a Rh-based catalyst. It was observed that while promotion with Pt had no significant effect on the H_2 yield, both Pd and Ni increased it relatively to the unpromoted catalyst, especially Ni. Furthermore, the Rh-Ni bimetallic catalyst showed higher CO and lower CH_4 production, thus indicating the promotion of CH_4 reforming. Bimetallic catalysts in which Ni was combined with Pt [118,119] and Au [120] have also been studied in the ESR reaction. While significant amounts of acetaldehyde were observed over monometallic Ni catalyst supported on detonation nanodiamond, the same compound was not observed over the bimetallic Pt-Ni on the same support [118]. Furthermore, higher production of H_2 and CO was observed over the bimetallic catalyst than over the monometallic Ni catalyst. It is proposed that the bimetallic catalyst exhibits a synergistic effect and that it could be associated with the influence of both the electronic structure of the catalyst surface and to the sorption properties of the catalyst [119]. The addition of Au to the Ni/SBA-15 catalyst also enhanced the ESR activity [120]. This has been once again attributed to the improved dispersion of the NiO/Ni phase, which resulted in smaller particles, and strengthened NiO/Ni-support interaction. Promotion with B also enhanced ESR activity towards H_2 production due to the formation of a Ni-B alloy [86]. Finally, W was also found to improve catalytic activity due to a synergism between W and Ni and the enhanced steam reforming of methane activity by WO_x [121].

Similar to what was observed for the MSR process, LDH-derived materials containing Ni have been tested in ESR [122–125]. Romero et al. [122] analyzed the effect of changing the Mg content in a Ni-Mg-Al mixed oxide, having found that the Mg/Ni ratio of 0.33 allowed maximum H_2 production and minimum amounts of ethylene and acetaldehyde. On the other hand, more CO and lower ethanol conversion were obtained compared to the materials with a lower Mg/Ni ratio. Such dependence on the Mg/Ni ratio has been attributed to the fact that it influences the interaction of Ni^0 in the oxide matrix, thus also changing the nature of the active sites. In a different work [123] Ce was impregnated into

a Ni-Mg-Al LDH derived catalyst, having been determined that 10 wt.% of Ce allows the highest ethanol conversion. The catalysts with more than 10 wt.% of ceria showed lower ESR activity due to ceria particles aggregation, which probably blocked the active sites catalyzing the desired reactions. Elsewhere [125], the introduction of Cu in the LDH structure enhanced Ni reducibility on the derived mixed oxide. Furthermore, the presence of Cu enhanced the production of H_2, as it promoted WGS. A Mg-Al LDH-derived mixed oxide has also been used as support to combine the high basicity of MgO and high activity of Al_2O_3 [124]. Ni supported on this material was able to reach higher ethanol conversion and H_2 production than Ni supported on either MgO or Al_2O_3. Furthermore, Cu-Ni-Co over the same support yielded an even better catalytic performance as the presence of the three metals provided restricted formation of intermediate products and coke, thus leading to higher H_2 yields.

In a general way, the mechanism of the ESR process involves the dehydrogenation of ethanol to yield several intermediates such as ethylene and acetaldehyde [126,127]. These last species can either decompose to CH_4 and CO or transform into ethane and H_2O [127].

3.2.2. Deactivation

Even though there are several possible reasons for catalyst deactivation, coke formation and sintering are the most common ones in the ESR process, as seen previously for the MSR reaction. Regarding coke, there are more coke formation pathways that can happen during ESR than during MSR due to the more complex reaction network of the first (cf. Figure 7).

A comparison in terms of overtime stability has been established between catalysts consisting of Ni over different supports (Al_2O_3, ZrO_2, MgO and CeO_2) [124]. It was observed that while the MgO supported catalyst kept stable activity for several cycles, the other catalysts suffered from practically constant deactivation over cycles. In another work [87] it was observed that while Ni/Al_2O_3 maintained stable activity for 24 h on stream, Ni/ZrO_2 suffered from deactivation. The different stability results regarding Al_2O_3 supported monometallic Ni catalyst between both works [87,124] could be due to the different conditions employed, namely temperature and Water to Ethanol Feed Ratio (WEFR). As for the deactivation suffered by the ZrO_2 supported catalyst, it was related to the formation of large deposits of amorphous carbon, observed by TEM, which could have blocked the access to the active sites. The authors attributed such significant carbon deposition to the large Ni particles and the weak interaction between Ni and the ZrO_2 support [87]. The addition of both CeO_2 and La_2O_3 to the support induced a change in the nature of the formed carbon deposits to filamentous carbon, which, contrarily to amorphous carbon, does not normally envelop the Ni nanoparticles [128]. Therefore, despite the observed formation of coke, no significant blockage of the active sites access took place and so no substantial deactivation was observed after 24 h. Such enhancement in stability was probably a result of the change in the properties of the support's surface and better Ni dispersion. As for the Al_2O_3 supported catalyst and the corresponding catalyst similarly modified, no considerable changes were observed regarding the nature of the deposited carbon (filamentous). Elsewhere [129], Ni supported on CeO_2-MgO converted ethanol completely while showing H_2 selectivity of approximately 70% after 18 h time on stream. Such results are probably associated with the high oxygen storage capacity of the catalyst, which probably allowed the gasification of carbon deposits, thus avoiding deactivation. The presence of Ce in the support could have also promoted water dissociation into –OH and –O species, which would also contribute to coke gasification into CO, CO_2 and H_2 and, consequently, the high H_2 selectivity [130]. Tahir et al. [131] tested a Ni/MMT-TiO_2 catalyst for the steam reforming of ethanol being observed high catalytic performance at 500 °C. After the experimental tests it was determined a significant amount of carbon deposition (graphitic nature), but this had little effect on catalyst activity over the 20 h of the long-term test.

It has been observed by Song et al. [92] that adding too much La$_2$O$_3$ to Al$_2$O$_3$ can not only affect negatively the catalytic activity, as already discussed in the previous section but also the stability over time. The authors observed that the catalyst with the highest La/Al ratio of 0.20 started deactivating rapidly after 3 h on stream, contrary to what was observed for the other materials with lower La content. The reason for such behavior was not coke formation, since the amount of deposited coke (amorphous and filamentous) decreased with increasing La/Al ratio, as observed by TPO and TEM. The formation of La$_2$O$_2$CO$_3$ could have contributed to carbon removal from the catalyst surface [132,133]. Furthermore, the enhanced basicity of the La-rich catalyst could have also played an important role in inhibiting ethylene formation, a main coke precursor. On the other hand, an increase in the size of the Ni particles was observed for the catalyst with the highest La content. This suggests that sintering occurred and could have been the main reason for the observed deactivation. Re-oxidation of metallic Ni did not occur.

In a different work [98] in which a WEFR of only 3 was used, a Ni/Al$_2$O$_3$ catalyst showed deactivation once again. However, it was observed that promoting Al$_2$O$_3$ with ZnO at a Zn/Al ratio of 2 resulted in stable ESR activity for 28 h on stream at 500 °C, probably due to coke formation inhibition, as shown by thermogravimetric analysis and scanning electron microscopy analysis. The calcined Ni/ZnO-Al$_2$O$_3$ precursor is mainly composed of NiO/ZnO crystalline phases dispersed over amorphous Al$_2$O$_3$, which is transformed into a metallic phase over ZnAl$_2$O$_4$ support during reduction (Figure 10). When Zn is in excess (Zn/Al of 2), a mixture of Ni$_x$Zn$_y$ intermetallic phase, containing only small amounts of pure Ni, is observed in the metallic phase of the reduced catalyst. It is possible that this dilution of Ni metal atoms in the NiZn alloy allowed the inhibition of carbon formation, thus resulting in the mentioned increased stability. Furthermore, the alloy was stable and, consequently, not destroyed during the reaction. On the other hand, for Zn/Al of 1/2, the reduced metal consists only of Ni^0, as the limited amount of Zn is only enough to form the ZnAl$_2$O$_4$ support. For this reason, filamentous carbon was formed and resulted in deactivation (Figure 10). Sintering was not significantly observed in either case. Despite this, the catalyst containing an excess of Zn suffered from deactivation at 400 °C and the authors propose that this is due to the re-oxidation of metallic Ni by water during the ESR process.
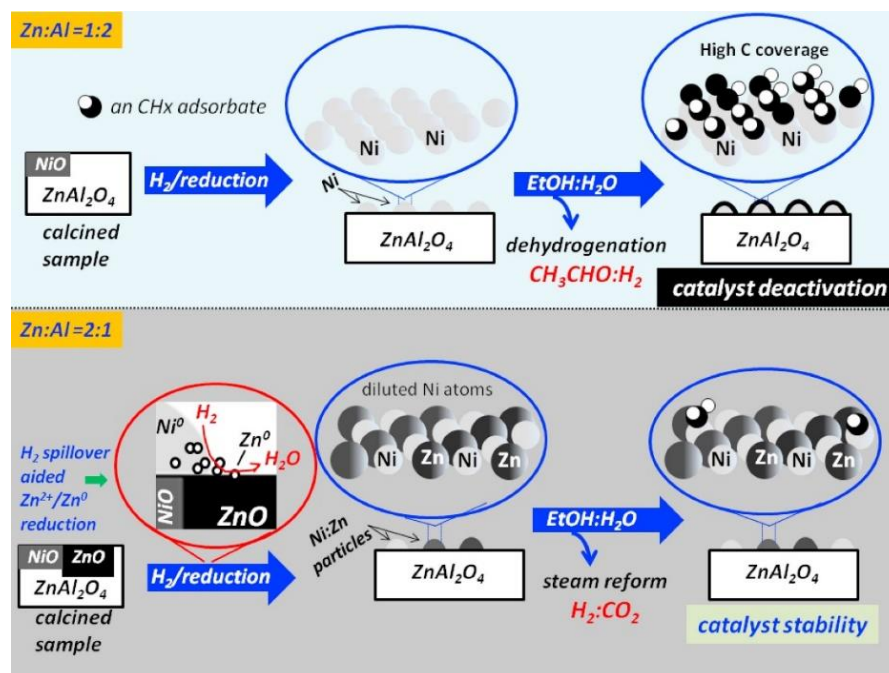
Figure 10. Phase transformation during reduction and reaction steps over Ni/ZnAl having two different Zn/Al molar ratios. Reprinted with permission from Ref. [98]. Copyright 2022 Elsevier.

Two catalysts having MMT in the support have shown promisingly stable behaviors [99,100]. A comparison between Ni/MMT-TiO$_2$ micro-particles and nano-composite at 500 °C showed that while the micro-particles-based catalyst deactivated over time, the nano-composite material did not show signs of deactivation after 20 h [99]. The enhanced stability of the last sample is probably associated with the total inhibition of ethylene formation at 500 °C. This indicates that the ethylene polymerization reaction leading to coke formation did not occur. Also, the presence of MMT in the support of the nano-composite catalyst was probably responsible for the low coke formation observed over this material, as it improved the dispersion of Ni on the surface. On the other hand, Xue-mei et al. [100] observed that Ni supported on MMT presented significant coke deposition accompanied by the formation of acetaldehyde and ethylene at 500 °C, which resulted in deactivation after 10 h of reaction. This indicates that a synergism between MMT and TiO$_2$ was probably what allowed the positive effect of MMT addition in the work of Mulewa et al. [99]. The modification of MMT with cetrimonium bromide in [100] resulted in enhanced catalytic stability (30 h) due to a reduction of carbon formation, accompanied by a significant reduction of acetaldehyde and ethylene formation. Such reduction was possible due to the immobilization of highly dispersed Ni on the interlayers of the organically modified MMT, which reduced the coating of metallic Ni with carbon.

Besides showing good catalytic activity, the two zeolite-supported monometallic Ni catalysts [103,104], also showed good catalytic stability. The intracrystalline mesoporous structure of the Ni/hierarchical beta zeolite was probably related to the lower deactivation rate compared to the non-hierarchical zeolite. The sol-gel method used also contributed to the observed stability [103]. As for the Ni over dealuminated BEA zeolite tested by Gac et al. [104], it showed superior over time stability than Ni supported on non-modified BEA zeolite. The deactivation of the last catalyst was mainly attributed to the formation of significant amounts of amorphous, graphitic and filamentous carbon deposits, probably associated with the high production of ethylene. On the other hand, much lower carbon deposits were formed over the catalyst whose zeolite support was dealuminated. The enhanced stability of this catalyst is probably related to the structural changes caused by dealumination, which led to enhanced dispersion of nickel nanoparticles (higher active nickel surface area), and a decrease of the acidity of the zeolite support (decreasing the coke formation).

The addition of Mg to Ni-based catalysts has also been reported to allow stable ESR activity [105,106]. Such improvement has been attributed to the suppression of both sintering and carbon deposition [105]. As for coke formation, the addition of Mg decreased the acidic strength of the catalyst, which resulted in lower ethylene formation and, consequently, less carbon deposition. Still, stable ESR activity for 50 h was only reached by the catalyst with the optimal Mg loading of 10 wt.%, which showed the strongest interaction between the Ni active phase and the support and, therefore, the lowest sintering and coke formation rates [105]. The authors attributed this behavior to the lower carbon deposition observed over the Sr promoted catalyst, probably due to its higher basicity (already discussed). As for the effect of Sr loading [107], it was observed that the unpromoted catalyst and the catalyst with the highest Sr loading of 10 wt.% slightly deactivated over a 1000 h period under 450 °C. Besides the presence of filamentous carbon, it was also observed that the 10 wt.% Sr catalyst (weakest metal-support interaction) suffered from sintering. Ultimately, the 6 wt.% Sr catalyst not only presented the best catalytic activity (as already discussed), but also remained stable for 1000 min on stream.

The effect of promoting a Ni/MgAl$_2$O$_4$ catalyst with K, CeO$_2$, ZrO$_2$ and combinations of these promoters (CeO$_2$-K, CeZrO$_4$, and K/CeZrO$_4$) on the catalytic stability has been studied [90]. As can be seen in Figure 11, the unpromoted catalyst (base) showed rapid deactivation over time. The Ce promoted catalyst showed similar behavior, but with a quicker deactivation during the first hour of reaction and subsequent deactivation (contrary to what was verified in previous works for other catalysts). On the other hand, promotion with K, CeO$_2$-K, CeZrO$_4$ and K/CeZrO$_4$ resulted in stable activity.

In fact, carbon deposition was lowered by factors of two to four over these promoted catalysts. It is possible that K blocked the active sites for carbon formation, while the re-dox-active promoters could have contributed to higher OH availability and/or provided lattice oxygen to react with coke precursors.
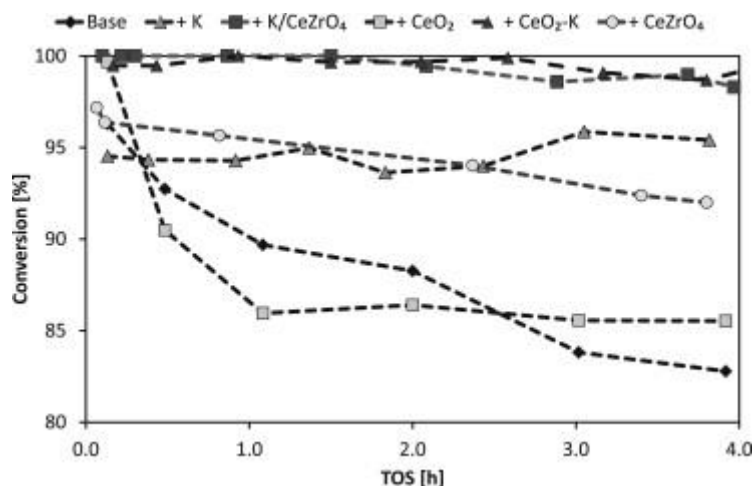

Figure 11. Ethanol conversion as a function of time on stream (TOS) for Ni/MgAl$_2$O$_4$ (base) with different promoters. Reprinted with permission from Ref. [90]. Copyright 2022 Elsevier.

Elsewhere [108], promotion of a Ni-based catalyst with Ce resulted in significantly improved stability over 50 h time on stream compared to the unpromoted material. As already mentioned, such enhancement was related to the suppression of both coke formation and sintering. On one side the high oxygen storage and transport capacity of Ce facilitates carbon species gasification and, on the other side, Ce strengthens the metal-support interaction, thus restraining the growth of Ni particles. Trane-Restrup et al. [90] have shown the formation of carbon whiskers. Such carbonaceous structures have been reported to break catalyst pellets with time, thus leading to increasing pressure drops on the catalyst bed and, consequently, local hot spots in industrial reactors [134]. Moreover, it was observed that Ni sintering contributed to the deactivation of both Ni/CeO$_2$-K/MgAl$_2$O$_4$ and Ni-K/MgAl$_2$O$_4$ catalysts. Finally, the authors tested the promotion with different amounts of sulfur of Ni-CeO$_2$/MgAl$_2$O$_4$, the addition of S having decreased coke deposition. Probably sulfur blocked the step sites on the Ni particles, responsible for carbon deposition. The sulfur loading of 0.03 wt.% allowed the minimum formation of carbon deposits [90]. The positive effect of promotion with Zr addressed by Trane-Restrup et al. [90] was also observed in other work [109], having once again been observed enhanced stability. The authors attributed this enhancement to sintering inhibition, higher dispersion of the Ni-Co active phase on the support and the formation of carbon nanotubes that were unable to deactivate the catalyst. Regarding this last aspect, the catalyst without Zr showed amorphous coke formation which, on contrary to the carbon nanotubes, resulted in ESR active sites deactivation.

The promotion of Ni with Co in the active phase has also been reported to improve the catalytic stability [110]. The authors tested three catalysts for 8 h under ESR reaction, two monometallic Ni and Co over MCM-41 and bimetallic Ni-Co over the same support. The Ni catalyst presented the highest coke formation among the three, followed by the Co catalyst and the bimetallic catalyst presented the lowest carbon deposition. This indicates that Co partially hinders coke formation. Elsewhere [111], a bimetallic Ni-Co/Al$_2$O$_3$ catalyst showed quite stable behavior for 100 h on stream. This improvement, partially caused by the promotion of Ni with Co in the active phase, has been associated with higher surface area, higher metal dispersion and lower particle size. Such enhancements were also caused by specific preparation conditions [111].

Besides improving the catalytic activity of the ESR reaction, promotion with Rh also allows higher long-term stability [115,116]. Campos et al. [115] reported a decrease in coke formation observed over a bimetallic Ni-Rh catalyst of 70 and 560 times relative to monometallic Rh and Ni catalysts, respectively. The authors attributed the enhanced coke resistance of the bimetallic catalyst to i) synergism between Ni and Rh catalytic activities; ii) favored WGS reaction; iii) improved capacity to gasify methyl groups resultant from the decomposition of intermediate products; and iv) no accumulation of CO and/or acetate species. The Rh-Ni/CeO_2-La_2O_3-Al_2O_3 catalyst was able to still convert more than 80% of ethanol after 144 h on stream at 500 °C. As already discussed for other catalysts, the addition of Rh was also reported to lead to the preferential formation of less encapsulating amorphous coke (which does not deactivate active sites), contrarily to monometallic Ni [116]. Au addition also suppressed, for the reason already mentioned in the previous section, both carbon deposition over Ni particles and their sintering, resulting in stable activity for 25 h on stream [120]. Both W [121] and B [86] promoted Ni catalysts have also shown remarkable stability compared to the respective monometallic Ni catalysts. In fact, the W promoted catalyst maintained an H_2 yield of around 80% for 80 h time on stream, to which the inhibition of sintering of Ni particles contributed [121]. As for the effect of B [86], the formation of a Ni-B alloy lowers coke deposition by enhancing the cracking of acetaldehyde and, consequently, avoiding the formation of acetone (coke precursor). Also, the simultaneous presence of Ce in the mixed support led to the formation of $CeBO_3$, which assisted in the removal of carbonaceous deposits. As a result, ethanol conversion was still around 96% after 50 h of reaction.

Finally, Romero et al. [122] observed that the Mg content in a Ni-Mg-Al mixed oxide influenced its stability, besides its catalytic activity (already discussed). More specifically, as shown by the TPO profiles of the used catalysts in Figure 12, higher Mg contents led to lower coke formation (lower gasification to CO_2). It has been claimed elsewhere [135,136] that higher Mg content in LDHs results in enhanced oxygen mobility and water adsorption-dissociation capacity, ultimately leading to improved carbon resistance. The presence of Cu in the LDH has also been reported to improve ESR catalytic stability by mitigating the deposition of carbon [125].
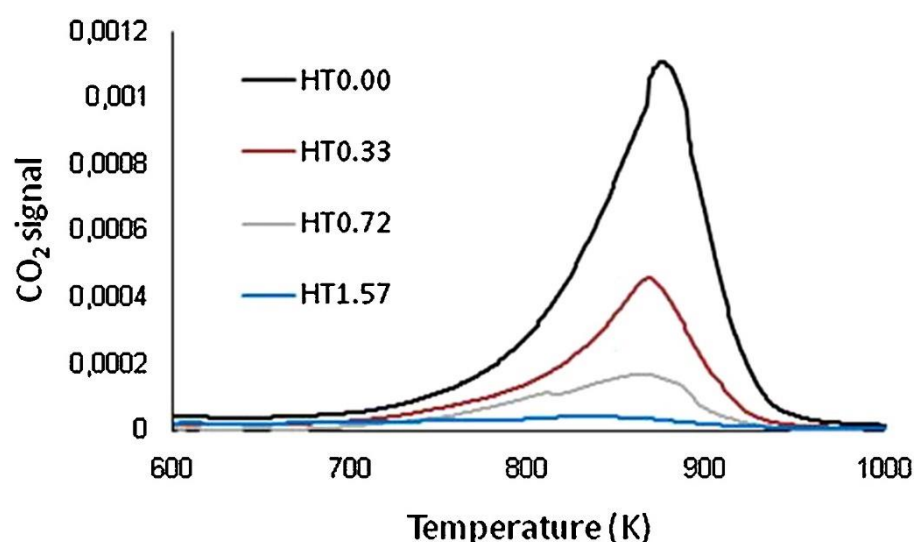
Figure 12. TPO profiles of LDH-derived mixed oxides with different Mg/Ni molar ratios (number in each sample) used in ESR. Reprinted with permission from Ref. [122]. Copyright 2022 Elsevier.

3.2.3. Effect of the Preparation Method

As previously seen for the MSR process, the method through which a catalyst is prepared can have a determining effect on its catalytic activity and stability. The same has been consistently observed for the ESR reaction. Once again, the impregnation method (wet impregnation and incipient wetness impregnation) has been the most commonly used for the preparation of ESR catalysts [87,90–92,98–100,106,107,109–111]. Zhao et al. [111] established a comparison between co-impregnation and sequential impregnation of bimetallic Ni and Co over Al_2O_3 in terms of ESR performance. As observed for MSR, co-impregnation once again led to higher ethanol conversion and H_2 selectivity (above 350 °C) than sequentially impregnated materials. At 350 °C, the co-impregnated material converted 68.7% of ethanol, while the $Co/Ni/Al_2O_3$ and $Ni/Co/Al_2O_3$ showed conversions of only 50.9% and 36.6%, respectively. Furthermore, the co-impregnated catalyst showed the lowest production of CO and CH_4. These results were mainly due to the higher metal dispersion, lower metal particle size and higher surface area of the co-impregnated material. For the same reasons, while the co-impregnated catalyst showed relatively stable activity for 100 h, both Co/Ni and Ni/Co started deactivating significantly after 60 h and 30 h, respectively. The authors also propose that the co-impregnated material might have benefited from H_2 spillover, which would have been responsible for the observed decrease in carbon deposits, possibly gasified into CH_4 [137].

Elsewhere [138], Ni/SBA-15 was prepared via incipient wetness impregnation using two different Ni precursors: nickel nitrate (commonly used) and nickel citrate. The citrate precursor strengthened the metal-support interaction and improved the dispersion of the smaller nickel particles. Furthermore, analysis of the spent catalysts after 25 h of ESR showed that not only less coke was formed on the catalyst synthesized with the citrate precursor, but it was also easily removable (contrarily to the catalyst prepared with nitrate precursor). This ultimately resulted in higher ESR activity and stability of the catalyst prepared using nickel citrate as a precursor.

The use of chelating agents in the wet impregnation method has also been tested [139]. The authors prepared four different $Ni/CeO_2-MgAl_2O_4$ catalysts, one without a chelating agent (conventional wet impregnation) and three others using different chelating agents: ethylenediaminetetraacetic acid, nitrilotriacetic acid and citric acid. The catalyst prepared with ethylenediaminetetraacetic acid as a chelating agent showed the best catalytic activity among the prepared samples. While the other three catalysts showed production of acetaldehyde and ethylene and a small decay in conversion after 7 h of reaction, the catalyst prepared using ethylenediaminetetraacetic acid did not show either of those. The results for the last catalyst were due to smaller NiO particles, which induced stronger $Ni-CeO_2$ interaction, and a higher Ce^{3+}/C^{4+} ratio, which means a higher capacity to store and release oxygen, thus leading to the observed higher resistance to coke formation [140]. The other chelating agents also improved such properties comparatively to the catalyst prepared through conventional impregnation, especially nitrilotriacetic acid, but to a lower extent. Contrarily to other methods or method modifications already discussed, this methodology keeps the simplicity of the conventional wet impregnation method. It also allows high synthesis reproducibility [141].

Wu et al. [86] compared the impregnation with the co-precipitation method in terms of their influence on ESR activity and stability. As can be observed in Figure 13, the catalysts prepared via co-precipitation presented higher ethanol conversions and higher stability than the respective B-promoted or unpromoted catalysts prepared through impregnation. First, the materials prepared through co-precipitation presented a higher surface area than the respective impregnated counterparts. This difference was higher between the boron promoted catalysts. The very low surface area obtained for the B promoted catalyst prepared via impregnation was caused by the calcination at 400 °C, which resulted in pore blocking. Despite showing the second higher ethanol conversion, this catalyst showed the lowest H_2 selectivity. Furthermore, co-impregnation improved the dispersion of NiO as a result of allowing Ni^{2+} to interpolate into the $Ce_{0.5}Zr_{0.5}O_2$ solid solution.
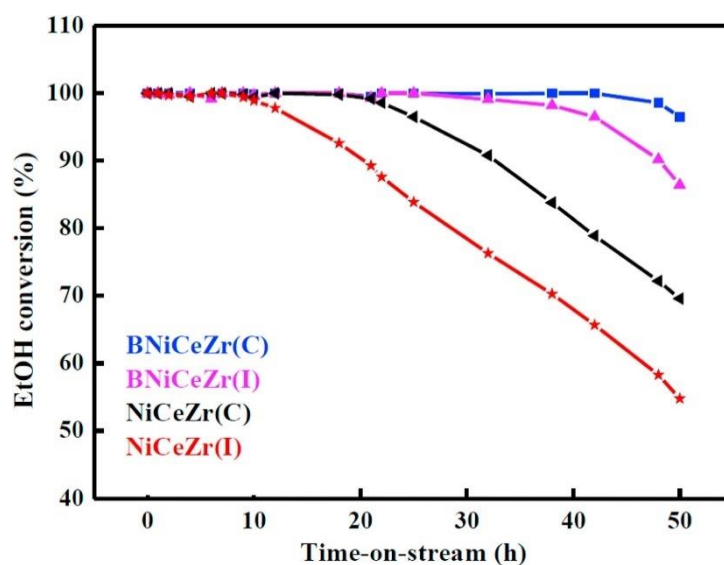
Figure 13. Influence of preparation method of Ni/Ce0.5Zr0.5O2 (C, co-precipitation; I, impregnation) on the catalytic activity of boron promoted and unpromoted catalysts. Reprinted with permission from Ref. [86]. Copyright 2022 Elsevier.

A sol-gel iso-volumetric impregnation method was used to prepare Ni/MBeta zeolite [103]. Comparatively to the iso-volumetric impregnation, used to prepare the same catalyst, the sol-gel method improved the same parameters previously discussed (smaller metal particles and improved dispersion), thus resulting in stronger metal-support interaction. This resulted in higher carbon deposition resistance, as the highly dispersed small metal particles make it more difficult for carbon deposits to accumulate on the metal surface and embed it. Therefore, higher conversion of ethanol into H_2 and more stable activity were, once again, obtained via the sol-gel-based method compared to the impregnation-based one. In a different work, Wu and co-workers [142] analyzed the effect of using different agents (HNO_3 or NH_4OH) at different ratios with tetraethyl silicate (0.04 or 0.20), which changed the acidity of the preparation solution, to prepare different Ni/SiO$_2$ catalysts. Essentially, changing the preparation solution's pH did not significantly influence the production of H_2, but it changed coke formation. The higher basicity of the solution resulted in larger SiO$_2$ particles and lower surface area and porosity and, consequently, higher coke formation.

The calcination conditions, such as temperature [143] and atmosphere [142], have also been the target of analysis in terms of impact on ESR activity and catalysts' stability. Nichele et al. [143] prepared Ni/TiO$_2$ catalysts calcined at 500 and 800 °C, being that calcination at 800 °C led to more stable behavior due to stronger metal-support interaction, which ultimately contributed to avoiding sintering. Elsewhere [142], the effect of calcining a Ni/SiO$_2$ catalyst under N_2 or air on the catalytic activity and stability in ESR was assessed. The results indicate that calcination under N_2 atmosphere resulted in higher H_2 yield and lower coke formation comparatively to preparation under air. Calcination under N_2 led to the formation of both Ni and NiO phases, while only NiO was formed when air was used. Furthermore, the first showed higher Ni dispersion (smaller Ni particles), probably the main cause of the enhanced activity towards H_2 production.

3.3. Summary

A summary of the ESR catalysts reviewed in this section that showed the most promising results is presented in Table 4. These three catalysts showed ethanol conversions of 100%, as well as quite high H_2 yields. In these studies, it was verified that the utilization of adequate promoters and supports could be very beneficial for the catalyst performance. For instance, in the work of Song et al. [92], it was observed that the addition of La_2O_3 in

a Ni/Al$_2$O$_3$ catalyst (La/Al between 0.05–0.15) improved significantly the catalytic performance of the material. Moreover, the utilization of graphene and zeolite as supports has shown to be a good solution to achieve high catalytic activities; concerning the study that used zeolite [103], the high performance of the material was attributed to the strong metal-support interaction and high active Ni surface area. In the work of Prasongthum et al. [97], the unique characteristics of the graphene (electron cloud) accelerate the rate of carbon gasification and help the regeneration of the active Ni surface.

Besides that, the impregnation method appears to be suitable to impregnate Ni on the support surface, although several studies indicate that co-precipitation increases the catalytic performance of the materials. Finally, the reduction methods adopted in these studies were performed at temperatures very similar to those used during the ESR reaction.

In the previous section, it was also verified that the most important catalyst properties to achieve proper catalytic performance (in terms of catalytic activity and stability) for the ESR process are the number of active sites available and the ability to gasify coke deposits. In this way, to reach high ethanol conversion, high H$_2$ production and low sub-products production, it is necessary to prepare a catalyst with a proper content of active phase (well dispersed) and promoted with basic oxides (e.g., MgO and CeO$_2$—these phases inhibited the coke production).

Taking into account the main results shown and discussed in Section 3.2 (and presented in Table 4), it is suggested the preparation of a Ni-based catalyst (for instance, prepared by impregnation) promoted with (or supported on) CeO$_2$ for the ESR process, to obtain high and stable catalytic performances.

Table 4. Comparison of some of the most promising ESR catalysts reviewed in this section.

Catalyst	Temperature	Feed Flow Rate	Mass of Catalyst	S/C [a]	Conversion of Ethanol	H$_2$ Yield/Selectivity	Stability	Preparation Method	Refs.
15 wt.% Ni/zeolite	550 °C	0.05 mL·min^{-1}	0.1 g	6	≈100%	76% [b]/n.d.	Result after 27 h (no significant deactivation)	Sol-gel + Impregnation	[103]
10 wt.% Ni/CNTs–SF	450 °C	8 g$_{cat}$·h·mol^{-1}	n.d.	9	≈100%	40% [b]/n.d.	Result after 22 h (no significant deactivation)	Sol-gel + Impregnation	[97]
Ni/Al-0.1La	450 °C	23,140 mL·h^{-1} g$_{cat}^{-1}$ [c]	0.1 g	6	100%	124% [b]/n.d.	Result after 15 h (no significant deactivation)	Epoxide-initiated sol-gel + Impregnation	[92]
15 wt.% Ni/Y-ZrO$_2$	650 °C	41,000 h^{-1} [c]	0.1 g	4.5	100%	91% [b]/74% [d]	Result after 8 h (no significant deactivation)	Sol-gel	[101]
13 wt.% Ni-4 wt.% Cu/CeO$_2$	600 °C	20,00 mL·h^{-1} g$_{cat}^{-1}$ [c]	0.3 g	6	≈100%	n.d./70 [d]	Result after 20 h (no significant deactivation)	Impregnation	[102]

[a] Steam to carbon molar feed ratio. [b] Yield (%) = $\frac{H_2}{H_{2\,Máx.}} \times 100$. [c] GHSV: gas hourly space velocity. [d] Selectivity (%) = $\frac{H_2}{\sum F_i} \times 100$. n.d.—Not determined

4. Other Oxygenates Steam Reforming
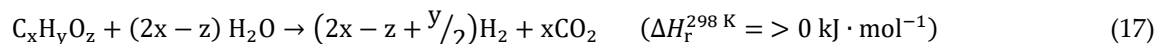
4.1. Introduction

Many recent studies are focused on the sustainable production of fuels and renewable energy sources, to decrease the dependency on fossil fuels and reduce the emissions of CO_2. One of the attractive alternatives for sustainable production of fuels is biomass, which is a renewable and CO_2-neutral emission fuel source [144]. Biomass conversion into different types of fuels can be performed through distinct processes, namely: biological, mechanical, or thermal processes [145–148]. For instance, pyrolysis is the thermal decomposition of the biomass (in the absence of O_2) that produces charcoal, fuel gas and bio-oil. Three different modes of pyrolysis can be differentiated: fast, intermediate, and slow [146,149,150]. The fast pyrolysis, which occurs at high heating rates, @ 450–600 °C and < 2 s of residence time, provides a higher yield in bio-oil, while the charcoal and fuel gas can be used to produce heat for the process itself [146]. Compared with biomass, bio-oil has a much higher energy density (ten times higher). Consequently, it is much more suitable for transportation [22,151]. The composition of bio-oil is highly variable depending on several factors such as residence time, heating rate and temperature of the process, and composition of the biomass source itself [152]. A typical composition of bio-oil consists of many different oxygenated species such as alcohols, acids, ketones, phenols, etc. [153–155]. In Table 4 is possible to see an example of bio-oil composition, produced through flash pyrolysis of two different types of biomass: a mix of 85% of pine and 15% of spruce [22].

Another possible attractive alternative of sustainable fuel composed of distinct oxygenated compounds is the olive mill wastewater (OMW, a polluting stream generated from the olive oil producing systems) since the composition of this stream (mainly polyphenols, carbohydrates, fatty acids and water) is very similar to the composition of the bio-oil. Several studies have shown that OMW disposal/discharge causes large environmental impacts due to its high content of organic matter and pollutant load [156–158]. The most referenced compounds are the following: vanillic acid, caffeic acid, tyrosol, p-coumaric acid, cinnamic acid, d-arabinose, d-galactose, d-galacturonic acid, syringic acid, gallic acid, protocatechuic acid, phenol, acetic acid, phenethyl alcohol, guaiacol and benzyl alcohol [159–176]. However, the composition of OMW is highly variable and it suggests that such compounds can be present in major or minor proportion, depending on several factors which include the maturation level of the olive, the region of cultivation, the age of the olive tree, the treatment of the tree, the method of extracting the oil and the weather conditions that the olive was been subjected to in the ripening process [164].

In addition to the polluting effluents already mentioned (bio-oil and OMW), there are other streams with a very similar composition and potential such as palm oil mill effluent (POME) and glycerol. POME is a polluting stream generated from the palm oil producing system, constituted by several oxygenated molecules [177], causing environmental impacts identical to OMW. The composition is also highly variable due to the reasons already mentioned for the composition of the OMW. About the glycerol, it is possible to verify that this oxygenate compound is the main by-product of biodiesel production (100 kg of glycerol/ton of biodiesel), without economic value so far.

These streams could be used directly as combustion fuels, but their poor volatility, high viscosity and coking formation result in problems for equipment. However, experimental studies of oxygenates steam reforming (OSR) showed that this technology is viable to produce hydrogen [178–187]. Additionally, several thermodynamic studies for the steam reforming of several oxygenates have already been performed, which also demonstrate the potential of this technology for the production of hydrogen [152,188–191], though only from the theoretical (thermodynamic) point of view. This technology would enable the production of green H_2, while reducing the pollutant load of these oxygenated

streams. The produced biofuel is environmentally attractive since it is renewable [192]. The OSR is described by the overall reaction shown in Equation (17):

$$C_xH_yO_z + (2x - z)\, H_2O \rightarrow \left(2x - z + \frac{y}{2}\right)H_2 + xCO_2 \qquad (\Delta H_r^{298\,K} = >0\ kJ \cdot mol^{-1}) \tag{17}$$

The OSR can be divided into two major reactions: oxygenates decomposition (Equation (18)) to yield syngas (mixture of hydrogen and carbon monoxide) followed by the WGS reaction (Equation (3)).

$$C_xH_yO_z + (x - z)H_2O \rightarrow \left(x - z + \frac{y}{2}\right)H_2 + xCO \qquad (\Delta H_r^{298\,K} = >0\ kJ \cdot mol^{-1}) \tag{18}$$

As it was aforementioned for MSR and ESR processes, there are also secondary reactions associated with this process that form some undesired by-products (e.g., methane, coke). For instance, the reactions represented by Equations (4)–(6). Therefore, choosing a proper catalyst, able to maximize conversion and selectivity for H_2 formation, is also required for this reaction.

Several catalysts were extensively studied for the steam reforming of individual model compounds that are present in the bio-oil, OMW, or POME. At the moment, the main challenge is to prepare highly reducible and with high oxygen mobility redox catalysts for OSR. These catalysts must present high performance with high stability. Numerous catalysts have been extensively studied for the steam reforming of individual compounds, which are the main species present in the pollutant effluents considered in this section. The molecules included in this group are acetic acid, phenol and toluene. The performance of such catalysts is affected by the type of support and the promoter agent(s); these topics are discussed in the next sub-section, but only for catalysts with Ni as the active phase. Besides that, some materials already developed for the steam reforming of bio-oil, OMW, glycerol or POME were also discussed.

4.2. Nickel-Based Catalysts

#### 4.2.1. Catalytic Activity and H_2 Selectivity

The Ni-based catalysts are the most used in the steam reforming of oxygenates since they are effective, commercially available and relatively cheap [193–197]. Metal loading is an important parameter in the study of such catalysts' performance. In the study of Zhang et al. [198] (focused on acetic acid steam reforming), it was concluded that the increase of Ni loading from 10 wt.% to higher values (in a Ni/Al_2O_3 catalyst prepared by a wetness impregnation method) did not significantly increase the activity of the catalysts when a steam to carbon feed ratio of two or five was used. However, high content of Ni in the catalyst did prevent coke formation, promoting its stability (due to the higher number of active sites available). In another study of acetic acid steam reforming, Borges et al. [199] verified that the higher is the Ni loading (in LHD-like precursors of Ni-Mg-Al prepared through co-precipitation), the lower will be the temperature and the time necessary for the reduction, since the interactions between Ni and Mg-Al oxides are weaker (TPR peaks shifted to lower temperatures)—c.f. Figure 14.
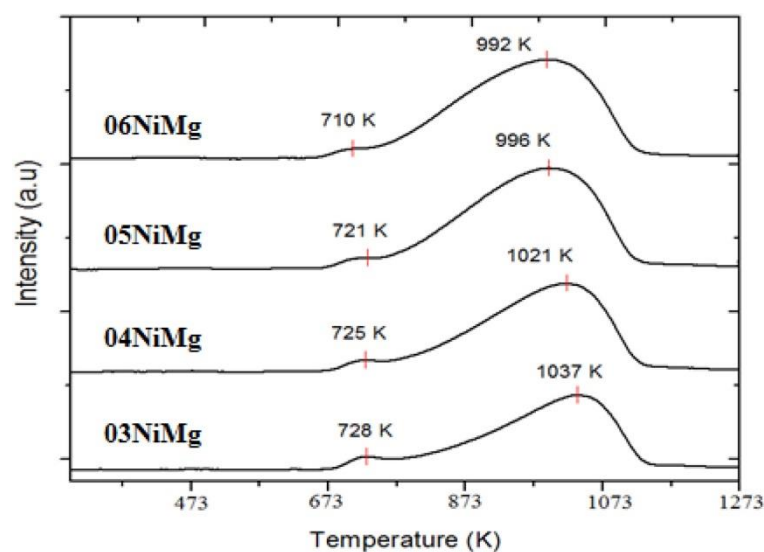
Figure 14. TPR analyses of the calcined hydrotalcite-like precursors (xNiMg) with different Ni loading (x is the molar ratio of Ni^{2+}/Mg^{2+}. Reprinted with permission from Ref. [199]. Copyright 2022 Elsevier.

In several studies, it was found that different supports significantly influenced the catalyst performance in the reforming reaction. Ni-based catalysts supported on various types of Al_2O_3 with different crystalline phases for the steam reforming of acetic acid were prepared and tested by Chen et al. [196]. The crystalline phases of Al_2O_3 support influence the intensity of the interaction between these supports and Ni and, consequently, the formation of metallic Ni. Since the surface of α-Al_2O_3 was mainly formed with bulk NiO, more metallic Ni was present on the Ni/α-Al_2O_3 catalyst after the reduction treatment. In this way, this catalyst presents a higher catalytic activity, as the metallic Ni content caused higher C-C and C-H bonds breaking capability.

In the work of He et al. [200] (toluene steam reforming), it was possible to verify that the high Ni dispersion in Ni/γ-Al_2O_3 increases toluene conversion and H_2 yield. On the other hand, a series of Ni core-shell catalysts with various shell species (i.e., SiO_2, Al_2O_3, CeO_2 and TiO_2) were prepared by Pu et al. [201]—see Figure 15. By comparing the catalytic activities of the catalysts with various shell materials, it was concluded that the improved Ni/Al_2O_3-*i* catalyst (the nickel precursor was reduced by $NaBH_4$) was the most suitable for the steam reforming of acetic acid, showing much higher catalytic activity than the other materials (Figure 16).
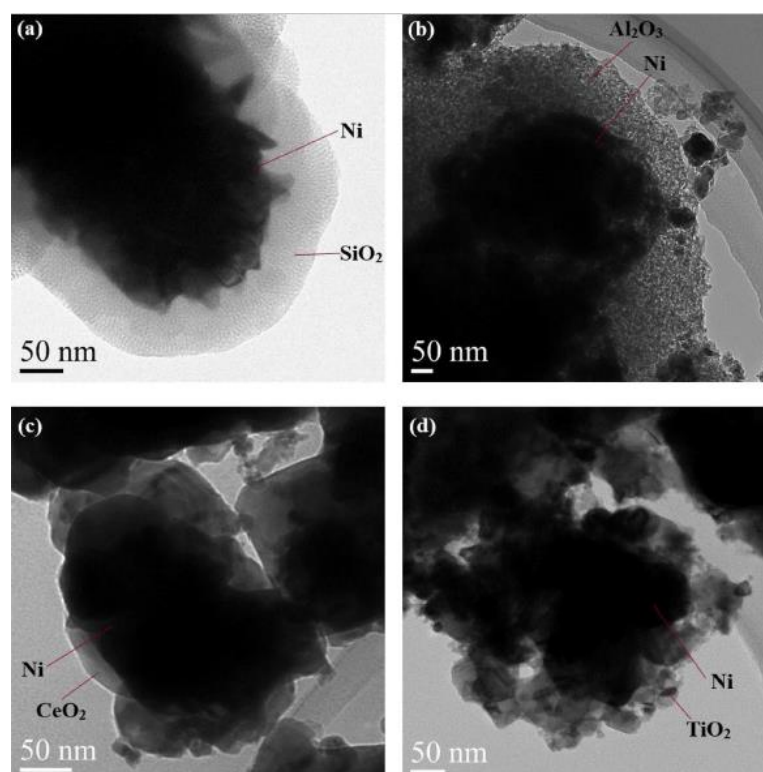
Figure 15. TEM images of the core-shell catalysts reduced at 600 °C: (**a**) Ni/iO$_2$, (**b**) Ni/Al$_2$O$_3$, (c) Ni/CeO$_2$, and (**d**) Ni/TiO$_2$. Reprinted with permission from Ref. [201]. Copyright 2022 Elsevier.
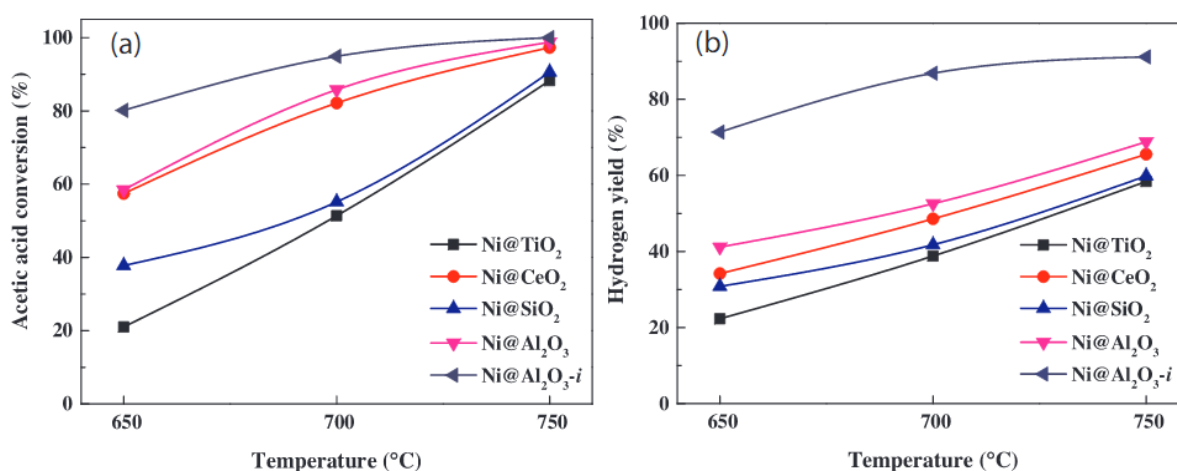
Figure 16. (**a**) Conversions of acetic acid and (**b**) H$_2$ yields in the steam reforming of acetic acid over different catalysts. Reaction conditions: 1 bar, WHSV = 21 h^{-1}, and steam to carbon molar feed ratio = 3.18. Reprinted with permission from Ref. [201]. Copyright 2022 Elsevier.

The nature of the support was also studied by Zhang et al. [202], using attapulgite (ATTP) and Al$_2$O$_3$ as support of Ni-based catalysts. ATTP has a lower specific surface area and lower thermal stability than Al$_2$O$_3$. The low thermal stability negatively affects the catalytic performance for steam reforming of acetic acid. However, the interaction between the Ni species and ATTP is much weaker than that of Ni with Al$_2$O$_3$, and, as a consequence, at the low Ni loading, the Ni/ATTP catalyst showed better performance. Chen et al. [203] studied the effect of using biochar as support in a Ni catalyst for the steam reforming of acetic acid. The catalyst characterization showed that after activation, the porosity of the biochar enlarged significantly, and both the surface area and the dispersions of Ni particles increased, increasing the catalytic activity. Kechagiopoulos et al. [204]

used a Ni-based catalyst supported in natural material (Ni/olivine) in a spouted bed reactor; it was observed that the catalyst presented a high catalytic activity for the steam reforming of representative model species of the aqueous phase of bio-oil. Besides, Liu et al. [205] stated that the porosity of the support could promote the catalytic performance in bio-oil steam reforming, by comparing the results obtained from a Ni-Mo catalyst supported on natural sepiolite and acidified sepiolite. The authors verified that the acidified support showed higher catalytic performance than the non-acidified sepiolite since the acid treatment changed the internal structure of the support to produce a higher number of pores, leading to an increase of the surface area of the material.

In several studies dealing with the steam reforming of long-chain oxygenates, the catalysts were often doped with promoters. Galdamez et al. [24], who addressed the steam reforming of bio-oil, concluded that the addition of La_2O_3 in the Ni-based catalyst does not increase the H_2 yield. Nevertheless, Garcia et al. [206] observed that the promotion of a Ni/Al_2O_3 catalyst with MgO and La_2O_3 enhanced the steam adsorption that facilitated the gasification of surface carbon (decreasing coke formation) also during bio-oil steam reforming. The increase in the performance of a Ni/Al_2O_3 catalyst caused by the incorporation of these two promoters was also reported by Bangala et al. [207] (though in naphthalene steam reforming). In the work of Zhang et al. [208] (acetic acid steam reforming), it was verified that the addition of KOH to Ni/Al_2O_3, with the lowest Ni loading, significantly enhances the catalytic activity. Choi et al. [209] studied the steam reforming of acetic acid by using Ni-based catalysts modified by Mg, La, Cu, and K elements; they found that the Ni/Al_2O_3 catalyst modified with Mg showed the best performance at low temperatures.

In the work of Charisiou et al. [210] (steam reforming of glycerol), it was studied the catalytic activity and stability of a Ni-based catalyst promoted with Y and Zr. It was concluded that the addition of Y stabilized the ZrO_2 phase and, for this reason, the utilization of these promotors enhanced the production of H_2 and increased the stability of the catalyst.

Souza et al. [211] prepared Ni-Pt monometallic and bimetallic materials supported on ZrO_2 for the acetic acid steam reforming. The addition of Pt to Ni catalysts caused an increase in the metallic dispersion and a decrease in the nickel reduction temperature; however, the catalytic performance was not improved by Pt addition. Ni monometallic catalyst presented the best catalytic behavior: 100% of conversion and 30% of H_2 yield at 500 °C, without any deactivation during 30 h on stream. The high activity and stability of Ni/ZrO_2 catalyst may be related to its high reduction degree, increasing the availability of metal sites, and its low acidity, reducing coke formation. The fast deactivation of Pt/ZrO_2 catalyst is associated with its highest rate of coke production.

Baamran et al. [212] prepared several Ni-based catalysts supported on TiO_2 for the steam reforming of phenol. As mentioned in previous works, the superior performance of the materials was related to the larger surface area, higher metal dispersion and no internal diffusion inside the pores (these properties were obtained due to the small particle size). The best catalyst (10 wt.% Ni/TiO_2) attained a 98.3% of phenol conversion, 76.9% of H_2 yield and high stability for more than 70 h. Besides that, another work of the research group of Baamran et al. [213] reported a synergistic effect between the TiO_2 and $ZnTiO_3$ phases in Ni-based materials, enhancing the Ni dispersion and, in this way, increasing the catalyst activity and stability. Moreover, Abbas et al. [214] prepared Ni/Co_3O_4-supported TiO_2 catalysts for the phenol steam reforming with continuous H_2 production. Using a feed rate of 10 mL/h, temperature equal to 700 °C, and 0.3 g of catalyst loading, a H_2 yield of 83.5%, a selectivity of 72.8%, and a phenol conversion of 92% were obtained. High stability in terms of production of H_2 after 100 h of reaction was obtained with the best material (no deactivation was verified). This stability was attributed to the strong interaction of the metal-support (improving the metal dispersion and enhancing the reducibility), minimizing the coke formation.

It was reported that the incorporation of Cr in a Ni/MgO-La$_2$O$_3$-Al$_2$O$_3$ catalyst inhibited the formation of Ni$_3$C [207], modified the metal sites forming alloys with Ni, and reduced the crystallite size (enhancing the crystallinity of the material), increasing the catalyst activity. Besides that, Bangala et al. [207] observed that the presence of TiO$_2$ decreases the conversion since it reduces the crystallinity and robustness of the material and destroys the Al$_2$O$_3$ matrix. It was also observed that the addition of CeO$_2$ improved the catalyst performance, namely through the inhibition of coke production due to the enhanced catalyst redox properties [195,197,215–218]. So, the addition of basic oxides (e.g., MgO, CeO$_2$, La$_2$O$_3$, etc.) or other promoters to the Al$_2$O$_3$ support, in a general way, enhanced the steam reforming catalytic performance.

Besides the monometallic Ni-based catalysts, other elements such as Pt, Co, Rh, Cu, and Fe were used along with Ni in bimetallic catalysts for the steam reforming of oxygenated molecules. A series of Ni-Cu bimetallic catalysts supported on sepiolite (Nix-Cuy/SEP) was prepared by Liang et al. [219] for the steam reforming of phenol. The results showed that the Ni-Cu alloys were successfully synthesized, and the addition of Cu decreased the Ni particle size, improving the redox ability and metal dispersion of bimetallic catalysts (in this case, Cu can be also considered as a promoter of the catalyst). Pant et al. [220] reported that Ni-Co, Ni-Co/CeO$_2$-ZrO$_2$, and Ni/La$_2$O$_3$-Al$_2$O$_3$ catalysts catalyze the acetic acid steam reforming reaction, being that among them, the Ni-Co catalyst was more effective. In this specific case, the unsupported catalyst presents a higher performance due to the combined action of the Ni and Co (Co catalyzes the WGS reaction [221,222]). Besides that, since Al$_2$O$_3$ allows the formation of a high quantity of coke, the unsupported catalyst presented higher stability. Mizuno et al. [223] studied the steam reforming of acetic acid over Ni-Co supported in MgAl$_2$O$_4$. The ketonization reaction occurred on the MgAl$_2$O$_4$ support and the presence of Co or Ni changed the reaction pathway of adsorbed species, which suppressed the formation of acetone.

Rocha et al. [224,225] tested one commercial catalyst and several prepared materials based on Ni in the OMW steam reforming process (using a synthetic OMW effluent). A catalytic screening was carried out with these materials (at 1 bar and 350/400 °C), and stability tests (at 1 bar and 400 °C) were performed with the most promising samples. The authors reported that the LDH-based catalysts and the Ni-Ru/SiO$_2$ catalyst prepared in the laboratory showed good catalytic properties (the last one with high deactivation resistance in the long-term test of 24 h) due to a high number of active sites available and high surface area. Using the commercial catalyst (Ni/Al$_2$O$_3$-SiO$_2$), this research group [224] observed that the H$_2$ and CO$_2$ production was very high during all of the screening experiments. Still, the CH$_4$ yield was very close to zero and CO was not detected during the experimental test.

Adhikari et al. [226] compared the catalytic activity of several Ni-based catalysts on different supports for the steam reforming of glycerol: MgO, CeO$_2$ and TiO$_2$. At 600 °C, it was found the following order of H$_2$ selectivity: CeO$_2$ > MgO > TiO$_2$. Pant et al. [227] observed that the incorporation of CeO$_2$ in the Ni-based catalysts affects the reduction of Ni species, enhancing the catalyst activity for the stem reforming of glycerol. In a general way, it was reported that the addition of a CeO$_2$ promoter enhances the catalytic performance of the Ni-based catalysts for steam reforming processes [228].

For the steam reforming of POME [186], a Ni/Al$_2$O$_3$ catalyst was demonstrated to be a good candidate for syngas production and reduction of the organic load of the pollutant stream.

Finally, mixed oxides such as LHD-type oxides (Ni-Mg-Al oxides) have been reported as promising catalyst precursors for the steam reforming of these types of oxygenates since they present high surface areas in comparison with other catalysts [199,229].

In the steam reforming of these oxygenates, it was possible to observe the formation of several surface intermediates. For instance, it was verified the formation of lactic acid, acetaldehyde, propyleneglycol, ethylene glycol, methanol, acetic acid, acetone, hydroxyacetone, acrolein and ethanol during the steam reforming of glycerol [230–232].

4.2.2. Deactivation

The formation of carbon deposits on the catalysts used in the OSR leads to catalyst deactivation (as verified in Sections 2.2.2 and 3.2.2). Therefore, to achieve continuous performance and sustainable H_2 production, it is necessary to study the deactivation of such catalysts.

In the study of Zhang et al. [198], it was verified that the increase of Ni content, from 10 wt.% to higher values, does not significantly affect the catalytic activity of the catalysts. Still, it enhanced the stability, and especially the resistance towards coking in the steam reforming of acetic acid. While the coke formed over the catalyst with the lower Ni loading was mostly amorphous, the coke formed over higher Ni loading was more fibrous [198]. In another work, Zhang et al. [208] also verified that the addition of KOH to Ni/Al_2O_3 with the low Ni loading not only significantly enhances the catalytic activity but also promotes gasification of the reactive intermediates such as methyl group, carbonyl group, etc. The effect of the support in the stability tests was studied by Zhang et al. [202] (also in acetic acid steam reforming), using attapulgite (ATTP) and Al_2O_3 as support of a Ni-based catalyst. The stability of the Ni/Al_2O_3 catalyst was higher than that of Ni/ATTP, due to the higher surface area of Al_2O_3, and to the nature of the coke formed on the surface of the Ni/Al_2O_3 catalyst (fibrous) instead of the coke formed on Ni/ATTP (amorphous). Hoang et al. [195] showed that Ni/HT gradually deactivates with the time-on-stream due to coke formation (competitive adsorption in the active sites)—see Figure 17.
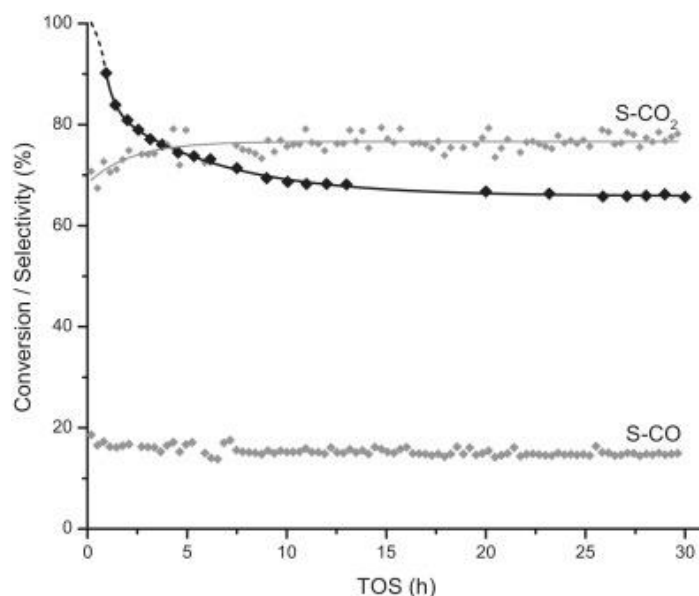
Figure 17. Steam reforming of acetic acid in presence of Ni/HT catalyst with steam to carbon ratio of 5, T = 700 °C, WHSV = 25.2 h^{-1}. Reprinted with permission from Ref. [195]. Copyright 2022 Elsevier.

In the work of Savuto et al. [197] (who studied the steam reforming of tar model compounds), mayenite ($Ca_{12}Al_{14}O_{33}$) was used as support of Ni, showing excellent oxidation properties that increase the resistance of the catalyst towards coke deposition. On the other hand, Choi et al. [209] verified that a Ni/Al_2O_3 catalyst with a large amount of weak basic sites and few middle and strong basic sites is required to improve the catalytic performance and minimize coke formation (in acetic acid steam reforming).

It was also reported that, for several Ni-based catalysts, La_2O_3 led to a decrease in coke formation [194,206,207,217,233,234] and KOH and MgO improved the stability [194,206,207,234–236]. It was also observed in several studies using Ni-based catalysts that the addition of CeO_2 improved the catalyst stability, namely through the decrease of coke production [195,197,215–218]. So, the addition of basic oxides to the Al_2O_3 support, in a

general way, enhanced the catalytic performance. The main role of these oxides is to enhance the redox properties of the material [237,238], which increases the oxidation of surface carbon and the stability of the catalyst.

In the study of Rocha et al. [225], it was observed that the increase of the CO production was related to the decreased extent of the WGS reaction (catalyst deactivation), decreasing the production of H_2. Besides that, it was concluded that the production of amorphous coke is the main route for the deactivation of the catalysts, as shown in multiple studies on the steam reforming processes.

Sánchez et al. [239] studied the utilization of a Ni-based catalyst for the steam reforming of glycerol. This work reported a catalyst deactivation after 8 h of a long-term test (at 600 and 650 °C) caused by coke deposition. However, Wen et al. [240] verified that Ni-based supported catalysts suffer quick deactivation for the glycerol steam reforming, but due to the sintering of the Ni particles during the reaction.

Finally, a brief reference to structured mesoporous silicate materials that were reported to be Ni supports less susceptible to deactivation due to coke formation than the conventional microporous supports. Apart from that, it is well known that they also cause less resistance to the diffusion of reactants to the active sites [241].

4.2.3. Effect of the Preparation Method

The preparation method (including the precursors of the species) used is also a very important parameter to be considered since it can affect the activity and stability of the catalysts. For instance, in a recent study by Yu et al. [242], the effect of the type of Ni precursors (used in the incipient wetness impregnation method) on the catalytic behaviors of Ni/Al_2O_3 during steam reforming of acetic acid was studied. It was found that the type of anion in the nickel precursors affects the properties and performance of the Ni/Al_2O_3 catalysts. $NiSO_4/Al_2O_3$ and $Ni(NH_2SO_3)_2/Al_2O_3$ did not show good catalytic activity, while $Ni(NO_3)_2/Al_2O_3$ and $Ni(CH_3COO)_2/Al_2O_3$ showed good and similar activity for the conversion of acetic acid. Nevertheless, $Ni(CH_3COO)_2/Al_2O_3$ was more stable and had a higher resistance toward coke production. Among the nickel precursors investigated, $Ni(CH_3COO)_2$ was more suitable as the CH_3COO^- anion.

Metal salts precursors have significant effects on the properties and catalytic performance of the final catalysts, which should be considered in the preparation of Ni-based catalysts. This topic is not very studied for the steam reforming long-chain oxygenates or even model compounds (apart from methanol and ethanol), and almost all Ni-based catalysts assessed for these reactions are prepared by the traditional impregnation method (see Table 5).

Table 5. Example of the composition of bio-oil [22].

Component	[wt.%]
Water	20–23
Acids	3–22
Sugars	4–9
Phenols	3–4
Lignin	2–18
PAH [a]	8 [ppm]
Others [b]	2–21

[a] Poly aromatic hydrocarbons. [b] Ketones, aldehydes, and alcohols.

4.3. Summary

A summary of the most promising OSR catalysts reviewed in this section is shown in Table 5. From those eleven catalysts, seven are monometallic and the others are bimetallic. Regarding the support, most of the supports are Al_2O_3-based. Besides that, it is

worth mentioning that almost all of the eleven catalysts presented in Table 5 were prepared by impregnation. All of these catalysts showed conversions close to 100% and high H_2 yields (always higher than 57%) and selectivities (always higher than 54%). In addition, several catalysts do not present any deactivation, even over long-term experimental tests (30 h).

Analyzing the results of oxygenates conversion, only the catalysts Ni/ABC (ABC—Activated Biochar) and 6.6 wt.% Ni–10 wt.% Fe/$(CeO_2)_{0.4}$-$PG^{0.6}$ (PG, palygorskite) did not convert completely the compounds fed [203,216]. Regarding the H_2 production, it was observed that the monometallic catalysts 15 wt.% Ni/α-Al_2O_3 and 3.5 wt.% Ni/5 wt.% La_2O_3-ZrO_2 demonstrated higher performance (H_2 yield of 90%) in comparison with the remaining materials [194,196]. It is also important to emphasize that two catalysts prepared by co-precipitation [216,233] did not demonstrate loss of activity (during 20 h of operation) through the stability tests (6.6 wt.% Ni–10 wt.% Fe/$(CeO_2)_{0.4}$-$PG_{0.6}$ and 10 wt.% Ni/La_2O_3-Al_2O_3). These results show how attractive Ni-based catalysts are for OSR.

Finally, it was also observed that the most crucial catalyst properties to reach a high catalytic activity/stability for the OSR processes are the number of active sites available (related to metal dispersion), the surface area and the basicity of the material. In this way, to reach high oxygenates conversion, high production of H_2 and low sub-products production, it is necessary to prepare a catalyst promoted with basic oxides, which presents high metal dispersion (defined by the strong interaction between the active phase and the support), and with high surface area (utilization of a proper porous support).

Taking into account the works discussed in Section 4.2 (and observing the data summarized in Table 6), to obtain high catalytic performances during long-term tests in the steam reforming of oxygenates it is suggested the preparation of a Ni-based catalyst by impregnation, supported on Al_2O_3, and promoted with a metal oxide (e.g., MgO or CeO_2—to inhibit the coke production).

Table 6. Comparison of some of the most promising OSR catalysts reviewed in this section.

Catalyst	Temperature	Feed Flow Rate	Mass of Catalyst	S/C [a]	Conversion	H₂ Yield/Selectivity	Stability	Preparation Method	Refs.
3.5 wt.% Ni/5 wt.% La_2O_3-ZrO_2 [1]	700 °C	240,000 h^{-1} [b]	0.050 g	5	100	87 [c]/64 [d]	Lost 7% of H₂ yield in 20 h	Impregnation	[194]
(2.5+2.5) wt.% Ni-Cu/Al_2O_3 [1]	750 °C	28 h^{-1} [e]	0.1 g	1.25	100	67 [c]/57 [d]	Result of 7.5 h (no deactivation)	Impregnation over support prepared by following evaporation-induced-self-assembly	[243]
15 wt.% Ni/α-Al_2O_3 [1]	600 °C	20 h^{-1} [e]	1.5 g	1	≈100	90 [c]/66 [d]	n.d.	Impregnation	[196]
10 wt.% Ni/La_2O_3-Al_2O_3 [1] (La_2O_3/Al_2O_3 = 1:3, weight ratio)	700 °C	10 h^{-1} [f]	0.2 g	2.5	100	73 [c]/59 [d]	Result of 30 h (no deactivation)	Co-precipitation	[233]
15 wt.% Ni/Al_2O_3 [1]	700 °C	7400–10,000 h^{-1} [b]	0.2 g	1	100	57 [c]/54 [d]	n.d.	Incipient wetness impregnation	[244]
5.5 wt.% Cu–2.5 wt.% Ni/$MgAl_2O_4$ [1]	450 °C	9 h^{-1} [e]	0.1 mg	2	100	83 [c]/63 [d]	n.d.	Impregnation	[223]

(6.6+10) wt.% Ni-Fe/(CeO$_2$)$_{0.4}$-PG$_{0.6}$ [1]	600 °C	14,427 h^{-1} [f]	n.d.	3	≈93	85 [c]/63 [d]	Result of 20 h (no deactivation)	Co-precipitation	[216]
Ni(NO$_3$)$_2$/Al$_2$O$_3$ [1]	600 °C	12.7 h^{-1} [f]	0.5 g	5	≈100	77 [c]/71 [d]	n.d.	Incipient wetness impregnation	[242]
Ni/ABC [1]	700 °C	10 h^{-1} [f]	0.15 g	2.5	91.2	71 [c]/61 [d]	n.d.	Impregnation	[203]
10 wt.% Ni/ATTP [1]	600 °C	7.2 h^{-1} [f]	0.5 g	5	≈100	75 [c]/65 [d]	n.d.	Impregnation	[202]
(10+1) wt.% Ni-Ru/SiO$_2$ [2]	400 °C	n.d.	0.65 g	694	≈100	84 [c]/68 [d]	Lost 10% of H$_2$ yield in 20 h	Co-precipitation	[225]

[a] Steam to Carbon Molar Feed Ratio. [b] GHSV: gas hourly space velocity. [c] Yield (%) = $\frac{H_2}{H_{2\,Máx.}} \times 100$. [d] Selectivity (%) = $\frac{H_2}{H_2+CH_4+CO_2+CO} \times 100$. [e] WHSV: weight hourly space velocity. [f] LHSV: liquid hourly space velocity. [1] Steam reforming of acetic acid. [2] Steam reforming of OMW. n.d—Not determined.

5. Conclusions

In the last years, the production of H_2 through the catalytic steam reforming of bio-mass-derived oxygenates was the target of several studies and such a process has been demonstrated to be a very attractive alternative for green H_2 production. In this way, and to improve the H_2 production, the selection of an appropriate catalyst is fundamental. Nickel-based materials have been widely studied due to their lower price and their performance as compared to noble metal-based materials. This review addressed steam reforming of different biomass-derived oxygenates, namely methanol, ethanol, and other oxygenates (bio-oil, acetic acid, OMW, etc.).

Most of the promising catalysts for the MSR are bimetallic, Ni and Cu-based. The materials demonstrated methanol conversions of around 90%, as well as high H_2 yields and selectivities. The materials with higher Cu content and lower amounts of Ni tend to be more selective towards the production of H_2 and CO_2 (in detriment of CO). The impregnation method for the preparations of these catalysts appears to be an appropriate choice and the annealing/reduction programs adopted were often carried out at temperatures very similar to those used during the MSR. Besides that, the LDH-based materials allowed to reach high methanol conversions and H_2 yields and showed very stable operation. These materials might be a potential option in a MSR process since they present a high potential to be used as hybrid sorbent-catalyst (i.e., dual-functional) materials.

Among the best catalysts for the ESR reaction, half are monometallic and the other half are bimetallic. It was concluded that the presence of CeO_2 in the catalyst composition enhanced the catalytic activity towards H_2 and stability. Several advantages resulting from promoting the catalysts with Rh were identified, despite the high cost of the noble metal (which is attenuated by using low loadings of Rh). The best catalysts used in the ESR process were prepared via simple impregnation techniques.

From the catalysts with the best performances for the OSR, six are monometallic and the others are bimetallic, and almost all of the catalysts presented Al_2O_3-based supports. Most of these catalysts were prepared by impregnation. The catalysts showed practically complete conversions of the oxygenates and moderate to high H_2 yields (>57%) and selectivities (>54%). Still, several catalysts do not present any deactivation in the stability tests, although they have not been tested for extended times on stream (<30 h).

Conflicts of Interest: The authors declare no conflict of interest.

Notation and Glossary

ABC	Activated Biochar
ATTP	Attapulgite
DFM	Dual Function Materials
ESR	Ethanol Steam Reforming
ISO	International Organization for Standardization
LDH	Layered Double Hydroxides
MSR	Methanol Steam Reforming
MMT	Montmorillonite
OMW	Olive Mill Wastewater
OSE	Oxygenates Steam Reforming
PF	Palygorskite
POME	Palm Oil Mill Effluent
TEM	Transmission Electron Microscopy
TPD	Temperature-Programmed Desorption
TPO	Temperature-Programmed Oxidation
TPR	Temperature-Programmed Reduction
WEFR	Water to Ethanol Feed Ratio
WGS	Water-Gas Shift
WHSV	Weight Hourly Space Velocity
XRD	X-Ray Diffraction

References

1. Dou, B.; Song, Y.; Wang, C.; Chen, H.; Xu, Y. Hydrogen production from catalytic steam reforming of biodiesel byproduct glycerol: Issues and challenges. *Renew. Sustain. Energy Rev.* **2014**, *30*, 950–960.
2. Ayalur Chattanathan, S.; Adhikari, S.; Abdoulmoumine, N. A review on current status of hydrogen production from bio-oil. *Renew. Sustain. Energy Rev.* **2012**, *16*, 2366–2372. https://doi.org/10.1016/j.rser.2012.01.051.
3. LeValley, T.L.; Richard, A.R.; Fan, M. The progress in water gas shift and steam reforming hydrogen production technologies–A review. *Int. J. Hydrog. Energy* **2014**, *39*, 16983–17000.
4. Mazloomi, K.; Gomes, C. Hydrogen as an energy carrier: Prospects and challenges. *Renew. Sustain. Energy Rev.* **2012**, *16*, 3024–3033. https://doi.org/10.1016/j.rser.2012.02.028.
5. Nikolaidis, P.; Poullikkas, A. A comparative overview of hydrogen production processes. *Renew. Sustain. Energy Rev.* **2017**, *67*, 597–611. https://doi.org/10.1016/j.rser.2016.09.044.
6. Balat, M. Potential importance of hydrogen as a future solution to environmental and transportation problems. *Int. J. Hydrog. Energy* **2008**, *33*, 4013–4029. https://doi.org/10.1016/j.ijhydene.2008.05.047.
7. Verhelst, S.; Wallner, T. Hydrogen-fueled internal combustion engines. *Prog. Energy Combust. Sci.* **2009**, *35*, 490–527. https://doi.org/10.1016/j.pecs.2009.08.001.
8. Wang, G.; Yu, Y.; Liu, H.; Gong, C.; Wen, S.; Wang, X.; Tu, Z. Progress on design and development of polymer electrolyte membrane fuel cell systems for vehicle applications: A review. *Fuel Processing Technol.* **2018**, *179*, 203–228. https://doi.org/10.1016/j.fuproc.2018.06.013.
9. Kothari, R.; Buddhi, D.; Sawhney, R.L. Comparison of environmental and economic aspects of various hydrogen production methods. *Renew. Sustain. Energy Rev.* **2008**, *12*, 553–563. https://doi.org/10.1016/j.rser.2006.07.012.
10. Ewan, B.C.R.; Allen, R.W.K. A figure of merit assessment of the routes to hydrogen. *Int. J. Hydrog. Energy* **2005**, *30*, 809–819. https://doi.org/10.1016/j.ijhydene.2005.02.003.
11. Baharudin, L.; Watson, M.J. Hydrogen applications and research activities in its production routes through catalytic hydrocarbon conversion. *Rev. Chem. Eng.* **2018**, *34*, 43–72, https://doi.org/doi:10.1515/revce-2016-0040.
12. Uddin, M.N.; Nageshkar, V.V.; Asmatulu, R. Improving water-splitting efficiency of water electrolysis process via highly conductive nanomaterials at lower voltages. *Energy Ecol. Environ.* **2020**, *5*, 108–117. https://doi.org/10.1007/s40974-020-00147-5.
13. Shamsul, N.S.; Kamarudin, S.K.; Rahman, N.A.; Kofli, N.T. An overview on the production of bio-methanol as potential renewable energy. *Renew. Sustain. Energy Rev.* **2014**, *33*, 578–588. https://doi.org/10.1016/j.rser.2014.02.024.
14. Iulianelli, A.; Ribeirinha, P.; Mendes, A.; Basile, A. Methanol steam reforming for hydrogen generation via conventional and membrane reactors: A review. *Renew. Sustain. Energy Rev.* **2014**, *29*, 355–368. https://doi.org/10.1016/j.rser.2013.08.032.
15. Xuan, J.; Leung, M.K.H.; Leung, D.Y.C.; Ni, M. A review of biomass-derived fuel processors for fuel cell systems. *Renew. Sustain. Energy Rev.* **2009**, *13*, 1301–1313. https://doi.org/10.1016/j.rser.2008.09.027.
16. Baneshi, J.; Haghighi, M.; Jodeiri, N.; Abdollahifar, M.; Ajamein, H. Urea–nitrate combustion synthesis of ZrO_2 and CeO_2 doped CuO/Al_2O_3 nanocatalyst used in steam reforming of biomethanol for hydrogen production. *Ceram. Int.* **2014**, *40*, 14177–14184. https://doi.org/10.1016/j.ceramint.2014.06.005.

17. Hou, T.; Zhang, S.; Chen, Y.; Wang, D.; Cai, W. Hydrogen production from ethanol reforming: Catalysts and reaction mechanism. *Renew. Sustain. Energy Rev.* **2015**, *44*, 132–148. https://doi.org/10.1016/j.rser.2014.12.023.

18. Badwal, S.P.S.; Giddey, S.; Kulkarni, A.; Goel, J.; Basu, S. Direct ethanol fuel cells for transport and stationary applications–A comprehensive review. *Appl. Energy* **2015**, *145*, 80–103. https://doi.org/10.1016/j.apenergy.2015.02.002.

19. Frusteri, F.; Freni, S. Bio-ethanol, a suitable fuel to produce hydrogen for a molten carbonate fuel cell. *J. Power Sources* **2007**, *173*, 200–209. https://doi.org/10.1016/j.jpowsour.2007.04.065.

20. Ni, M.; Leung, D.Y.C.; Leung, M.K.H. A review on reforming bio-ethanol for hydrogen production. *Int. J. Hydrog. Energy* **2007**, *32*, 3238–3247. https://doi.org/10.1016/j.ijhydene.2007.04.038.

21. Nabgan, W.; Tuan Abdullah, T.A.; Mat, R.; Nabgan, B.; Gambo, Y.; Ibrahim, M.; Ahmad, A.; Jalil, A.A.; Triwahyono, S.; Saeh, I. Renewable hydrogen production from bio-oil derivative via catalytic steam reforming: An overview. *Renew. Sustain. Energy Rev.* **2017**, *79*, 347–357. https://doi.org/10.1016/j.rser.2017.05.069.

22. Trane, R.; Dahl, S.; Skjøth-Rasmussen, M.S.; Jensen, A.D. Catalytic steam reforming of bio-oil. *Int. J. Hydrog. Energy* **2012**, *37*, 6447–6472. https://doi.org/10.1016/j.ijhydene.2012.01.023.

23. Arregi, A.; Amutio, M.; Lopez, G.; Bilbao, J.; Olazar, M. Evaluation of thermochemical routes for hydrogen production from biomass: A review. *Energy Convers. Manag.* **2018**, *165*, 696–719. https://doi.org/10.1016/j.enconman.2018.03.089.

24. Galdámez, J.R.; García, L.; Bilbao, R. Hydrogen Production by Steam Reforming of Bio-Oil Using Coprecipitated Ni−Al Catalysts. Acetic Acid as a Model Compound. *Energy Fuels* **2005**, *19*, 1133–1142. https://doi.org/10.1021/ef049718g.

25. Somerville, C.; Youngs, H.; Taylor, C.; Davis, S.C.; Long, S.P. Feedstocks for Lignocellulosic Biofuels. *Science* **2010**, *329*, 790–792. https://doi.org/10.1126/science.1189268.

26. Sá, S.; Silva, H.; Brandão, L.; Sousa, J.M.; Mendes, A. Catalysts for methanol steam reforming—A review. *Appl. Catal. B Environ.* **2010**, *99*, 43–57. https://doi.org/10.1016/j.apcatb.2010.06.015.

27. Li, D.; Nakagawa, Y.; Tomishige, K. Development of Ni-Based Catalysts for Steam Reforming of Tar Derived from Biomass Pyrolysis. *Chin. J. Catal.* **2012**, *33*, 583–594. https://doi.org/10.1016/S1872-2067(11)60359-8.

28. Baddour, F.G.; Snowden-Swan, L.; Super, J.D.; Van Allsburg, K.M. Estimating Precommercial Heterogeneous Catalyst Price: A Simple Step-Based Method. *Org. Process Res. Dev.* **2018**, *22*, 1599–1605. https://doi.org/10.1021/acs.oprd.8b00245.

29. Angeli, S.D.; Monteleone, G.; Giaconia, A.; Lemonidou, A.A. State-of-the-art catalysts for CH4 steam reforming at low temperature. *Int. J. Hydrog. Energy* **2014**, *39*, 1979–1997. https://doi.org/10.1016/j.ijhydene.2013.12.001.

30. Llorca, J.; Corberán, V.C.; Divins, N.J.; Fraile, R.O.; Taboada, E. Chapter 7-Hydrogen from Bioethanol. In *Renewable Hydrogen Technologies*; Gandía, L.M., Arzamendi, G., Diéguez, P.M., Eds.; Elsevier: Amsterdam, The Netherlands, 2013; pp. 135–169. https://doi.org/10.1016/B978-0-444-56352-1.00007-6.

31. Bao, Z.; Yu, F. Chapter Two-Catalytic Conversion of Biogas to Syngas via Dry Reforming Process. In *Advances in Bioenergy*; Li, Y., Ge, X., Eds.; Elsevier: Amsterdam, The Netherlands, 2018; Volume 3, pp. 43–76.

32. Silva, J.M.; Soria, M.A.; Madeira, L.M. Challenges and strategies for optimization of glycerol steam reforming process. *Renew. Sustain. Energy Rev.* **2015**, *42*, 1187–1213. https://doi.org/10.1016/j.rser.2014.10.084.

33. Molino, A.; Chianese, S.; Musmarra, D. Biomass gasification technology: The state of the art overview. *J. Energy Chem.* **2016**, *25*, 10–25. https://doi.org/10.1016/j.jechem.2015.11.005.

34. International Organization for Standardization. *Hydrogen Fuel-Product Specification-Part 2: Proton Exchange Membrane Fuel Cell Applications for Road Vehicles*; International Organization for Standardization: Geneva, Switzerland, 2012.

35. Kurtz, M.; Wilmer, H.; Genger, T.; Hinrichsen, O.; Muhler, M. Deactivation of Supported Copper Catalysts for Methanol Synthesis. *Catal. Lett.* **2003**, *86*, 77–80. https://doi.org/10.1023/A:1022663125977.

36. Deshmane, V.G.; Owen, S.L.; Abrokwah, R.Y.; Kuila, D. Mesoporous nanocrystalline TiO2 supported metal (Cu, Co, Ni, Pd, Zn, and Sn) catalysts: Effect of metal-support interactions on steam reforming of methanol. *J. Mol. Catal. A Chem.* **2015**, *408*, 202–213. https://doi.org/10.1016/j.molcata.2015.07.023.

37. Abrokwah, R.Y.; Deshmane, V.G.; Kuila, D. Comparative performance of M-MCM-41 (M: Cu, Co, Ni, Pd, Zn and Sn) catalysts for steam reforming of methanol. *J. Mol. Catal. A Chem.* **2016**, *425*, 10–20. https://doi.org/10.1016/j.molcata.2016.09.019.

38. Liu, Z.; Yao, S.; Johnston-Peck, A.; Xu, W.; Rodriguez, J.A.; Senanayake, S.D. Methanol steam reforming over Ni-CeO2 model and powder catalysts: Pathways to high stability and selectivity for H_2/CO_2 production. *Catal. Today* **2018**, *311*, 74–80. https://doi.org/10.1016/j.cattod.2017.08.041.

39. Shetty, K.; Zhao, S.; Cao, W.; Siriwardane, U.; Seetala, N.V.; Kuila, D. Synthesis and characterization of non-noble nanocatalysts for hydrogen production in microreactors. *J. Power Sources* **2007**, *163*, 630–636. https://doi.org/10.1016/j.jpowsour.2006.04.130.

40. Luo, X.; Hong, Y.; Wang, F.; Hao, S.; Pang, C.; Lester, E.; Wu, T. Development of nano NixMgyO solid solutions with outstanding anti-carbon deposition capability for the steam reforming of methanol. *Appl. Catal. B Environ.* **2016**, *194*, 84–97. https://doi.org/10.1016/j.apcatb.2016.04.031.

41. Bobadilla, L.F.; Palma, S.; Ivanova, S.; Domínguez, M.I.; Romero-Sarria, F.; Centeno, M.A.; Odriozola, J.A. Steam reforming of methanol over supported Ni and Ni–Sn nanoparticles. *Int. J. Hydrog. Energy* **2013**, *38*, 6646–6656. https://doi.org/10.1016/j.ijhydene.2013.03.143.

42. Xu, C.; Koel, B.E. Influence of alloyed Sn atoms on the chemisorption properties of Ni(111) as probed by RAIRS and TPD studies of CO adsorption. *Surf. Sci.* **1995**, *327*, 38–46. https://doi.org/10.1016/0039-6028(94)00816-7.

43. Khzouz, M.; Gkanas, E.I.; Du, S.; Wood, J. Catalytic performance of Ni-Cu/Al2O3 for effective syngas production by methanol steam reforming. *Fuel* **2018**, *232*, 672–683. https://doi.org/10.1016/j.fuel.2018.06.025.

44. Qing, S.; Hou, X.; Liu, Y.; Wang, L.; Li, L.; Gao, Z. Catalytic performance of Cu-Ni-Al spinel for methanol steam reforming to hydrogen. *J. Fuel Chem. Technol.* **2018**, *46*, 1210–1217. https://doi.org/10.1016/S1872-5813(18)30050-1.

45. Lytkina, A.A.; Orekhova, N.V.; Ermilova, M.M.; Belenov, S.V.; Guterman, V.E.; Efimov, M.N.; Yaroslavtsev, A.B. Bimetallic carbon nanocatalysts for methanol steam reforming in conventional and membrane reactors. *Catal. Today* **2016**, *268*, 60–67. https://doi.org/10.1016/j.cattod.2016.01.003.

46. Huang, Y.-H.; Wang, S.-F.; Tsai, A.-P.; Kameoka, S. Catalysts prepared from copper–nickel ferrites for the steam reforming of methanol. *J. Power Sources* **2015**, *281*, 138–145. https://doi.org/10.1016/j.jpowsour.2015.01.168.

47. Khzouz, M.; Wood, J.; Pollet, B.; Bujalski, W. Characterization and activity test of commercial Ni/Al2O3, Cu/ZnO/Al2O3 and prepared Ni–Cu/Al2O3 catalysts for hydrogen production from methane and methanol fuels. *Int. J. Hydrog. Energy* **2013**, *38*, 1664–1675. https://doi.org/10.1016/j.ijhydene.2012.07.026.

48. Pérez-Hernández, R.; Gutiérrez-Martínez, A.; Espinosa-Pesqueira, M.E.; Estanislao, M.L.; Palacios, J. Effect of the bimetallic Ni/Cu loading on the ZrO2 support for H2 production in the autothermal steam reforming of methanol. *Catal. Today* **2015**, *250*, 166–172. https://doi.org/10.1016/j.cattod.2014.08.009.

49. Tahay, P.; Khani, Y.; Jabari, M.; Bahadoran, F.; Safari, N. Highly porous monolith/TiO2 supported Cu, Cu-Ni, Ru, and Pt catalysts in methanol steam reforming process for H2 generation. *Appl. Catal. A Gen.* **2018**, *554*, 44–53. https://doi.org/10.1016/j.apcata.2018.01.022.

50. Yang, R.-X.; Chuang, K.-H.; Wey, M.-Y. Hydrogen production through methanol steam reforming: Effect of synthesis parameters on Ni–Cu/CaO–SiO2 catalysts activity. *Int. J. Hydrog. Energy* **2014**, *39*, 19494–19501. https://doi.org/10.1016/j.ijhydene.2014.09.140.

51. Suetsuna, T.; Suenaga, S.; Fukasawa, T. Monolithic Cu–Ni-based catalyst for reforming hydrocarbon fuel sources. *Appl. Catal. A Gen.* **2004**, *276*, 275–279. https://doi.org/10.1016/j.apcata.2004.08.018.

52. Lorenzut, B.; Montini, T.; De Rogatis, L.; Canton, P.; Benedetti, A.; Fornasiero, P. Hydrogen production through alcohol steam reforming on Cu/ZnO-based catalysts. *Appl. Catal. B Environ.* **2011**, *101*, 397–408. https://doi.org/10.1016/j.apcatb.2010.10.009.

53. Lytkina, A.A.; Zhilyaeva, N.A.; Ermilova, M.M.; Orekhova, N.V.; Yaroslavtsev, A.B. Influence of the support structure and composition of Ni–Cu-based catalysts on hydrogen production by methanol steam reforming. *Int. J. Hydrog. Energy* **2015**, *40*, 9677–9684. https://doi.org/10.1016/j.ijhydene.2015.05.094.

54. Duprez, D.; Pereira, P.; Miloudi, A.; Maurel, R. Steam dealkylation of aromatic hydrocarbons: II. Role of the support and kinetic pathway of oxygenated species in toluene steam dealkylation over group VIII metal catalysts. *J. Catal.* **1982**, *75*, 151–163. https://doi.org/10.1016/0021-9517(82)90130-0.

55. Duprez, D. Selective steam reforming of aromatic compounds on metal catalysts. *Appl. Catal. A Gen.* **1992**, *82*, 111–157. https://doi.org/10.1016/0926-860X(92)85001-R.

56. Takezawa, N.; Iwasa, N. Steam reforming and dehydrogenation of methanol: Difference in the catalytic functions of copper and group VIII metals. *Catal. Today* **1997**, *36*, 45–56. https://doi.org/10.1016/S0920-5861(96)00195-2.

57. Lytkina, A.A.; Orekhova, N.V.; Ermilova, M.M.; Yaroslavtsev, A.B. The influence of the support composition and structure (MXZr1-XO2-δ) of bimetallic catalysts on the activity in methanol steam reforming. *Int. J. Hydrog. Energy* **2018**, *43*, 198–207. https://doi.org/10.1016/j.ijhydene.2017.10.182.

58. Huang, H.-K.; Chih, Y.-K.; Chen, W.-H.; Hsu, C.-Y.; Lin, K.-J.; Lin, H.-P.; Hsu, C.-H. Synthesis and regeneration of mesoporous Ni–Cu/Al2O4 catalyst in sub-kilogram-scale for methanol steam reforming reaction. *Int. J. Hydrog. Energy* **2021**. https://doi.org/10.1016/j.ijhydene.2021.12.080.

59. Pérez-Hernández, R. Reactivity of Pt/Ni supported on CeO2-nanorods on methanol steam reforming for H2 production: Steady state and DRIFTS studies. *Int. J. Hydrog. Energy* **2021**, *46*, 25954–25964. https://doi.org/10.1016/j.ijhydene.2021.03.125.

60. Penkova, A.; Bobadilla, L.; Ivanova, S.; Domínguez, M.I.; Romero-Sarria, F.; Roger, A.C.; Centeno, M.A.; Odriozola, J.A. Hydrogen production by methanol steam reforming on NiSn/MgO–Al2O3 catalysts: The role of MgO addition. *Appl. Catal. A Gen.* **2011**, *392*, 184–191. https://doi.org/10.1016/j.apcata.2010.11.016.

61. Lu, J.; Li, X.; He, S.; Han, C.; Wan, G.; Lei, Y.; Chen, R.; Liu, P.; Chen, K.; Zhang, L.; et al. Hydrogen production via methanol steam reforming over Ni-based catalysts: Influences of Lanthanum (La) addition and supports. *Int. J. Hydrog. Energy* **2017**, *42*, 3647–3657. https://doi.org/10.1016/j.ijhydene.2016.08.165.

62. Kim, W.; Mohaideen, K.K.; Seo, D.J.; Yoon, W.L. Methanol-steam reforming reaction over Cu-Al-based catalysts derived from layered double hydroxides. *Int. J. Hydrog. Energy* **2017**, *42*, 2081–2087. https://doi.org/10.1016/j.ijhydene.2016.11.014.

63. Qi, C.; Amphlett, J.C.; Peppley, B.A. Product composition as a function of temperature over NiAl-layered double hydroxide derived catalysts in steam reforming of methanol. *Appl. Catal. A Gen.* **2006**, *302*, 237–243. https://doi.org/10.1016/j.apcata.2006.01.013.

64. Qi, C.; Amphlett, J.C.; Peppley, B.A. Hydrogen production by methanol reforming on NiAl layered double hydroxide derived catalyst: Effect of the pretreatment of the catalyst. *Int. J. Hydrog. Energy* **2007**, *32*, 5098–5102. https://doi.org/10.1016/j.ijhydene.2007.06.033.

65. Qi, C.; Amphlett, J.C.; Peppley, B.A. K (Na)-promoted Ni, Al layered double hydroxide catalysts for the steam reforming of methanol. *J. Power Sources* **2007**, *171*, 842–849. https://doi.org/10.1016/j.jpowsour.2007.06.018.

66. Frank, B.; Jentoft, F.C.; Soerijanto, H.; Kröhnert, J.; Schlögl, R.; Schomäcker, R. Steam reforming of methanol over copper-containing catalysts: Influence of support material on microkinetics. *J. Catal.* **2007**, *246*, 177–192. https://doi.org/10.1016/j.jcat.2006.11.031.

67. Bepari, S.; Kuila, D. Steam reforming of methanol, ethanol and glycerol over nickel-based catalysts-A review. *Int. J. Hydrog. Energy* **2020**, *45*, 18090–18113. https://doi.org/10.1016/j.ijhydene.2019.08.003.

68. Mosińska, M.; Szynkowska-Jóźwik, M.I.; Mierczyński, P. Catalysts for Hydrogen Generation via Oxy–Steam Reforming of Methanol Process. *Materials* **2020**, *13*, 5601.

69. Boskovic, G.; Baerns, M. Catalyst Deactivation. In *Basic Principles in Applied Catalysis*; Baerns, M., Ed.; Springer: Berlin/Heidelberg, Germany, 2004; pp. 477–503. https://doi.org/10.1007/978-3-662-05981-4_14.

70. Figueiredo, J.L.; Ramôa Ribeiro, F. *Catálise Heterogénea*, 2nd ed.; Gulbenkian, F.C., Ed.; Fundação Calouste Gulbenkian: Lisbon, Portugal, 2007.

71. Liu, Y.; Kang, H.; Hou, X.; Zhang, L.; Qing, S.; Gao, Z.; Xiang, H. Cu-Ni-Al spinel catalyzed methanol steam reforming for hydrogen production: Effect of Al content. *J. Fuel Chem. Technol.* **2020**, *48*, 1112–1121. https://doi.org/10.1016/S1872-5813(20)30075-X.

72. Munnik, P.; de Jongh, P.E.; de Jong, K.P. Recent Developments in the Synthesis of Supported Catalysts. *Chem. Rev.* **2015**, *115*, 6687–6718. https://doi.org/10.1021/cr500486u.

73. Pérez-Hernández, R.; Mendoza-Anaya, D.; Martínez, A.G.; Gómez-Cortés, A. Catalytic steam reforming of methanol to produce hydrogen on supported metal catalysts. In *Hydrogen Energy-Challenges and Perspectives*; Minic, D., Ed.; InTech: London, UK, 2012; pp. 149–174.

74. López, P.; Mondragón-Galicia, G.; Espinosa-Pesqueira, M.E.; Mendoza-Anaya, D.; Fernández, M.E.; Gómez-Cortés, A.; Bonifacio, J.; Martínez-Barrera, G.; Pérez-Hernández, R. Hydrogen production from oxidative steam reforming of methanol: Effect of the Cu and Ni impregnation on ZrO2 and their molecular simulation studies. *Int. J. Hydrog. Energy* **2012**, *37*, 9018–9027. https://doi.org/10.1016/j.ijhydene.2012.02.105.

75. Yang, W.; Parr, R.G. Hardness, softness, and the fukui function in the electronic theory of metals and catalysis. *Proc. Natl. Acad. Sci. USA* **1985**, *82*, 6723–6726. https://doi.org/10.1073/pnas.82.20.6723.

76. Chen, D.-H.; He, X.-R. Synthesis of nickel ferrite nanoparticles by sol-gel method. *Mater. Res. Bull.* **2001**, *36*, 1369–1377. https://doi.org/10.1016/S0025-5408(01)00620-1.

77. Bhosale, R.; Shende, R.; Puszynski, J. H₂ Generation From Thermochemical Water-Splitting Using Sol-Gel Synthesized Zn/Sn/Mn-doped Ni-Ferrite. *I.RE.CH.E.* **2010**, *2*, 852–862.

78. Wu, C.; Williams, P.T. A Novel Nano-Ni/SiO₂ Catalyst for Hydrogen Production from Steam Reforming of Ethanol. *Environ. Sci. Technol.* **2010**, *44*, 5993–5998. https://doi.org/10.1021/es100912w.

79. Sols, Gels, and Organic Chemistry. In *Ceramic Materials: Science and Engineering*; Carter, C.B., Norton, M.G., Eds.; Springer New York: New York, NY, USA, 2007; pp. 400–411. https://doi.org/10.1007/978-0-387-46271-4_22.

80. Fiévet, F.; Ammar-Merah, S.; Brayner, R.; Chau, F.; Giraud, M.; Mammeri, F.; Peron, J.; Piquemal, J.Y.; Sicard, L.; Viau, G. The polyol process: A unique method for easy access to metal nanoparticles with tailored sizes, shapes and compositions. *Chem. Soc. Rev.* **2018**, *47*, 5187–5233. https://doi.org/10.1039/C7CS00777A.

81. Wang, G.; Takeguchi, T.; Yamanaka, T.; Muhamad, E.N.; Mastuda, M.; Ueda, W. Effect of preparation atmosphere of Pt–SnOx/C catalysts on the catalytic activity for H₂/CO electro-oxidation. *Appl. Catal. B Environ.* **2010**, *98*, 86–93. https://doi.org/10.1016/j.apcatb.2010.05.016.

82. Silva, J.M.; Trujillano, R.; Rives, V.; Soria, M.A.; Madeira, L.M. High temperature CO₂ sorption over modified hydrotalcites. *Chem. Eng. J.* **2017**, *325*, 25–34. https://doi.org/10.1016/j.cej.2017.05.032.

83. Silva, J.M.; Trujillano, R.; Rives, V.; Soria, M.A.; Madeira, L.M. Dynamic behaviour of a K-doped Ga substituted and microwave aged hydrotalcite-derived mixed oxide during CO₂ sorption experiments. *J. Ind. Eng. Chem.* **2019**, *72*, 491–503. https://doi.org/10.1016/j.jiec.2019.01.005.

84. Rocha, C.; Soria, M.A.; Madeira, L.M. Effect of interlayer anion on the CO₂ capture capacity of hydrotalcite-based sorbents. *Sep. Purif. Technol.* **2019**, *219*, 290–302. https://doi.org/10.1016/j.seppur.2019.03.026.

85. Zabed, H.; Sahu, J.N.; Suely, A.; Boyce, A.N.; Faruq, G. Bioethanol production from renewable sources: Current perspectives and technological progress. *Renew. Sustain. Energy Rev.* **2017**, *71*, 475–501. https://doi.org/10.1016/j.rser.2016.12.076.

86. Wu, R.-C.; Tang, C.-W.; Huang, H.-H.; Wang, C.-C.; Chang, M.-B.; Wang, C.-B. Effect of boron doping and preparation method of Ni/Ce0.5Zr0.5O2 catalysts on the performance for steam reforming of ethanol. *Int. J. Hydrog. Energy* **2019**, *44*, 14279–14289. https://doi.org/10.1016/j.ijhydene.2019.02.065.

87. Dan, M.; Mihet, M.; Tasnadi-Asztalos, Z.; Imre-Lucaci, A.; Katona, G.; Lazar, M.D. Hydrogen production by ethanol steam reforming on nickel catalysts: Effect of support modification by CeO2 and La2O3. *Fuel* **2015**, *147*, 260–268. https://doi.org/10.1016/j.fuel.2015.01.050.

88. Bussi, J.; Musso, M.; Veiga, S.; Bespalko, N.; Faccio, R.; Roger, A.-C. Ethanol steam reforming over NiLaZr and NiCuLaZr mixed metal oxide catalysts. *Catal. Today* **2013**, *213*, 42–49. https://doi.org/10.1016/j.cattod.2013.04.013.

89. Biswas, P.; Kunzru, D. Steam reforming of ethanol for production of hydrogen over Ni/CeO2–ZrO2 catalyst: Effect of support and metal loading. *Int. J. Hydrog. Energy* **2007**, *32*, 969–980. https://doi.org/10.1016/j.ijhydene.2006.09.031.

90. Trane-Restrup, R.; Dahl, S.; Jensen, A.D. Steam reforming of ethanol: Effects of support and additives on Ni-based catalysts. *Int. J. Hydrog. Energy* **2013**, *38*, 15105–15118. https://doi.org/10.1016/j.ijhydene.2013.09.027.

91. Dancini-Pontes, I.; DeSouza, M.; Silva, F.A.; Scaliante, M.H.N.O.; Alonso, C.G.; Bianchi, G.S.; Medina Neto, A.; Pereira, G.M.; Fernandes-Machado, N.R.C. Influence of the CeO2 and Nb2O5 supports and the inert gas in ethanol steam reforming for H2 production. *Chem. Eng. J.* **2015**, *273*, 66–74. https://doi.org/10.1016/j.cej.2015.03.032.

92. Song, J.H.; Yoo, S.; Yoo, J.; Park, S.; Gim, M.Y.; Kim, T.H.; Song, I.K. Hydrogen production by steam reforming of ethanol over Ni/Al2O3-La2O3 xerogel catalysts. *Mol. Catal.* **2017**, *434*, 123–133. https://doi.org/10.1016/j.mcat.2017.03.009.

93. Di Cosimo, J.I.; Díez, V.K.; Xu, M.; Iglesia, E.; Apesteguía, C.R. Structure and Surface and Catalytic Properties of Mg-Al Basic Oxides. *J. Catal.* **1998**, *178*, 499–510. https://doi.org/10.1006/jcat.1998.2161.

94. Rioche, C.; Kulkarni, S.; Meunier, F.C.; Breen, J.P.; Burch, R. Steam reforming of model compounds and fast pyrolysis bio-oil on supported noble metal catalysts. *Appl. Catal. B Environ.* **2005**, *61*, 130–139. https://doi.org/10.1016/j.apcatb.2005.04.015.

95. Takanabe, K.; Aika, K.; Seshan, K.; Lefferts, L. Sustainable hydrogen from bio-oil—Steam reforming of acetic acid as a model oxygenate. *J. Catal.* **2004**, *227*, 101–108. https://doi.org/10.1016/j.jcat.2004.07.002.

96. Matas Güell, B.; Babich, I.; Nichols, K.P.; Gardeniers, J.G.E.; Lefferts, L.; Seshan, K. Design of a stable steam reforming catalyst— A promising route to sustainable hydrogen from biomass oxygenates. *Appl. Catal. B Environ.* **2009**, *90*, 38–44. https://doi.org/10.1016/j.apcatb.2009.02.008.

97. Prasongthum, N.; Xiao, R.; Zhang, H.; Tsubaki, N.; Natewong, P.; Reubroycharoen, P. Highly active and stable Ni supported on CNTs-SiO2 fiber catalysts for steam reforming of ethanol. *Fuel Processing Technol.* **2017**, *160*, 185–195. https://doi.org/10.1016/j.fuproc.2017.02.036.

98. Anjaneyulu, C.; Costa, L.O.O.d.; Ribeiro, M.C.; Rabelo-Neto, R.C.; Mattos, L.V.; Venugopal, A.; Noronha, F.B. Effect of Zn addition on the performance of Ni/Al2O3 catalyst for steam reforming of ethanol. *Appl. Catal. A Gen.* **2016**, *519*, 85–98. https://doi.org/10.1016/j.apcata.2016.03.008.

99. Mulewa, W.; Tahir, M.; Amin, N.A.S. MMT-supported Ni/TiO2 nanocomposite for low temperature ethanol steam reforming toward hydrogen production. *Chem. Eng. J.* **2017**, *326*, 956–969. https://doi.org/10.1016/j.cej.2017.06.012.

100. Yin, X.-m.; Xie, X.-m.; Wu, X.; An, X. Catalytic performance of nickel immobilized on organically modified montmorillonite in the steam reforming of ethanol for hydrogen production. *J. Fuel Chem. Technol.* **2016**, *44*, 689–697. https://doi.org/10.1016/S1872-5813(16)30033-0.

101. Musso, M.; Cardozo, A.; Romero, M.; Faccio, R.; Segobia, D.; Apesteguía, C.; Bussi, J. High performance Ni-catalysts supported on rare-earth zirconates (La and Y) for hydrogen production through ethanol steam reforming. Characterization and assay. *Catal. Today* **2021**. https://doi.org/10.1016/j.cattod.2021.07.001.

102. Niazi, Z.; Irankhah, A.; Wang, Y.; Arandiyan, H. Cu, Mg and Co effect on nickel-ceria supported catalysts for ethanol steam reforming reaction. *Int. J. Hydrog. Energy* **2020**, *45*, 21512–21522. https://doi.org/10.1016/j.ijhydene.2020.06.001.

103. Wang, S.; He, B.; Tian, R.; Sun, C.; Dai, R.; Li, X.; Wu, X.; An, X.; Xie, X. Ni-hierarchical Beta zeolite catalysts were applied to ethanol steam reforming: Effect of sol gel method on loading Ni and the role of hierarchical structure. *Mol. Catal.* **2018**, *453*, 64–73. https://doi.org/10.1016/j.mcat.2018.04.034.

104. Gac, W.; Greluk, M.; Słowik, G.; Millot, Y.; Valentin, L.; Dzwigaj, S. Effects of dealumination on the performance of Ni-containing BEA catalysts in bioethanol steam reforming. *Appl. Catal. B Environ.* **2018**, *237*, 94–109. https://doi.org/10.1016/j.apcatb.2018.05.040.

105. Chen, M.; Wang, Y.; Yang, Z.; Liang, T.; Liu, S.; Zhou, Z.; Li, X. Effect of Mg-modified mesoporous Ni/Attapulgite catalysts on catalytic performance and resistance to carbon deposition for ethanol steam reforming. *Fuel* **2018**, *220*, 32–46. https://doi.org/10.1016/j.fuel.2018.02.013.

106. Song, J.H.; Han, S.J.; Yoo, J.; Park, S.; Kim, D.H.; Song, I.K. Hydrogen production by steam reforming of ethanol over Ni–X/Al2O3–ZrO2 (X=Mg, Ca, Sr, and Ba) xerogel catalysts: Effect of alkaline earth metal addition. *J. Mol. Catal. A Chem.* **2016**, *415*, 151–159. https://doi.org/10.1016/j.molcata.2016.02.010.

107. Song, J.H.; Han, S.J.; Yoo, J.; Park, S.; Kim, D.H.; Song, I.K. Effect of Sr content on hydrogen production by steam reforming of ethanol over Ni-Sr/Al2O3-ZrO2 xerogel catalysts. *J. Mol. Catal. A Chem.* **2016**, *418–419*, 68–77. https://doi.org/10.1016/j.molcata.2016.03.035.

108. Li, L.; Tang, D.; Song, Y.; Jiang, B.; Zhang, Q. Hydrogen production from ethanol steam reforming on Ni-Ce/MMT catalysts. *Energy* **2018**, *149*, 937–943. https://doi.org/10.1016/j.energy.2018.02.116.

109. Gharahshiran, V.S.; Yousefpour, M. Synthesis and characterization of Zr-promoted Ni-Co bimetallic catalyst supported OMC and investigation of its catalytic performance in steam reforming of ethanol. *Int. J. Hydrog. Energy* **2018**, *43*, 7020–7037. https://doi.org/10.1016/j.ijhydene.2018.02.139.

110. Nejat, T.; Jalalinezhad, P.; Hormozi, F.; Bahrami, Z. Hydrogen production from steam reforming of ethanol over Ni-Co bimetallic catalysts and MCM-41 as support. *J. Taiwan Inst. Chem. Eng.* **2019**, *97*, 216–226. https://doi.org/10.1016/j.jtice.2019.01.025.

111. Zhao, X.; Lu, G. Modulating and controlling active species dispersion over Ni–Co bimetallic catalysts for enhancement of hydrogen production of ethanol steam reforming. *Int. J. Hydrog. Energy* **2016**, *41*, 3349–3362. https://doi.org/10.1016/j.ijhydene.2015.09.063.

112. Llorca, J.; Homs, N.; Ramirez de la Piscina, P. In situ DRIFT-mass spectrometry study of the ethanol steam-reforming reaction over carbonyl-derived Co/ZnO catalysts. *J. Catal.* **2004**, *227*, 556–560. https://doi.org/10.1016/j.jcat.2004.08.024.

113. Sutton, D.; Kelleher, B.; Ross, J.R.H. Review of literature on catalysts for biomass gasification. *Fuel Processing Technol.* **2001**, *73*, 155–173. https://doi.org/10.1016/S0378-3820(01)00208-9.

114. Davda, R.R.; Shabaker, J.W.; Huber, G.W.; Cortright, R.D.; Dumesic, J.A. A review of catalytic issues and process conditions for renewable hydrogen and alkanes by aqueous-phase reforming of oxygenated hydrocarbons over supported metal catalysts. *Appl. Catal. B Environ.* **2005**, *56*, 171–186. https://doi.org/10.1016/j.apcatb.2004.04.027.

115. Campos, C.H.; Pecchi, G.; Fierro, J.L.G.; Osorio-Vargas, P. Enhanced bimetallic Rh-Ni supported catalysts on alumina doped with mixed lanthanum-cerium oxides for ethanol steam reforming. *Mol. Catal.* **2019**, *469*, 87–97. https://doi.org/10.1016/j.mcat.2019.03.007.

116. Mondal, T.; Pant, K.K.; Dalai, A.K. Oxidative and non-oxidative steam reforming of crude bio-ethanol for hydrogen production over Rh promoted Ni/CeO2-ZrO2 catalyst. *Appl. Catal. A Gen.* **2015**, *499*, 19–31. https://doi.org/10.1016/j.apcata.2015.04.004.

117. Le Valant, A.; Can, F.; Bion, N.; Duprez, D.; Epron, F. Hydrogen production from raw bioethanol steam reforming: Optimization of catalyst composition with improved stability against various impurities. *Int. J. Hydrog. Energy* **2010**, *35*, 5015–5020. https://doi.org/10.1016/j.ijhydene.2009.09.008.

118. Mironova, E.Y.; Lytkina, A.A.; Ermilova, M.M.; Efimov, M.N.; Zemtsov, L.M.; Orekhova, N.V.; Karpacheva, G.P.; Bondarenko, G.N.; Muraviev, D.N.; Yaroslavtsev, A.B. Ethanol and methanol steam reforming on transition metal catalysts supported on detonation synthesis nanodiamonds for hydrogen production. *Int. J. Hydrog. Energy* **2015**, *40*, 3557–3565. https://doi.org/10.1016/j.ijhydene.2014.11.082.

119. Mironova, E.Y.; Ermilova, M.M.; Orekhova, N.V.; Muraviev, D.N.; Yaroslavtsev, A.B. Production of high purity hydrogen by ethanol steam reforming in membrane reactor. *Catal. Today* **2014**, *236*, 64–69. https://doi.org/10.1016/j.cattod.2014.01.014.

120. He, S.; He, S.; Zhang, L.; Li, X.; Wang, J.; He, D.; Lu, J.; Luo, Y. Hydrogen production by ethanol steam reforming over Ni/SBA-15 mesoporous catalysts: Effect of Au addition. *Catal. Today* **2015**, *258*, 162–168. https://doi.org/10.1016/j.cattod.2015.04.031.

121. Kim, D.; Kwak, B.S.; Min, B.-K.; Kang, M. Characterization of Ni and W co-loaded SBA-15 catalyst and its hydrogen production catalytic ability on ethanol steam reforming reaction. *Appl. Surf. Sci.* **2015**, *332*, 736–746. https://doi.org/10.1016/j.apsusc.2014.12.180.

122. Romero, A.; Jobbágy, M.; Laborde, M.; Baronetti, G.; Amadeo, N. Ni(II)–Mg(II)–Al(III) catalysts for hydrogen production from ethanol steam reforming: Influence of the Mg content. *Appl. Catal. A Gen.* **2014**, *470*, 398–404. https://doi.org/10.1016/j.apcata.2013.10.054.

123. Bepari, S.; Basu, S.; Pradhan, N.C.; Dalai, A.K. Steam reforming of ethanol over cerium-promoted Ni-Mg-Al hydrotalcite catalysts. *Catal. Today* **2017**, *291*, 47–57. https://doi.org/10.1016/j.cattod.2017.01.027.

124. Shejale, A.D.; Yadav, G.D. Cu promoted Ni-Co/hydrotalcite catalyst for improved hydrogen production in comparison with several modified Ni-based catalysts via steam reforming of ethanol. *Int. J. Hydrog. Energy* **2017**, *42*, 11321–11332. https://doi.org/10.1016/j.ijhydene.2017.03.052.

125. Passos, A.R.; Pulcinelli, S.H.; Santilli, C.V.; Briois, V. Operando monitoring of metal sites and coke evolution during non-oxidative and oxidative ethanol steam reforming over Ni and NiCu ex-hydrotalcite catalysts. *Catal. Today* **2019**, *336*, 122–130. https://doi.org/10.1016/j.cattod.2018.12.054.

126. Wang, F. *Hydrogen Production from Steam Reforming of Ethanol Over an Ir/Ceria-Based Catalyst: Catalyst Ageing Analysis and Performance Improvement upon Ceria Doping*; Université Claude Bernard-Lyon I: Villeurbanne, France, 2012.

127. Mhadmhan, S.; Natewong, P.; Prasongthum, N.; Samart, C.; Reubroycharoen, P. Investigation of Ni/SiO2 Fiber Catalysts Prepared by Different Methods on Hydrogen production from Ethanol Steam Reforming. *Catalysts* **2018**, *8*, 319.

128. Xu, W.; Liu, Z.; Johnston-Peck, A.C.; Senanayake, S.D.; Zhou, G.; Stacchiola, D.; Stach, E.A.; Rodriguez, J.A. Steam Reforming of Ethanol on Ni/CeO2: Reaction Pathway and Interaction between Ni and the CeO2 Support. *ACS Catal.* **2013**, *3*, 975–984. https://doi.org/10.1021/cs4000969.

129. Santander, J.A.; Tonetto, G.M.; Pedernera, M.N.; López, E. Ni/CeO2–MgO catalysts supported on stainless steel plates for ethanol steam reforming. *Int. J. Hydrog. Energy* **2017**, *42*, 9482–9492. https://doi.org/10.1016/j.ijhydene.2017.03.169.

130. Zhuang, Q.; Qin, Y.; Chang, L. Promoting effect of cerium oxide in supported nickel catalyst for hydrocarbon steam-reforming. *Appl. Catal.* **1991**, *70*, 1–8. https://doi.org/10.1016/S0166-9834(00)84149-4.

131. Tahir, M.; Mulewa, W.; Amin, N.A.S.; Zakaria, Z.Y. Thermodynamic and experimental analysis on ethanol steam reforming for hydrogen production over Ni-modified TiO2/MMT nanoclay catalyst. *Energy Convers. Manag.* **2017**, *154*, 25–37. https://doi.org/10.1016/j.enconman.2017.10.042.

132. Chen, X.; Liu, Y.; Niu, G.; Yang, Z.; Bian, M.; He, A. High temperature thermal stabilization of alumina modified by lanthanum species. *Appl. Catal. A Gen.* **2001**, *205*, 159–172. https://doi.org/10.1016/S0926-860X(00)00575-5.

133. Carrera Cerritos, R.; Fuentes Ramírez, R.; Aguilera Alvarado, A.F.; Martínez Rosales, J.M.; Viveros García, T.; Galindo Esquivel, I.R. Steam Reforming of Ethanol over Ni/Al2O3–La2O3 Catalysts Synthesized by Sol–Gel. *Ind. Eng. Chem. Res.* **2011**, *50*, 2576–2584. https://doi.org/10.1021/ie100636f.

134. Lee, S. Concepts in Syngas Manufacture. By Jens Rostrup-Nielsen and Lars J. Christiansen. *Energy Technol.* **2013**, *1*, 419–420. https://doi.org/10.1002/ente.201305007.

135. Melo, F.; Morlanés, N. Synthesis, characterization and catalytic behaviour of NiMgAl mixed oxides as catalysts for hydrogen production by naphtha steam reforming. *Catal. Today* **2008**, *133–135*, 383–393. https://doi.org/10.1016/j.cattod.2007.12.070.

136. Melo, F.; Morlanés, N. Naphtha steam reforming for hydrogen production. *Catal. Today* **2005**, *107-108*, 458-466. https://doi.org/10.1016/j.cattod.2005.07.028.

137. Conner, W.C.; Falconer, J.L. Spillover in Heterogeneous Catalysis. *Chem. Rev.* **1995**, *95*, 759–788. https://doi.org/10.1021/cr00035a014.

138. He, S.; Mei, Z.; Liu, N.; Zhang, L.; Lu, J.; Li, X.; Wang, J.; He, D.; Luo, Y. Ni/SBA-15 catalysts for hydrogen production by ethanol steam reforming: Effect of nickel precursor. *Int. J. Hydrog. Energy* **2017**, *42*, 14429–14438. https://doi.org/10.1016/j.ijhydene.2017.02.115.

139. Villagrán-Olivares, A.C.; Gomez, M.F.; Barroso, M.N.; Abello, M.C. Hydrogen production from ethanol: Synthesis of Ni catalysts assisted by chelating agents. *Mol. Catal.* **2020**, *481*, 110164. https://doi.org/10.1016/j.mcat.2018.08.006.

140. Tarditi, A.M.; Barroso, N.; Galetti, A.E.; Arrúa, L.A.; Cornaglia, L.; Abello, M.C. XPS study of the surface properties and Ni particle size determination of Ni-supported catalysts. *Surf. Interface Anal.* **2014**, *46*, 521–529. https://doi.org/10.1002/sia.5549.

141. van Dillen, A.J.; Terörde, R.J.A.M.; Lensveld, D.J.; Geus, J.W.; de Jong, K.P. Synthesis of supported catalysts by impregnation and drying using aqueous chelated metal complexes. *J. Catal.* **2003**, *216*, 257–264. https://doi.org/10.1016/S0021-9517(02)00130-6.

142. Wu, C.; Dupont, V.; Nahil, M.A.; Dou, B.; Chen, H.; Williams, P.T. Investigation of Ni/SiO2 catalysts prepared at different conditions for hydrogen production from ethanol steam reforming. *J. Energy Inst.* **2017**, *90*, 276–284. https://doi.org/10.1016/j.joei.2016.01.002.

143. Nichele, V.; Signoretto, M.; Menegazzo, F.; Rossetti, I.; Cruciani, G. Hydrogen production by ethanol steam reforming: Effect of the synthesis parameters on the activity of Ni/TiO2 catalysts. *Int. J. Hydrog. Energy* **2014**, *39*, 4252–4258. https://doi.org/10.1016/j.ijhydene.2013.12.178.

144. Bridgwater, A.V. Review of fast pyrolysis of biomass and product upgrading. *Biomass Bioenergy* **2012**, *38*, 68–94. https://doi.org/10.1016/j.biombioe.2011.01.048.

145. Akhtar, J.; Amin, N.A.S. A review on process conditions for optimum bio-oil yield in hydrothermal liquefaction of biomass. *Renew. Sustain. Energy Rev.* **2011**, *15*, 1615–1624. https://doi.org/10.1016/j.rser.2010.11.054.

146. Bridgwater, T. Biomass for energy. *J. Sci. Food Agric.* **2006**, *86*, 1755–1768. https://doi.org/10.1002/jsfa.2605.

147. Faba, L.; Díaz, E.; Ordóñez, S. Recent developments on the catalytic technologies for the transformation of biomass into biofuels: A patent survey. *Renew. Sustain. Energy Rev.* **2015**, *51*, 273–287. https://doi.org/10.1016/j.rser.2015.06.020.

148. Sadhukhan, J.; Martinez-Hernandez, E.; Murphy, R.J.; Ng, D.K.S.; Hassim, M.H.; Siew Ng, K.; Yoke Kin, W.; Jaye, I.F.M.; Leung Pah Hang, M.Y.; Andiappan, V. Role of bioenergy, biorefinery and bioeconomy in sustainable development: Strategic pathways for Malaysia. *Renew. Sustain. Energy Rev.* **2018**, *81*, 1966–1987. https://doi.org/10.1016/j.rser.2017.06.007.

149. Dhyani, V.; Bhaskar, T. A comprehensive review on the pyrolysis of lignocellulosic biomass. *Renew. Energy* **2018**, *129*, 695–716. https://doi.org/10.1016/j.renene.2017.04.035.

150. Mondal, P.; Dang, G.S.; Garg, M.O. Syngas production through gasification and cleanup for downstream applications—Recent developments. *Fuel Processing Technol.* **2011**, *92*, 1395–1410. https://doi.org/10.1016/j.fuproc.2011.03.021.

151. Raffelt, K.; Henrich, E.; Koegel, A.; Stahl, R.; Steinhardt, J.; Weirich, F. The BTL2 process of biomass utilization entrained-flow gasification of pyrolyzed biomass slurries. *Appl. Biochem. Biotechnol.* **2006**, *129*, 153–164. https://doi.org/10.1385/abab:129:1:153.

152. Soria, M.A.; Barros, D.; Madeira, L.M. Hydrogen production through steam reforming of bio-oils derived from biomass pyrolysis: Thermodynamic analysis including in situ CO2 and/or H2 separation. *Fuel* **2019**, *244*, 184–195. https://doi.org/10.1016/j.fuel.2019.01.156.

153. Basagiannis, A.C.; Verykios, X.E. Reforming reactions of acetic acid on nickel catalysts over a wide temperature range. *Appl. Catal. A Gen.* **2006**, *308*, 182–193. https://doi.org/10.1016/j.apcata.2006.04.024.

154. Marquevich, M.; Czernik, S.; Chornet, E.; Montané, D. Hydrogen from Biomass: Steam Reforming of Model Compounds of Fast-Pyrolysis Oil. *Energy Fuels* **1999**, *13*, 1160–1166. https://doi.org/10.1021/ef990034w.

155. Radlein, D.; Piskorz, J.; Scott, D.S. Fast pyrolysis of natural polysaccharides as a potential industrial process. *J. Anal. Appl. Pyrolysis* **1991**, *19*, 41–63. https://doi.org/10.1016/0165-2370(91)80034-6.

156. Paredes, M.J.; Moreno, E.; Ramos-Cormenzana, A.; Martinez, J. Characteristics of soil after pollution with wastewaters from olive oil extraction plants. *Chemosphere* **1987**, *16*, 1557–1564.

157. DellaGreca, M.; Monaco, P.; Pinto, G.; Pollio, A.; Previtera, L.; Temussi, F. Phytotoxicity of low-molecular-weight phenols from olive mill wastewaters. *Bull. Environ. Contam. Toxicol.* **2001**, *67*, 352–359.

158. Rana, G.; Rinaldi, M.; Introna, M. Volatilisation of substances alter spreading olive oil waste water on the soil in a Mediterranean environment. *Agric. Ecosyst. Environ.* **2003**, *96*, 49–58.

159. Montero, C.; Oar-Arteta, L.; Remiro, A.; Arandia, A.; Bilbao, J.; Gayubo, A.G. Thermodynamic comparison between bio-oil and ethanol steam reforming. *Int. J. Hydrog. Energy* **2015**, *40*, 15963–15971. https://doi.org/10.1016/j.ijhydene.2015.09.125.

160. Casanovas, A.; Galvis, A.; Llorca, J. Catalytic steam reforming of olive mill wastewater for hydrogen production. *Int. J. Hydrog. Energy* **2015**, *40*, 7539–7545. https://doi.org/10.1016/j.ijhydene.2014.11.083.

161. Tosti, S.; Fabbricino, M.; Pontoni, L.; Palma, V.; Ruocco, C. Catalytic reforming of olive mill wastewater and methane in a Pd-membrane reactor. *Int. J. Hydrog. Energy* **2016**, *41*, 5465–5474. https://doi.org/10.1016/j.ijhydene.2016.02.014.

162. Tosti, S.; Accetta, C.; Fabbricino, M.; Sansovini, M.; Pontoni, L. Reforming of olive mill wastewater through a Pd-membrane reactor. *Int. J. Hydrog. Energy* **2013**, *38*, 10252–10259. https://doi.org/10.1016/j.ijhydene.2013.06.027.

163. Gebreyohannes, A.Y.; Mazzei, R.; Giorno, L. Trends and current practices of olive mill wastewater treatment: Application of integrated membrane process and its future perspective. *Sep. Purif. Technol.* **2016**, *162*, 45–60. https://doi.org/10.1016/j.seppur.2016.02.001.

164. Aggoun, M.; Arhab, R.; Cornu, A.; Portelli, J.; Barkat, M.; Graulet, B. Olive mill wastewater microconstituents composition according to olive variety and extraction process. *Food Chem.* **2016**, *209*, 72–80. https://doi.org/10.1016/j.foodchem.2016.04.034.

165. El-Abbassi, A.; Kiai, H.; Hafidi, A. Phenolic profile and antioxidant activities of olive mill wastewater. *Food Chem.* **2012**, *132*, 406–412. https://doi.org/10.1016/j.foodchem.2011.11.013.

166. Daâssi, D.; Lozano-Sánchez, J.; Borrás-Linares, I.; Belbahri, L.; Woodward, S.; Zouari-Mechichi, H.; Mechichi, T.; Nasri, M.; Segura-Carretero, A. Olive oil mill wastewaters: Phenolic content characterization during degradation by Coriolopsis gallica. *Chemosphere* **2014**, *113*, 62–70. https://doi.org/10.1016/j.chemosphere.2014.04.053.

167. Fki, I.; Allouche, N.; Sayadi, S. The use of polyphenolic extract, purified hydroxytyrosol and 3,4-dihydroxyphenyl acetic acid from olive mill wastewater for the stabilization of refined oils: A potential alternative to synthetic antioxidants. *Food Chem.* **2005**, *93*, 197–204. https://doi.org/10.1016/j.foodchem.2004.09.014.

168. Dermeche, S.; Nadour, M.; Larroche, C.; Moulti-Mati, F.; Michaud, P. Olive mill wastes: Biochemical characterizations and valorization strategies. *Process Biochem.* **2013**, *48*, 1532–1552. https://doi.org/10.1016/j.procbio.2013.07.010.

169. Kyriacou, A.; Lasaridi, K.E.; Kotsou, M.; Balis, C.; Pilidis, G. Combined bioremediation and advanced oxidation of green table olive processing wastewater. *Process Biochem.* **2005**, *40*, 1401–1408. https://doi.org/10.1016/j.procbio.2004.06.001.

170. Araújo, M.; Pimentel, F.B.; Alves, R.C.; Oliveira, M.B.P.P. Phenolic compounds from olive mill wastes: Health effects, analytical approach and application as food antioxidants. *Trends Food Sci. Technol.* **2015**, *45*, 200–211. https://doi.org/10.1016/j.tifs.2015.06.010.

171. Kaleh, Z.; Geißen, S.U. Selective isolation of valuable biophenols from olive mill wastewater. *J. Environ. Chem. Eng.* **2016**, *4*, 373–384. https://doi.org/10.1016/j.jece.2015.11.010.

172. Caputo, A.C.; Scacchia, F.; Pelagagge, P.M. Disposal of by-products in olive oil industry: Waste-to-energy solutions. *Appl. Therm. Eng.* **2003**, *23*, 197–214. https://doi.org/10.1016/S1359-4311(02)00173-4.

173. Vlyssides, A.G.; Loizides, M.; Karlis, P.K. Integrated strategic approach for reusing olive oil extraction by-products. *J. Clean. Prod.* **2004**, *12*, 603–611. https://doi.org/10.1016/S0959-6526(03)00078-7.

174. Paredes, C.; Cegarra, J.; Roig, A.; Sánchez-Monedero, M.A.; Bernal, M.P. Characterization of olive mill wastewater (alpechin) and its sludge for agricultural purposes. *Bioresour. Technol.* **1999**, *67*, 111–115. https://doi.org/10.1016/S0960-8524(98)00106-0.

175. Feki, M.; Allouche, N.; Bouaziz, M.; Gargoubi, A.; Sayadi, S. Effect of storage of olive mill wastewaters on hydroxytyrosol concentration. *Eur. J. Lipid Sci. Technol.* **2006**, *108*, 1021–1027. https://doi.org/10.1002/ejlt.200500348.

176. Hamden, K.; Allouche, N.; Damak, M.; Elfeki, A. Hypoglycemic and antioxidant effects of phenolic extracts and purified hydroxytyrosol from olive mill waste in vitro and in rats. *Chem.-Biol. Interact.* **2009**, *180*, 421–432. https://doi.org/10.1016/j.cbi.2009.04.002.

177. O-Thong, S.; Suksong, W.; Promnuan, K.; Thipmunee, M.; Mamimin, C.; Prasertsan, P. Two-stage thermophilic fermentation and mesophilic methanogenic process for biohythane production from palm oil mill effluent with methanogenic effluent recirculation for pH control. *Int. J. Hydrog. Energy* **2016**, *41*, 21702–21712. https://doi.org/10.1016/j.ijhydene.2016.07.095.

178. Bizkarra, K.; Bermudez, J.M.; Arcelus-Arrillaga, P.; Barrio, V.L.; Cambra, J.F.; Millan, M. Nickel based monometallic and bimetallic catalysts for synthetic and real bio-oil steam reforming. *Int. J. Hydrog. Energy* **2018**, *43*, 11706–11718. https://doi.org/10.1016/j.ijhydene.2018.03.049.

179. Kechagiopoulos, P.N.; Voutetakis, S.S.; Lemonidou, A.A.; Vasalos, I.A. Hydrogen Production via Steam Reforming of the Aqueous Phase of Bio-Oil in a Fixed Bed Reactor. *Energy Fuels* **2006**, *20*, 2155–2163. https://doi.org/10.1021/ef060083q.

180. Remiro, A.; Arandia, A.; Oar-Arteta, L.; Bilbao, J.; Gayubo, A.G. Regeneration of NiAl2O4 spinel type catalysts used in the reforming of raw bio-oil. *Appl. Catal. B Environ.* **2018**, *237*, 353–365. https://doi.org/10.1016/j.apcatb.2018.06.005.

181. Remiro, A.; Valle, B.; Aguayo, A.T.; Bilbao, J.; Gayubo, A.G. Operating conditions for attenuating Ni/La2O3–αAl2O3 catalyst deactivation in the steam reforming of bio-oil aqueous fraction. *Fuel Processing Technol.* **2013**, *115*, 222–232. https://doi.org/10.1016/j.fuproc.2013.06.003.

182. Valle, B.; Aramburu, B.; Olazar, M.; Bilbao, J.; Gayubo, A.G. Steam reforming of raw bio-oil over Ni/La2O3-αAl2O3: Influence of temperature on product yields and catalyst deactivation. *Fuel* **2018**, *216*, 463–474. https://doi.org/10.1016/j.fuel.2017.11.149.

183. Xie, H.; Yu, Q.; Wei, M.; Duan, W.; Yao, X.; Qin, Q.; Zuo, Z. Hydrogen production from steam reforming of simulated bio-oil over Ce–Ni/Co catalyst with in continuous CO2 capture. *Int. J. Hydrog. Energy* **2015**, *40*, 1420–1428. https://doi.org/10.1016/j.ijhydene.2014.11.137.

184. Silva, J.M.; Ribeiro, L.S.; Órfão, J.J.M.; Soria, M.A.; Madeira, L.M. Low temperature glycerol steam reforming over a Rh-based catalyst combined with oxidative regeneration. *Int. J. Hydrog. Energy* **2019**, *44*, 2461–2473. https://doi.org/10.1016/j.ijhydene.2018.11.234.

185. Rocha, C.; Soria, M.A.; Madeira, L.M. Olive mill wastewater valorization through steam reforming using hybrid multifunctional reactors for high-purity H2 production. *Chem. Eng. J.* **2022**, *430*, 132651. https://doi.org/10.1016/j.cej.2021.132651.

186. Ng, K.H.; Cheng, Y.W.; Lee, Z.S.; Cheng, C.K. A study into syngas production from catalytic steam reforming of palm oil mill effluent (POME): A new treatment approach. *Int. J. Hydrog. Energy* **2019**, *44*, 20900–20913. https://doi.org/10.1016/j.ijhydene.2018.04.232.

187. Cheng, Y.W.; Ng, K.H.; Lam, S.S.; Lim, J.W.; Wongsakulphasatch, S.; Witoon, T.; Cheng, C.K. Syngas from catalytic steam reforming of palm oil mill effluent: An optimization study. *Int. J. Hydrog. Energy* **2019**, *44*, 9220–9236. https://doi.org/10.1016/j.ijhydene.2019.02.061.

188. Ighalo, J.O.; Adeniyi, A.G. Factor effects and interactions in steam reforming of biomass bio-oil. *Chem. Pap.* **2020**, *74*, 1459–1470. https://doi.org/10.1007/s11696-019-00996-3.

189. Rocha, C.; Soria, M.A.; Madeira, L.M. Steam reforming of olive oil mill wastewater with in situ hydrogen and carbon dioxide separation–Thermodynamic analysis. *Fuel* **2017**, *207*, 449–460. https://doi.org/10.1016/j.fuel.2017.06.111.

190. Rocha, C.; Soria, M.A.; Madeira, L.M. Thermodynamic analysis of olive oil mill wastewater steam reforming. *J. Energy Inst.* **2019**, *92*, 1599–1609. https://doi.org/10.1016/j.joei.2018.06.017.

191. Macedo, M.S.; Soria, M.A.; Madeira, L.M. Glycerol steam reforming for hydrogen production: Traditional versus membrane reactor. *Int. J. Hydrog. Energy* **2019**, *44*, 24719–24732. https://doi.org/10.1016/j.ijhydene.2019.07.046.

192. Leal, A.L.; Soria, M.A.; Madeira, L.M. Autothermal reforming of impure glycerol for H₂ production: Thermodynamic study including in situ CO₂ and/or H₂ separation. *Int. J. Hydrog. Energy* **2016**, *41*, 2607–2620. https://doi.org/10.1016/j.ijhydene.2015.11.132.

193. Medrano, J.A.; Oliva, M.; Ruiz, J.; Garcia, L.; Arauzo, J. Catalytic steam reforming of acetic acid in a fluidized bed reactor with oxygen addition. *Int. J. Hydrog. Energy* **2008**, *33*, 4387–4396. https://doi.org/10.1016/j.ijhydene.2008.05.023.

194. Matas Güell, B.; Silva, I.M.T.d.; Seshan, K.; Lefferts, L. Sustainable route to hydrogen–Design of stable catalysts for the steam gasification of biomass related oxygenates. *Appl. Catal. B Environ.* **2009**, *88*, 59–65. https://doi.org/10.1016/j.apcatb.2008.09.018.

195. Hoang, T.M.C.; Geerdink, B.; Sturm, J.M.; Lefferts, L.; Seshan, K. Steam reforming of acetic acid–A major component in the volatiles formed during gasification of humin. *Appl. Catal. B Environ.* **2015**, *163*, 74–82. https://doi.org/10.1016/j.apcatb.2014.07.046.

196. Chen, G.; Tao, J.; Liu, C.; Yan, B.; Li, W.; Li, X. Steam reforming of acetic acid using Ni/Al2O3 catalyst: Influence of crystalline phase of Al2O3 support. *Int. J. Hydrog. Energy* **2017**, *42*, 20729–20738. https://doi.org/10.1016/j.ijhydene.2017.07.027.

197. Savuto, E.; Navarro, R.M.; Mota, N.; Di Carlo, A.; Bocci, E.; Carlini, M.; Fierro, J.L.G. Steam reforming of tar model compounds over Ni/Mayenite catalysts: Effect of Ce addition. *Fuel* **2018**, *224*, 676–686. https://doi.org/10.1016/j.fuel.2018.03.081.

198. Zhang, Z.; Hu, X.; Li, J.; Gao, G.; Dong, D.; Westerhof, R.; Hu, S.; Xiang, J.; Wang, Y. Steam reforming of acetic acid over Ni/Al2O3 catalysts: Correlation of nickel loading with properties and catalytic behaviors of the catalysts. *Fuel* **2018**, *217*, 389–403. https://doi.org/10.1016/j.fuel.2017.12.114.

199. Borges, R.P.; Ferreira, R.A.R.; Rabelo-Neto, R.C.; Noronha, F.B.; Hori, C.E. Hydrogen production by steam reforming of acetic acid using hydrotalcite type precursors. *Int. J. Hydrog. Energy* **2018**, *43*, 7881–7892. https://doi.org/10.1016/j.ijhydene.2018.03.028.

200. He, L.; Hu, S.; Jiang, L.; Liao, G.; Chen, X.; Han, H.; Xiao, L.; Ren, Q.; Wang, Y.; Su, S.; et al. Carbon nanotubes formation and its influence on steam reforming of toluene over Ni/Al2O3 catalysts: Roles of catalyst supports. *Fuel Processing Technol.* **2018**, *176*, 7–14. https://doi.org/10.1016/j.fuproc.2018.03.007.

201. Pu, J.; Nishikado, K.; Wang, N.; Nguyen, T.T.; Maki, T.; Qian, E.W. Core-shell nickel catalysts for the steam reforming of acetic acid. *Appl. Catal. B Environ.* **2018**, *224*, 69–79. https://doi.org/10.1016/j.apcatb.2017.09.058.

202. Zhang, C.; Hu, X.; Yu, Z.; Zhang, Z.; Chen, G.; Li, C.; Liu, Q.; Xiang, J.; Wang, Y.; Hu, S. Steam reforming of acetic acid for hydrogen production over attapulgite and alumina supported Ni catalysts: Impacts of properties of supports on catalytic behaviors. *Int. J. Hydrog. Energy* **2019**, *44*, 5230–5244. https://doi.org/10.1016/j.ijhydene.2018.09.071.

203. Chen, J.; Wang, M.; Wang, S.; Li, X. Hydrogen production via steam reforming of acetic acid over biochar-supported nickel catalysts. *Int. J. Hydrog. Energy* **2018**, *43*, 18160–18168. https://doi.org/10.1016/j.ijhydene.2018.08.048.

204. Kechagiopoulos, P.N.; Voutetakis, S.S.; Lemonidou, A.A.; Vasalos, I.A. Hydrogen Production via Reforming of the Aqueous Phase of Bio-Oil over Ni/Olivine Catalysts in a Spouted Bed Reactor. *Ind. Eng. Chem. Res.* **2009**, *48*, 1400–1408. https://doi.org/10.1021/ie8013378.

205. Liu, S.; Chen, M.; Chu, L.; Yang, Z.; Zhu, C.; Wang, J.; Chen, M. Catalytic steam reforming of bio-oil aqueous fraction for hydrogen production over Ni–Mo supported on modified sepiolite catalysts. *Int. J. Hydrog. Energy* **2013**, *38*, 3948–3955. https://doi.org/10.1016/j.ijhydene.2013.01.117.

206. Garcia, L.a.; French, R.; Czernik, S.; Chornet, E. Catalytic steam reforming of bio-oils for the production of hydrogen: Effects of catalyst composition. *Appl. Catal. A Gen.* **2000**, *201*, 225–239. https://doi.org/10.1016/S0926-860X(00)00440-3.

207. Bangala, D.N.; Abatzoglou, N.; Chornet, E. Steam reforming of naphthalene on Ni–Cr/Al2O3 catalysts doped with MgO, TiO2, and La2O3. *AIChE J.* **1998**, *44*, 927–936. https://doi.org/10.1002/aic.690440418.

208. Zhang, Z.; Hu, X.; Gao, G.; Wei, T.; Dong, D.; Wang, Y.; Hu, S.; Xiang, J.; Liu, Q.; Geng, D. Steam reforming of acetic acid over NiKOH/Al2O3 catalyst with low nickel loading: The remarkable promotional effects of KOH on activity. *Int. J. Hydrog. Energy* **2019**, *44*, 729–747. https://doi.org/10.1016/j.ijhydene.2018.10.244.

209. Choi, I.-H.; Hwang, K.-R.; Lee, K.-Y.; Lee, I.-G. Catalytic steam reforming of biomass-derived acetic acid over modified Ni/γ-Al2O3 for sustainable hydrogen production. *Int. J. Hydrog. Energy* **2019**, *44*, 180–190. https://doi.org/10.1016/j.ijhydene.2018.04.192.

210. Charisiou, N.D.; Siakavelas, G.; Tzounis, L.; Dou, B.; Sebastian, V.; Hinder, S.J.; Baker, M.A.; Polychronopoulou, K.; Goula, M.A. Ni/Y2O3–ZrO2 catalyst for hydrogen production through the glycerol steam reforming reaction. *Int. J. Hydrog. Energy* **2020**, *45*, 10442–10460. https://doi.org/10.1016/j.ijhydene.2019.04.237.

211. Souza, I.C.A.; Manfro, R.L.; Souza, M.M.V.M. Hydrogen production from steam reforming of acetic acid over Pt–Ni bimetallic catalysts supported on ZrO2. *Biomass Bioenergy* **2022**, *156*, 106317. https://doi.org/10.1016/j.biombioe.2021.106317.

212. Baamran, K.S.; Tahir, M.; Mohamed, M.; Hussain Khoja, A. Effect of support size for stimulating hydrogen production in phenol steam reforming using Ni-embedded TiO2 nanocatalyst. *J. Environ. Chem. Eng.* **2020**, *8*, 103604. https://doi.org/10.1016/j.jece.2019.103604.

213. Baamran, K.S.; Tahir, M. Ni-embedded TiO2-ZnTiO3 reducible perovskite composite with synergistic effect of metal/support towards enhanced H2 production via phenol steam reforming. *Energy Convers. Manag.* **2019**, *200*, 112064. https://doi.org/10.1016/j.enconman.2019.112064.

214. Abbas, T.; Tahir, M.; Saidina Amin, N.A. Enhanced Metal–Support Interaction in Ni/Co3O4/TiO2 Nanorods toward Stable and Dynamic Hydrogen Production from Phenol Steam Reforming. *Ind. Eng. Chem. Res.* **2019**, *58*, 517–530. https://doi.org/10.1021/acs.iecr.8b03542.

215. Pu, J.; Ikegami, F.; Nishikado, K.; Qian, E.W. Effect of ceria addition on NiRu/CeO2Al2O3 catalysts in steam reforming of acetic acid. *Int. J. Hydrog. Energy* **2017**, *42*, 19733–19743. https://doi.org/10.1016/j.ijhydene.2017.06.120.

216. Wang, Y.; Chen, M.; Yang, J.; Liu, S.; Yang, Z.; Wang, J.; Liang, T. Hydrogen Production from Steam Reforming of Acetic Acid over Ni-Fe/Palygorskite Modified with Cerium. *BioResources* **2017**, *12*, 4830–4853.

217. Li, L.; Jiang, B.; Tang, D.; Zhang, Q.; Zheng, Z. Hydrogen generation by acetic acid steam reforming over Ni-based catalysts derived from La1−xCexNiO3 perovskite. *Int. J. Hydrog. Energy* **2018**, *43*, 6795–6803. https://doi.org/10.1016/j.ijhydene.2018.02.128.

218. Zhao, X.; Xue, Y.; Lu, Z.; Huang, Y.; Guo, C.; Yan, C. Encapsulating Ni/CeO2-ZrO2 with SiO2 layer to improve it catalytic activity for steam reforming of toluene. *Catal. Commun.* **2017**, *101*, 138–141. https://doi.org/10.1016/j.catcom.2017.08.013.

219. Liang, T.; Wang, Y.; Chen, M.; Yang, Z.; Liu, S.; Zhou, Z.; Li, X. Steam reforming of phenol-ethanol to produce hydrogen over bimetallic NiCu catalysts supported on sepiolite. *Int. J. Hydrog. Energy* **2017**, *42*, 28233–28246. https://doi.org/10.1016/j.ijhydene.2017.09.134.

220. Pant, K.K.; Mohanty, P.; Agarwal, S.; Dalai, A.K. Steam reforming of acetic acid for hydrogen production over bifunctional Ni–Co catalysts. *Catal. Today* **2013**, *207*, 36–43. https://doi.org/10.1016/j.cattod.2012.06.021.

221. Lee, Y.-L.; Jha, A.; Jang, W.-J.; Shim, J.-O.; Jeon, K.-W.; Na, H.-S.; Kim, H.-M.; Lee, D.-W.; Yoo, S.-Y.; Jeon, B.-H.; et al. Optimization of Cobalt Loading in Co–CeO2 Catalyst for the High Temperature Water–Gas Shift Reaction. *Top. Catal.* **2017**, *60*, 721–726. https://doi.org/10.1007/s11244-017-0776-2.

222. Sabnis, K.D. *Structure-Activity Relationships for the Water-Gas Shift Reaction over Supported Metal Catalysts*; Purdue University: West Lafayette, IN, USA, 2015.

223. Mizuno, S.C.M.; Braga, A.H.; Hori, C.E.; Santos, J.B.O.; Bueno, J.M.C. Steam reforming of acetic acid over MgAl2O4-supported Co and Ni catalysts: Effect of the composition of Ni/Co and reactants on reaction pathways. *Catal. Today* **2017**, *296*, 144–153. https://doi.org/10.1016/j.cattod.2017.04.023.

224. Rocha, C.; Soria, M.A.; Madeira, L.M. Screening of commercial catalysts for steam reforming of olive mill wastewater. *Renew. Energy* **2021**, *169*, 765–779. https://doi.org/10.1016/j.renene.2020.12.139.

225. Rocha, C.; Soria, M.A.; Madeira, L.M. Use of Ni-containing catalysts for synthetic olive mill wastewater steam reforming. *Renew. Energy* **2022**, *185*, 1329–1342. https://doi.org/10.1016/j.renene.2021.12.052.

226. Adhikari, S.; Fernando, S.D.; To, S.D.F.; Bricka, R.M.; Steele, P.H.; Haryanto, A. Conversion of Glycerol to Hydrogen via a Steam Reforming Process over Nickel Catalysts. *Energy Fuels* **2008**, *22*, 1220–1226. https://doi.org/10.1021/ef700520f.

227. Pant, K.K.; Jain, R.; Jain, S. Renewable hydrogen production by steam reforming of glycerol over Ni/CeO2 catalyst prepared by precipitation deposition method. *Korean J. Chem. Eng.* **2011**, *28*, 1859. https://doi.org/10.1007/s11814-011-0059-8.

228. Buffoni, I.N.; Pompeo, F.; Santori, G.F.; Nichio, N.N. Nickel catalysts applied in steam reforming of glycerol for hydrogen production. *Catal. Commun.* **2009**, *10*, 1656–1660. https://doi.org/10.1016/j.catcom.2009.05.003.

229. Silva, O.C.V.; Silveira, E.B.; Rabelo-Neto, R.C.; Borges, L.E.P.; Noronha, F.B. Hydrogen Production Through Steam Reforming of Toluene Over Ni Supported on MgAl Mixed Oxides Derived from Hydrotalcite-Like Compounds. *Catal. Lett.* **2018**, *148*, 1622–1633. https://doi.org/10.1007/s10562-018-2390-8.

230. Manfro, R.L.; Ribeiro, N.F.P.; Souza, M.M.V.M. Production of hydrogen from steam reforming of glycerol using nickel catalysts supported on Al2O3, CeO2 and ZrO2. *Catal. Sustain. Energy* **2013**, *1*, 60–70, doi:doi:10.2478/cse-2013-0001.

231. Carrero, A.; Calles, J.A.; García-Moreno, L.; Vizcaíno, A.J. Production of Renewable Hydrogen from Glycerol Steam Reforming over Bimetallic Ni-(Cu,Co,Cr) Catalysts Supported on SBA-15 Silica. *Catalysts* **2017**, *7*, 55.

232. Cheng, F.; Dupont, V. Nickel catalyst auto-reduction during steam reforming of bio-oil model compound acetic acid. *Int. J. Hydrog. Energy* **2013**, *38*, 15160–15172. https://doi.org/10.1016/j.ijhydene.2013.09.111.

233. Wang, M.; Zhang, F.; Wang, S. Effect of La2O3 replacement on γ-Al2O3 supported nickel catalysts for acetic acid steam reforming. *Int. J. Hydrog. Energy* **2017**, *42*, 20540–20548. https://doi.org/10.1016/j.ijhydene.2017.06.147.

234. Matas Güell, B.; Babich, I.V.; Lefferts, L.; Seshan, K. Steam reforming of phenol over Ni-based catalysts–A comparative study. *Appl. Catal. B Environ.* **2011**, *106*, 280–286. https://doi.org/10.1016/j.apcatb.2011.05.012.

235. Frusteri, F.; Freni, S.; Chiodo, V.; Spadaro, L.; Di Blasi, O.; Bonura, G.; Cavallaro, S. Steam reforming of bio-ethanol on alkali-doped Ni/MgO catalysts: Hydrogen production for MC fuel cell. *Appl. Catal. A Gen.* **2004**, *270*, 1–7. https://doi.org/10.1016/j.apcata.2004.03.052.

236. Ahmed, T.; Xiu, S.; Wang, L.; Shahbazi, A. Investigation of Ni/Fe/Mg zeolite-supported catalysts in steam reforming of tar using simulated-toluene as model compound. *Fuel* **2018**, *211*, 566–571. https://doi.org/10.1016/j.fuel.2017.09.051.

237. Fally, F.; Perrichon, V.; Vidal, H.; Kaspar, J.; Blanco, G.; Pintado, J.M.; Bernal, S.; Colon, G.; Daturi, M.; Lavalley, J.C. Modification of the oxygen storage capacity of CeO2–ZrO2 mixed oxides after redox cycling aging. *Catal. Today* **2000**, *59*, 373–386. https://doi.org/10.1016/S0920-5861(00)00302-3.

238. Vidal, H.; Kašpar, J.; Pijolat, M.; Colon, G.; Bernal, S.; Cordón, A.; Perrichon, V.; Fally, F. Redox behavior of CeO2–ZrO2 mixed oxides: II. Influence of redox treatments on low surface area catalysts. *Appl. Catal. B Environ.* **2001**, *30*, 75–85. https://doi.org/10.1016/S0926-3373(00)00221-6.

239. Sánchez, E.A.; D'Angelo, M.A.; Comelli, R.A. Hydrogen production from glycerol on Ni/Al₂O₃ catalyst. *Int. J. Hydrog. Energy* **2010**, *35*, 5902–5907. https://doi.org/10.1016/j.ijhydene.2009.12.115.

240. Wen, G.; Xu, Y.; Ma, H.; Xu, Z.; Tian, Z. Production of hydrogen by aqueous-phase reforming of glycerol. *Int. J. Hydrog. Energy* **2008**, *33*, 6657–6666. https://doi.org/10.1016/j.ijhydene.2008.07.072.

241. Cakiryilmaz, N.; Arbag, H.; Oktar, N.; Dogu, G.; Dogu, T. Effect of W incorporation on the product distribution in steam reforming of bio-oil derived acetic acid over Ni based Zr-SBA-15 catalyst. *Int. J. Hydrog. Energy* **2018**, *43*, 3629–3642. https://doi.org/10.1016/j.ijhydene.2018.01.034.

242. Yu, Z.; Hu, X.; Jia, P.; Zhang, Z.; Dong, D.; Hu, G.; Hu, S.; Wang, Y.; Xiang, J. Steam reforming of acetic acid over nickel-based catalysts: The intrinsic effects of nickel precursors on behaviors of nickel catalysts. *Appl. Catal. B Environ.* **2018**, *237*, 538–553. https://doi.org/10.1016/j.apcatb.2018.06.020.

243. Pekmezci Karaman, B.; Cakiryilmaz, N.; Arbag, H.; Oktar, N.; Dogu, G.; Dogu, T. Performance comparison of mesoporous alumina supported Cu & Ni based catalysts in acetic acid reforming. *Int. J. Hydrog. Energy* **2017**, *42*, 26257–26269. https://doi.org/10.1016/j.ijhydene.2017.08.155.

244. Goicoechea, S.; Kraleva, E.; Sokolov, S.; Schneider, M.; Pohl, M.-M.; Kockmann, N.; Ehrich, H. Support effect on structure and performance of Co and Ni catalysts for steam reforming of acetic acid. *Appl. Catal. A Gen.* **2016**, *514*, 182–191. https://doi.org/10.1016/j.apcata.2015.12.025.